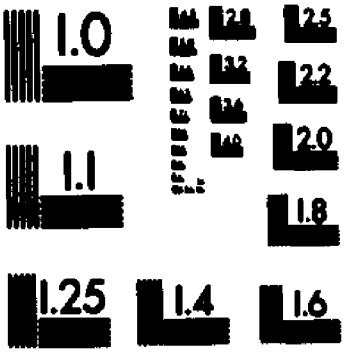

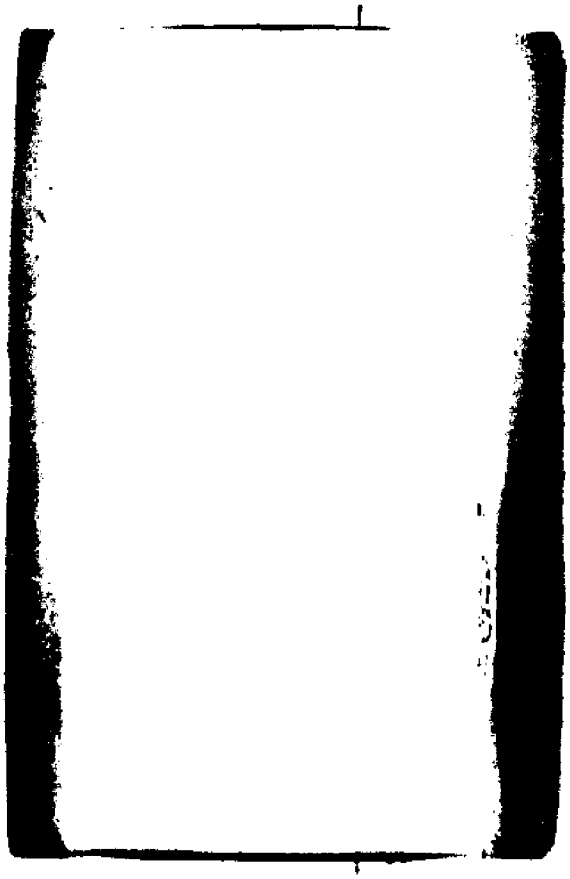

MARINOVIC, NENAD M.

THE WIGNER DISTRIBUTION AND THE AMBIGUITY FUNCTION: GENERALIZATIONS, ENHANCEMENT, COMPRESSION AND SOME APPLICATIONS

City University of New York PH.D. 1986

PLEASE NOTE:

In all cases this material has been filmed in the best possible way from the available copy. Problems encountered with this document have been identified here with a check mark __✓__.

1. Glossy photographs or pages _____
2. Colored illustrations, paper or print _____
3. Photographs with dark background ✓
4. Illustrations are poor copy _____
5. Pages with black marks, not original copy _____
6. Print shows through as there is text on both sides of page _____
7. Indistinct, broken or small print on several pages ✓
8. Print exceeds margin requirements _____
9. Tightly bound copy with print lost in spine _____
10. Computer printout pages with indistinct print _____
11. Page(s) _____ lacking when material received, and not available from school or author.
12. Page(s) _____ seem to be missing in numbering only as text follows.
13. Two pages numbered _____. Text follows.
14. Curling and wrinkled pages _____
15. Dissertation contains pages with print at a slant, filmed as received _____
16. Other _____

_____

_____

University
Microfilms
International

THE WIGNER DISTRIBUTION AND THE AMBIGUITY FUNCTION: GENERALIZATIONS, ENHANCEMENT, COMPRESSION AND SOME APPLICATIONS

by

NENAD M. MARINOVIC

A dissertation submitted to the Graduate Faculty in Engineering in partial fulfillment of the requirements for the degree of Doctor of Philosophy, The City University of New York.

1986

This manuscript has been read and accepted for the Graduate Faculty in Engineering in satisfaction of the dissertation requirements for the degree of Doctor of Philosophy.

1/10/86
Date

Prof. George Eichmann
Chair of Examining Committee

1/23/86
Date

Prof. Paul Karmel
Executive Officer

Supervisory Committee:

Prof. Richard Tolimieri
Prof. Leonid Roytman
Prof. Joseph Barba
Dr. Wallace A. Smith - Philips Laboratories

The City University of New York

Acknowledgements

I would like to use this opportunity to thank all the persons and institutions who have contributed to the successfull completion of many years of my formal education.

For nurturing my intellectual curiosity, and for all the love, dedication, sacrifices, support and guidance, I express my deepest gratitude to my mother and my father. For her love, faith and encouragement, I am grateful to my wife Sofia who took mostly upon herself to bring up our sons, to free the time that I needed to complete this work. To my brother, I am thankful for giving me an example to follow and for support when I needed it most.

Outside my family, there are many others deserving special thanks. Professors Mansour Javid and Paul Karmel provided me with the opportunity to pursue Ph.D. studies at the City University of New York by awarding me with the initial financial support. Professor Se Jeung Oh gave many words of friendly advice and guidance. Most of all, I am grateful to my adviser, Professor George Eichmann, for suggesting the topic of this research, for guiding me through it, and for being a constant source of challenging ideas.

For the extensive support provided, I wish to thank the management and employees of Philips Laboratories in Briarcliff Manor, New York; most of this research was done using the computational facilities, library and

documentation services of the Labs. Finally, I am especially indebted to Dr. Wallace A. Smith, my supervisor at Phillips Laboratories, whose technical insights, suggestions, encouragement and support throughout the course of this research, were invaluable.

This research was also supported, in part, by grants from the Air Force Office of Scientific Research.

Riverdale, New York
November 1985

Table of Contents

Chapter 1

Introduction

The Wigner distribution and the ambiguity function are well-characterized signal processing tools used in a variety of applications[1-6]. This thesis addresses the issues of modifying these representations to extend the range of their applications, and post-processing them to increase their effectiveness in existing applications.

An essential feature of the Wigner distribution and ambiguity function is their invariance to time and frequency shifts in the signal. It is this property that makes them appropriate for the analysis and processing of signals in shift-invariant systems. However, there are many shift-variant systems that cannot be treated in the same way - they lack corresponding tools. Among such systems, scale-invariant optical and electronic systems have received a lot of attention recently. A number of applications of scale-invariant signal processing techniques have been reported: in restoration of images with spatially-variant degradations[7,8], in spectral analysis[9] and signal recovery[10], in the deformation-invariant and scale-independent pattern recognition[11-13], in Doppler signal processing[14], in signal detection and estimation[15], in speech analysis[16], and in speech bandwidth compression and word recognition[17]. In view of this, it is beneficial to extend the concepts of Wigner distribution and ambiguity function to conform with scale-invariance rather than shift-invariance. That can make these powerful signal analysis and synthesis tools available for scale-invariant signal processing and characterization of scale-invariant systems. With this aim, generalized scale-invariant signal representations will be proposed and fully characterized.

Conventional bilinear signal representations, especially the Wigner distribution, have not been utilized to their full potential for several reasons. Being the two-dimensional representations of one-dimensional signals they contain a lot of redundancy. This increased amount of data often prohibits their effective use in applications like signal detection and pattern recognition. Hence, it is of practical interest to find methods of data compression to be applied on time-frequency representations. One particular form of the redundancy is represented by interfering cross-terms. These terms prevent the visual interpretation of results and sometimes make estimation of signal parameters rather difficult. Suppression of these terms is desired since it would make representations like the Wigner distribution more useful for both qualitative and quantitative signal characterization.

Related to this is the issue of the noise sensitivity of bilinear signal representations. Namely, if the signal is contaminated by noise, its auto-representation contains a correlated, linear noise term and an uncorrelated, quadratic noise term. Consequently, the signal to noise ratio (SNR) in the representation is significantly lower than in the original signal, and at low SNR's there is a threshold in their functional relationship. This prevents successful application of auto-representation of the signal at low SNR's. One of the aims of this research is to find procedures for data compression, interference elimination and noise suppression in bilinear time-frequency signal representations, in general, and in the Wigner distribution and the ambiguity function in particular.

In summary, two research directions are explored in this thesis. One is to find scale-invariant bilinear signal representations with properties corresponding to the conventional Wigner distribution and ambiguity functions. The other is to increase the utility of these conventional representations by

developing methods for their compression and enhancement. An overview of the current state of the art in time-frequency signal representations is presented in Chapter 2. In Chapter 3, the utility of the Wigner distribution for characterization and analysis of the filtering action of ultrasonic transducers is demonstrated. The discussion is actually applicable to linear systems in general. Scale-invariant modifications of the Wigner distribution and the ambiguity function are proposed and their properties are extensively analyzed in Chapter 4. A series expansion for the Wigner distribution (and ambiguity function, also) is presented in Chapter 5; properties of the expansion coefficients are analyzed and related to the physical characteristics of the signal. This expansion is shown to be useful for data compression and enhancement of the Wigner distribution. The coefficients of the expansion, regarded as a generalized "spectrum" of the signal, are used as descriptors of 2-D shapes for shape classification in image analysis. Finally, in Chapter 7, components of the generalized "spectrum", defined in Chapter 5, are used for estimation of the ultrasonic attenuation in tissues.

References

1. E. P. Wigner, "On the Quantum Correction for Thermo-dynamic Equilibrium," *Phys. Rew.* 40, pp. 749-759, 1932.

2. J. Ville, "Theorie et Applications de la Notion de Signal Analitique," *Cables et Transmission* 2, No. 1, pp. 61-74, 1948.

3. P. M. Woodward, *Probability and Information Theory with Application to Radar,* Pergamon Press, London, 1953.

4. A. W. Rihaczek, *Principles of High Resolution Radar,* McGraw-Hill, New York, 1969.

5. N. G. DeBruijn, "A Theory of Generalized Functions with Applications to Wigner Distribution and Weyl Correspondence," *Nieuw Arch. Wiskunde* 21, pp. 205-280, 1973.

6. T. A. C. M. Claasen and W. F. G. Mecklenbrauker, "The Wigner Distribution - A Tool for Time-Frequency Signal Analysis," Parts I, II, III, *Philips J. Res.* 35, pp. 217-250, 276-300, 372-389, 1980.

7. G. M. Robbins and T. S. Huang, "Inverse Filtering for Linear Shift-Variant Imaging Systems," *Proc. IEEE* 60, pp. 862-872, July 1972.

8. A. Sawchuk, "Space Invariant Image Restoration by Coordinate Transformations," *J. Opt. Soc. Am.* 64, pp. 138-144, Feb. 1974.

9. H. E. Moses and A. F. Quesada, "The Power Spectrum of the Mellin Transformation with Applications to Scaling of Physical Quantities," *J. Math. Phys.* 15, pp. 748-752, June 1974.

10. H. E. Moses and B. T. Prosser, "Phases of Complex Functions from the Amplitudes of the Functions and the Amplitudes of the Fourier and Mellin Transforms," *J. Opt. Soc. Am.* 73, pp. 1451-1454, Nov. 1983.

11. D. Casasent and D. Psaltis, "Deformation Invariant, Space-Variant Optical Pattern Recognition," pp. 289-356 in *Progress in Optics XVI* (ed. E. Wolf), North-Holand, 1978.

12. C. Braccini, G. Gambardella and A. Grattarola, "Digital Image Processing by Means of Generalized Scale-Invariant Filters," pp. 315-329, in *Issues in Acoustic Signal-Image Processing and Recognition* (ed. C. H. Chen), NATO ASI Series, Springer-Verlag, 1983.

13. R. A. Messner and H. H. Szu, "Simultaneous Image Processing and Feature Extraction for Two-Dimensional Non-Uniform Sensors," *Proc. SPIE* 449, pp. 693-710, Nov. 1983.

14. D. Psaltis, D. Casasent, and A. Sexton, "Optical Signal Processing of Non-Linear Coded Waveforms," *Proc. 1978 IEEE Opt. Comp. Symp.*, pp. 80-85, 1978.

15. C. Braccini, G. Gambardella, "Signal Detection and Estimation Techniques Based on Linear Shift-Variant Filtering and Short-Space Frequency Variant Spectral Analysis," *Proc. of the Workshop Italy-USA on Digital Signal Processing,* pp. 157-170, Portovenere, Italy, Aug. 1981.

16. R. A. Altes, "The Fourier-Mellin Transform and Mammalian Hearing," *J. Acoust. Soc. Am.* 63, No. 1, pp. 174-183, Jan. 1978.

17. D. Malah, "Time-Domain Algorithms for Harmonic Bandwidth Reduction and Time Scaling of Speech Signals," *IEEE Trans. ASSP* ASSP-27, No.2, pp. 121-133, Apr. 1979.

Chapter 2

Background

1. Introduction

Finite energy signals are commonly encountered in many diverse engineering and scientific disciplines - communications, radar, sonar, acoustics, geophysics, optics, biomedical engineering, to name a few. Conventional time or frequency representations of such signals do not explicitly display all the information that is present. In a number of signal processing problems joint time-frequency signal representations reveal more and serve as a better starting point for the analysis and synthesis. Although most of these representations were proposed and defined a long time ago[1-7], only the spectrogram and ambiguity function have found widespread use. More recently, there has been revived interest in others, sparked by the series of papers on Wigner distribution by Claasen and Mecklenbraüker[8]. This has also instigated research into unified characterization and categorization of joint time-frequency signal representations[9-13].

Most of these representations can be classified as being either of the convolution-type (or 'energy-type') or of the correlation-type. Members of the first class display how the signal energy is distributed in time and frequency. Members of the second class display correlation characteristics of the signal in the direction of time and frequency shifts. Since both energy and correlation are bilinear, all representations in these two classes are bilinear too. Recently, two new classes of multi-linear time-frequency signal representations have been proposed[9-11], but they lack the practical appeal of bilinear ones.

2. Bilinear Time-Frequency Signal Representations

A time-frequency representation can be classified as bilinear if it obeys the following "bilinear superposition principle". Let x(t) and y(t) be superpositions of finite energy complex signals:

$$x(t) = \sum_k a_k x_k(t), \qquad y(t) = \sum_k b_k y_k(t) \tag{1}$$

Then, any bilinear joint time-frequency cross-representation $T_{xy}(t,f)$ is expressible as

$$T_{xy}(t,f) = \sum_k \sum_l a_k b_l^* \, T_{x_k y_l}(t,f) \tag{2}$$

where * denotes complex conjugation. Corresponding auto-representation equals the sum of the auto-terms of individual component signals and the cross-terms among each pair of components:

$$T_x(t,f) \equiv T_{xx}(t,f) = \sum_k |a_k|^2 \, T_{x_k}(t,f) + \sum_k \sum_{l \neq k} a_k a_l^* \, T_{x_k x_l}(t,f) \tag{3}$$

A comprehensive theory of bilinear time-frequency signal representations can be given in terms of linear operators[12,13]. As a basis of this theory, four elementary bilinear signal representations are used:

- the time signal product

$$q_{xy}(t,\tau) = x(t+\tau/2)\; y^*(t-\tau/2) \tag{4}$$

- the frequency signal product

$$Q_{xy}(f,\nu) = X(f+\nu/2)\; Y^*(f-\nu/2) \tag{5}$$

where X(f) and Y(f) are Fourier transforms of x(t) and y(t);

- the Wigner distribution (WD)

$$W_{xy}(t,f) = \int_{-\infty}^{\infty} q_{xy}(t,\tau) e^{-j2\pi f \tau} d\tau = \int_{-\infty}^{\infty} Q_{xy}(f,\nu) e^{j2\pi\nu t} d\nu \tag{6}$$

- the ambiguity function (AF)

$$A_{xy}(\tau,\nu) = \int_{-\infty}^{\infty} q_{xy}(t,\tau)e^{-j2\pi\nu t}dt = \int_{-\infty}^{\infty} Q_{xy}(f,\nu)e^{j2\pi f\tau}df \tag{7}$$

From (6) and (7) it follows that the WD and the AF are a two-dimensional Fourier transform pair. It can be shown that any bilinear signal representation can be obtained from the elementary ones by linear transformations:

$$T_{xy}(t,f) = \int_{-\infty}^{\infty}\int_{-\infty}^{\infty} q_{xy}(t',\tau)u_T(t,f;t',\tau)dt'd\tau = \tag{8}$$

$$= \int_{-\infty}^{\infty}\int_{-\infty}^{\infty} Q_{xy}(f',\nu)U_T(t,f;f',\nu)df'd\nu = \tag{9}$$

$$= \int_{-\infty}^{\infty}\int_{-\infty}^{\infty} W_{xy}(t',f')v_T(t,f;t',f')dt'df' = \tag{10}$$

$$= \int_{-\infty}^{\infty}\int_{-\infty}^{\infty} A_{xy}(\tau,\nu)V_T(t,f;\nu,\tau)d\nu d\tau \tag{11}$$

or in more compact operator notation:

$$T = \underline{u}_T q = \underline{U}_T Q = \underline{v}_T W = \underline{V}_T A \tag{12}$$

Consequently, any bilinear time-frequency signal representation is uniquely characterized by the linear operators $\underline{u}_T$,$\underline{U}_T$,$\underline{v}_T$, and $\underline{V}_T$ with kernels u_T,U_T,v_T, and V_T. These kernels, like the elementary bilinear signal representations (4) - (7), are related by one- and two-dimensional Fourier transformations, and only one of them is sufficient to completely specify T. Equations (8) - (12) are convenient starting points for the analysis of the properties of bilinear time-frequency signal representations. Most of these properties can be expressed in terms of simple constraints on the kernels u_T and U_T. These two kernels can be regarded as time and frequency impulse responses of the representations ($T=u_T$ if x and y are impulses, and $T=U_T$ if X and Y are

impulses).

A bilinear time-frequency representation is of the convolution-type if shifts in time and frequency of the signal result in corresponding shifts of the representation[12,13]. Such a representation has impulse responses of the form:

$$u_T(t,f;t',\tau) = \phi_T(t-t',\tau)\, e^{-j2\pi f\tau}, \qquad U_T(t,f;f',\nu) = \Phi_T(f-f',\nu)\, e^{j2\pi t\nu} \quad (13)$$

where ϕ_T and Φ_T define a two-dimensional Fourier transform pair. Special cases are:

- the spectrogram with window w(t) (see Eqs. (4) and (5))

$$\phi_S(t,\tau) = q_{ww}(t+\tau/2,t-\tau/2), \qquad \Phi_S(f,\nu) = Q_{ww}(f-\nu/2,f+\nu/2) \quad (14)$$

- the Rihaczek distribution

$$\phi_R(t,\tau) = \delta(t+\tau/2), \qquad \Phi_R(f,\nu) = \delta(f-\nu/2) \quad (15)$$

- the Wigner distribution

$$\phi_W(t,\tau) = \delta(t), \qquad \Phi_W(f,\nu) = \delta(f) \quad (16)$$

The unique character of the WD is a consequence of its ideally concentrated and symmetric impulse responses. Namely, for this class of representations, the kernel v_T in (10) has to be of the convolution-type:

$$v_T(t,f;t',f') = \rho_T(t-t',f-f') \quad (17)$$

From (10) it follows, then, that all convolution-type representations can be constructed from the WD by performing the two-dimensional convolution:

$$T = \underline{v}_T W = \rho_T * W \quad (18)$$

In particular, v - kernel for the spectrogram $S(t,f)$ is the WD of the window used

$$v_S(t,f;t',f') = W_{ww}(t'-t,f-f') \tag{19}$$

and as a result

$$S(t,f) = \int_{-\infty}^{\infty}\int_{-\infty}^{\infty} W(t',f')W_{ww}(t'-t,f-f')dt'df' \tag{20}$$

So, the spectrogram is obtained by two-dimensional convolution of WD's of the signal and of the window.

The correlation-type bilinear signal representations are defined by the requirement that $T_{xy}(t,0)$ and $T_{xy}(0,f)$ are the cross-correlations of x and y in time and frequency domains, respectively[12]. It can be shown that every such representation is a two-dimensional Fourier transform of some convolution-type representation. The time and frequency impulse responses of these representations are:

$$u_T(t,f;t',\tau)=\psi_T(t,f)\delta(t-\tau)e^{-j2\pi ft'}, \quad U_T(t,f;f',\nu)=\psi_T(t,f)\delta(f-\nu)e^{j2\pi tf} \tag{21}$$

where

$$\psi_T(t,f) = \int_{-\infty}^{\infty} \phi_T(\tau,t)e^{-j2\pi f\tau}\,d\tau = \int_{-\infty}^{\infty} \Phi_T(\nu,f)e^{j2\pi t\nu}\,d\nu. \tag{22}$$

For T to be a proper correlation representation it is required that

$$\psi_T(t,0)=\psi_T(0,f)=1, \tag{23}$$

which is equivalent to the constraint

$$\int_{-\infty}^{\infty} \phi_T(\tau,t)d\tau = \int_{-\infty}^{\infty} \Phi_T(\nu,f)d\nu = 1 \tag{24}$$

that ensures proper energy interpretation of the corresponding convolution-type representation. Substitution of (22) into (8) or (9) yields

$$T_{xy}(t,f) = \psi_T(t,f)\, A_{xy}(t,f). \tag{25}$$

Hence, every correlation-type representation can be derived from the AF by multiplication with the Fourier transform of the impulse response of the corresponding convolution-type representation. This is a consequence of the Fourier transform relationships between the WD and the AF, and between convolution-type and correlation-type representations (see Eq. (18)). The choice $\psi_T(t,f)=1$ yields the symmetric form of the AF (7), while the choice $\psi_T(t,f)=e^{j\pi ft}$ yields the asymmetric form of the AF which is the two-dimensional Fourier transform of the Rihaczek distribution.

Equations (10), (11), (18), (23), together with corresponding expressions for the impulse responses, underscore the unique role that the WD and the AF have among bilinear time-frequency signal representations.

3. The Wigner Distribution (WD)

Historically, this distribution was proposed in 1932 for phase-space description of the relationship between the position and the momentum of a particle in quantum-mechanics[1]. However, it may be defined for any pair of quantities that are related through Fourier transform. Independently, Ville has defined it in 1948[3] as a tool for signal analysis. It took thirty years for his idea to get significant following, and currently the WD is a very active research topic in signal processing.

Following are the properties of the WD that make it useful in signal analysis and linear system characterization. They can be derived from the definition of the WD (6) and from the properties of the Fourier transform[8].

The WD is always real and for a real signal it is an even function of frequency. In the time domain the WD has the same support as the signal, and in the frequency domain it has the support of the Fourier transform of the signal. Shifting the signal in time (or, equivalently, introducing the phase shift in

frequency domain) causes identical displacement of its WD in the time direction. Modulation of the signal by $exp(j2\pi f_o t)$ (or, equivalently, a shift in the frequency domain by f_o) results in a displacement f_o of the WD in the frequency direction. Shifting in time followed by a modulation produces the corresponding displacements of the WD in the time and frequency directions. Multiplication of signals in the time domain yields a one-dimensional convolution of their WD in the frequency direction. The time convolution of two signals results in a one-dimensional convolution of their WD in the time direction.

The volume under the WD is equal to the signal energy.

$$\int_{-\infty}^{\infty}\int_{-\infty}^{\infty} W_x(t,f)dtdf = E_x \tag{26}$$

Projection of the WD onto the time axis is equal to the squared magnitude (instantaneous power) of the signal:

$$|x(t)|^2 = \int_{-\infty}^{\infty} W_x(t,f)df \tag{27}$$

The energy density spectrum can be obtained from the WD as its projection onto the frequency axis:

$$|X(f)|^2 = \int_{-\infty}^{\infty} W_x(t,f)dt \tag{28}$$

Last two equations define marginals of the distribution. The instantaneous frequency, which is meaningfully defined only on the analytic signal associated with a real bandpass signal, is the first local moment in the frequency variable of the WD of that analytic signal:

$$f_i(t) = \frac{\int_{-\infty}^{\infty} f\ W_x(t,f)\ df}{|x(t)|^2} \tag{29}$$

The first local moment of the WD in the time variable is equal to the group delay of the signal:

$$\tau_g(f) = \frac{\int_{-\infty}^{\infty} t\ W_x(t,f)\ dt}{|X(f)|^2} \tag{30}$$

Because of the properties (26) - (30), the WD is sometimes loosely called the "energy density" of the signal in the time-frequency plane. However, since the WD can have negative values, its interpretation as the pointwise energy density is inappropriate. A properly-weighted integral of the WD over a Heisenberg cell ($\Delta t \Delta f = 1/4\pi$, where Δt and Δf are the rms widths in time and frequency of the weighting functions) gives the signal energy in that cell[14]. Only in that sense the WD can be interpreted as the distribution of signal energy in the time-frequency plane.

4. The Ambiguity Function (AF)

Analyzing the radar signal detection problem in early 1950's, Woodward developed the concept of generalized matched-filter/correlator receiver. In order to describe and analyze its operation and the correlation properties of the radar signal, he defined the ambiguity function[4]. Ever since then, it has been widely used in radar and sonar system analysis and design, in communications and, more recently, in optics and pattern recognition. Its usefulness is a natural consequence of the many convenient properties that are discussed next.

In many instances it is preferable to deal with the real-valued squared magnitude of the AF, called the ambiguity surface. From the definition of the AF (7) and the characteristics of the Fourier transform, the following properties of these two representations may be deduced[15-17].

In general, the AF is complex-valued. For purely even or purely odd signals it is real-valued. Moreover, the AF for such signals is equal to the scaled version of their WD. The ambiguity surface is symmetric with respect to the origin of the time-frequency plane where it has its peak:

$$|A_x(\tau,\nu)|^2 \leq |A_x(0,0)|^2 = E_x^2 = [\int_{-\infty}^{\infty} |x(t)|^2\, dt\,]^2 \tag{31}$$

The volume under this surface is independent of the signal shape and is equal to the square of the signal energy:

$$\int_{-\infty}^{\infty}\int_{-\infty}^{\infty} |A_x(\tau,\nu)|^2\, d\tau d\nu = E_x^2 \tag{32}$$

This implies that for a given energy constraint, the peak value and the volume of the ambiguity surface are fixed and only the distribution of that volume may be altered by the change of signal shape.

Time and frequency shifts in the signal introduce a phase factor into the AF, leaving the ambiguity surface unaffected. Similarly, the magnitude of a cross-AF is invariant if both signals are time and frequency shifted by the same amount. If, however, only one of the signals is shifted in time, the phase factor will be introduced whereas the cross-ambiguity surface will be shifted by the corresponding amount in the direction of the delay axis - τ. Modulation (shift in frequency) of only one signal produces a phase factor in the cross-AF and a corresponding shift of the cross-ambiguity surface in the direction of the Doppler axis - ν. These facts demonstrate the shift invariance property of the ambiguity surface. The AF of the product of two signals is equal to the one-dimensional convolution of their individual AF's in the direction of the Doppler axis. The convolution of two signals results in the one-dimensional convolution of their AF's in the direction of the delay axis.

Introducing the quadratic phase factor into the frequency spectrum of the signal (by passing the signal through a dispersive filter) produces a shearing of the AF parallel to the delay axis. Similarly, shearing parallel to the Doppler axis is achieved when a quadratic phase is introduced in the time domain by linear FM. Compression of the time axis of the signal results in the corresponding compression of the delay axis and expansion of the Doppler axis in the AF. By carrying out all three transformations in sequence with suitably selected parameters, a rotation of the original AF may be achieved.

The following important property relates the products of the cross-AF's through the two-dimensional Fourier transform:

$$\int_{-\infty}^{\infty}\int_{-\infty}^{\infty} A_{xy}(t,f)\, A_{uv}^{*}(t,f)\, e^{j2\pi(t\nu-\tau f)}\, dt\, df = A_{xu}(\tau,\nu)\, A_{yv}^{*}(\tau,\nu) \qquad (33)$$

Two special cases of this relation are of interest. If $x=u$ and $y=v$, it follows that the two-dimensional Fourier transform of the cross-ambiguity surface is equal to the product of the individual auto-AF's:

$$\int_{-\infty}^{\infty}\int_{-\infty}^{\infty} |A_{xy}(t,f)|^2 e^{j2\pi(t\nu-\tau f)}\, dt\, df = A_x(\tau,\nu)\, A_y^{*}(\tau,\nu) \qquad (34)$$

Moreover, the auto-ambiguity surface is its own two-dimensional Fourier transform (if x=y above):

$$\int_{-\infty}^{\infty}\int_{-\infty}^{\infty} |A_x(t,f)|^2 e^{j2\pi(t\nu-\tau f)}\, dt\, df = |A_x(\tau,\nu)|^2 \qquad (35)$$

Not all non-negative self-transforming functions (those that satisfy (35)) are ambiguity surfaces. Relation (32) follows from (31) and (35) for $\tau=0$ and $\nu=0$.

5. Applications

Although the WD was introduced into signal processing earlier than the

AF, it has found wide acceptance much later. So, it may be considered as a relatively new tool with still undeveloped range of applications. Revival of interest in the WD in mid-seventies began when it was used to describe the concept of rays in geometrical optics[18-20]. There, the value of WD at some position and in some direction was interpreted as the intensity of a light ray at that point and direction. Projections of the WD give the intensity of the ray and its spectrum.

However, it was the thorough analysis of the WD and its properties by Claasen and Mecklenbraüker[8] that provided the foundation for successful application of this tool in signal processing. Their claim that the WD should be useful for the analysis of linear systems and time-varying and transient signals was soon supported in practice. In acoustics, the WD has been successfully applied to characterization of loudspeakers[21]. It has been used in robotics for image representation and pattern recognition[22,23]. Also, it has been proposed to use the WD as a coding procedure in covert optical communication systems[24]. The WD is especially useful for estimation of signal parameters like instantaneous frequency of the non-stationary, phase-modulated signals that are common in radar, sonar, seismic and bio-medical applications. For example, it has been used for the analysis of bat sonar signals[25], seismic signals[26], and for the estimation of target range and azimuth in array processing[27]. The definition of the WD has also been extended to cover non-stationary harmonizable random signals[28]. This was used then to partition random signals into locally stationary segments[29,30] and to classify such signals according to the degree of non-stationarity[31]. Detection of modulated signals with a specific variation of instantaneous frequency with time has been performed in the WD domain and proven to be optimal[32-34]. Synthesis of a signal from its WD has been also achieved[35,36], which makes possible time-

varying filtering and separation of multi-component signals in the time-frequency plane[37]. Claims have been raised that the WD is also a better speech analysis tool than the short-time Fourier transform, in the sense that it better represents the transient behavior of this signal[38].

Unlike the WD, the AF has been widely used for over three decades and has reached level of maturity in a variety of applications where it is now routinely applied. The AF reflects inherent time and frequency correlation characteristics of the signal. That makes it suitable for use in detection and estimation of radar and sonar signals, especially in high-resolution applications. In this respect, the AF has been widely used to design, evaluate and compare the performance of various radar signals like chirp, uniform pulse trains, pseudo-noise sequences, Barker codes, phase-reversal codes, polyphase codes, and complementary signals[15,16]. It has become a standard tool of the radar system analysts and designers. Moreover, it has found use in spread-spectrum communications[39] and in modeling of time-varying and multipath communication channels[40]. In radio astronomy and geophysics it has been used for exploration of the surface of the heavenly bodies and Earth[42,43]. More recently, the AF has found application in the analysis of optical systems[44] and optical pattern recognition[20,24,45,46].

References

1. E. P. Wigner, "On the Quantum Correction for Thermo-Dynamic Equilibrium," *Phys. Rew.* 40, pp. 749-759, 1932.

2. W. Koenig, H. K. Dunn, and L. Y. Lacy, "The Sound Spectrograph," *J. Acoust. Soc. Am.* 17, pp. 19-49, July 1947.

3. J. Ville, "Theorie et Applications de la Notion de Signal Analitique," *Cables et Transmission* 2, No. 1, pp. 61-74, 1948.

4. P. M. Woodward, *Probability and Information Theory with Application to Radar,* Pergamon Press, London, 1953.

5. L. Cohen, "Generalized Phase-Space Distribution Functions," *J. Math. Phys.* 7, pp. 781-786, 1966.

6. A. W. Rihaczek, "Signal Energy Distribution in Time and Frequency," *IEEE Trans. Info. Theory,* IT-14, pp. 369-374, 1968.

7. B. Escudie, "Representation Temps-Frequence dans L'Analyse et Synthese des Signaux," *6 Congres International de Cybernetique,* pp. 277-299, 1972.

8. T. A. C. M. Claasen and W. F. G. Mecklenbraüker, "The Wigner Distribution - A Tool for Time-Frequency Signal Analysis," Parts I, II, III, *Philips J. Res.* 35, pp. 217-250, 276-300, 372-389, 1980.

9. L. Cohen, "Distributions in Signal Theory," *Proc. ICASSP-84,* pp. 41B.1.1-4, San Diego, Calif., 1984.

10. L. Cohen and T. E. Posch, "Positive Time-Frequency Distribution Functions," *IEEE Trans. ASSP,* ASSP-34, No. 1, pp.31-37, Feb. 1985.

11. L. Cohen and T. E. Posch, "Generalized Ambiguity Functions", Proc. ICASSP-85, pp. 1033-1036., Tampa, Fla., 1985.

12. F. Hlawatsch, "Theory of Bilinear Time-Frequency Signal Representa-

tions," *IEEE ASSP 1984 Dig. Sign. Process. Workshop,* pp. 7.5.1-7.5.2, Chatham, Mass., Oct. 1984.

13. F. Hlawatsch, "Transformation, Inversion and Conversion of Bilinear Signal Representations," *Proc. ICASSP-85,* pp. 1029-1032, Tampa, Fla., 1985.

14. N. G. DeBruijn, "A Theory of Generalized Functions with Applications to Wigner Distribution and Weyl Correspondence," *Nieuw Arch. Wiskunde* 21, pp. 205-280, 1973.

15. D. E. Vakman, *Sophisticated Signals and the Uncertainty Principle in Radar,* Springer-Verlag, New York, 1968.

16. A. W. Rihaczek, *Principles of High Resolution Radar,* McGraw-Hill, New York, 1969.

17. H. L. Van Trees, *Detection, Estimation, and Modulation Theory,* Part III, J. Wiley, New York, 1971.

18. M. J. Bastiaans, "The Wigner Distribution Function Applied to Optical Signals and Systems," *Opt. Comm.* 25, pp. 26-30, 1978.

19. M. J. Bastiaans, "The Wigner Distribution Function and its Application to First Order Optics," *J. Opt. Soc. Am.* 69, pp. 1710-1716, 1979.

20. M. J. Bastiaans, "The Wigner Distribution Function and its Applications to Optics," pp. 292-312 in *Optics in Four Dimensions,* M. A. Machado and L. M. Narducci, eds., Amer. Inst. of Physics, New York, 1981.

21. C. P. Janse and A. J. M. Kaizer, "Time-Frequency Distributions of Loudspeakers: the Application of the Wigner Distribution," *J. Audio Eng. Soc.* 31, No. 4, pp. 198-223, 1983.

22. L. Jacobson and H. Wechsler, "The Wigner Distribution and Its Usefulness for 2-D Image Processing," *Sixth Int. Joint Conf. Pattern Recogn.,*

Munich, W. Germany, Oct. 1982.

23. L. Jacobson and H. Wechsler, "Invariant Image Representation: a Path Toward Solving the Bin Picking Problem" *1984 IEEE Conf. on Robotics*, pp. 190-199, Atlanta, Ga., March 1984.

24. H. H. Szu and J. A. Blodgett, "Wigner Distribution and Ambiguity Function," pp. 355-381 in *Optics in Four Dimensions*, M. A. Machado and L. M. Narducci, eds., Amer. Inst. of Physics, New York, 1981.

25. P. Flandrin and B. Escudie, "An Interpretation of the Pseudo-Wigner-Ville Distribution," *Signal Processing* 6, pp. 27-36, 1984.

26. B. Bouachache, "Wigner-Ville Analysis of Time-Varying Signals: an Application in Seismic Prospecting," *EUSIPCO-83: Second Eur. Assoc. Sig. Proc. Conf.*, Erlangen, W. Germany, Sept. 1983.

27. B. R. Breed and T. E. Posch, "A Range and Azimuth Estimator Based on Forming the Spatial Wigner Distribution," *Proc. ICASSP-84*, pp. 41B.9.1-4, San Diego, Calif., March 1984.

28. W. Martin, "Time-Frequency Analysis of Random Signals," *Proc. ICASSP-82*, pp. 1325-1328, Paris, France, May 1982.

29. P. Flandrin and W. Martin, "Pseudo-Wigner Estimators for the Analysis of Non-Stationary Processes," *IEEE ASSP Spectrum Estimation Workshop II*, Tampa, Fla., Nov. 1983.

30. W. Martin and P. Flandrin, "Analysis of Non-Stationary Processes: Short-Time Periodogram Versus a Pseudo-Wigner Estimator," *EURASIP-83*, pp. 455-458, Elsevier Science Publ., 1983.

31. W. Martin, "Measuring the Degree of Non-Stationarity by Using the Wigner-Ville Spectrum," *Proc. ICASSP-84*, pp. 41B.3.1-4, San Diego, Calif., March 1984.

32. B. Bouachache and F. Rodriguez, "Recognition of Time-Varying Signals in the Time-Frequency Domain by Means of the Wigner Distribution," *Proc. ICASSP-84,* pp. 22.5.1-4, San Diego, Calif., March 1984.

33. B. V. K. V. Kumar and C. W. Carroll, "Performance of Wigner Distribution Function Based Detection Methods," *Opt. Eng.* 23, pp. 732-737, Nov. 1984.

34. S. Kay and G. F. Boudreaux-Bartels, "On the Optimality of the Wigner Distribution for Detection," *Proc. ICASSP-85,* pp. 1017-1020, Tampa, Fla., March 1985.

35. G. F. Boudreaux-Bartels, "Time-Frequency Signal Processing Algorithms: Analysis and Synthesis Using Wigner Distributions," Ph.D. Dissertation, Rice University, Houston, Tex., Dec. 1983.

36. K. B. Yu and S. Cheng, "Signal Synthesis from Wigner Distribution," *Proc. ICASSP-85,* pp. 1037-1040, Tampa, Fla., March 1985.

37. G. F. Boudreaux-Bartels and T. W. Parks, "Signal Estimation Using Modified Wigner Distributions," *Proc. ICASSP-84,* pp. 22.3.1-4, San Diego, Calif., March 1984.

38. D. Chester, F. J. Taylor, and M. Doyle, "Application of the Wigner Distribution to Speech Processing," *IEEE ASSP Spectrum Estimation Workshop II,* pp. 98-102, Tampa, Fla., Nov. 1983.

39. R. A. Scholtz, "The Origin of Spread-Spectrum Communications - Review," *IEEE Commun. R.* 30, pp 822-854, 1982.

40. T. Kailath, "Time-Variant Communication Channels," *IEEE Trans. Info. Theory* IT-9, No. 4, pp. 233-237, Oct. 1963.

41. J. Goldman, "Estimation of a Random Time-Varying Transfer Function," *IEEE Trans. Info. Theory* IT-14, No. 4, pp. 598-599, July 1968.

42. R. Price and P. Green Jr., "Signal Processing in Radar Astronomy - Communication via Fluctuating Multipath Media," Tech. Rept. No. 234, MIT Lincoln Lab, Lexington, Mass., Oct. 1960.

43. R. A. Shuchmann, C. F. Davis, and P. L. Jackson, "Contour Strip Mine Detection and Identification with Imaging Radar," *IEEE Trans. Aer. El. Sys.*, AES-11, 1975.

44. A. Papoulis, "Ambiguity function in Fourier Optics," *J. Opt. Soc. Am.* 64, pp. 779-788, June 1974.

45. J.-P. Guigay, "The Ambiguity Function in Diffraction and Isoplanatic Imaging by Partially Coherent Beams," *Opt. Commun.* 26, pp. 136-138, 1978.

46. H. H. Szu, "Two-Dimensional Optical Processing of One-Dimensional Acoustic Data," *Opt. Eng.* 21, pp. 804-813, 1982.

Chapter 3

Characterization of Ultrasonic Transducers

1. Introduction

The Wigner distribution (WD) [1-4] provides a mean to analyze the spectral and temporal characteristics of linear systems in general. This approach to the linear system analysis reveals in detail how an impulse response is distributed in the time-frequency domain. Indeed, the value of the WD at a given time and frequency can be heuristically related to the signal energy at that time and frequency. Here, the WD is used to study the impulse response of medical ultrasonic transducers. It provides a characterization of ultrasonic transducers that goes well beyond the conventional measures such as the bandwidth and the ring-down (settling) time.

Plots of the WD in the time-frequency plane show the delay and spread of each spectral component of the impulse response; they reveal how the instantaneous frequency and bandwidth vary over the pulse length. These plots display the information contained in the transducers phase-frequency transfer function in the time domain where it can be directly interpreted. If the phase variation in an incident acoustic signal is to be accurately transduced into the electrical output, a transducer should have a constant delay and uniform temporal spread over its entire bandwidth. Typically, this is a requirement in medical ultrasound applications, where the phase of the echo is sometimes used for the determination of the tissue characteristics.

The method of analysis is illustrated using both the simulated and the measured transducer impulse responses. The WD captures all the relevant

information about these impulse responses in a single time-frequency plane picture - both for quantitative calculation and qualitative apperception.

In this chapter, the basic properties of the WD, that make it useful for characterization of linear systems, are discussed. To demonstrate its utility, the WD based analyses of simulated impulse responses of ultrasonic transducers were performed and related to their physical characteristics. The WD's of experimentally measured impulse responses were calculated and used to evaluate several commercial transducers. It is shown that the Wigner distribution provides a convenient and complete single-plot characterization of the transducer filtering action.

2. The Wigner Distribution of Band-Pass Signals

The Wigner distribution $W_x(t,f)$ is a quadratic transformation of a one-dimensional signal $x(t)$. It is defined as [1]

$$W_x(t,f) = \int_{-\infty}^{\infty} x(t+\tau/2)\, x^*(t-\tau/2)\, e^{-j2\pi f\tau} d\tau$$
$$= \int_{-\infty}^{\infty} X(f+\nu/2)\, X^*(f-\nu/2)\, e^{j2\pi t\nu} d\nu \qquad (1)$$

where $X(f)$ is the Fourier transform (FT) of $x(t)$.

The discrete approximation to the WD may be obtained from the signal oversampled by a factor of two through the following sequence of steps [1,2]:

(1) the signal is shifted in one, while its complex conjugate is shifted in the opposite direction by an equal amount, and their products are formed for all possible shifts;

(2) for every value of the time index, the FT of the product is determined with respect to the shift index, and the result is multiplied by two.

Following is a brief review of the WD properties[1,2]. The WD is real, and for a real signal, it is an even function of frequency. In the time domain, the WD has the same support as the signal, and in the frequency domain it has the support of the FT of the signal. Figure 1 shows both perspective and contour plots of the WD of the complex analytic signal corresponding to a Gaussian radio-frequency pulse. Since the analytic signal spectrum is zero for negative frequencies, its WD, having the same support, vanishes there also. Hence, only positive frequencies are depicted. For convenience, therefore, the remaining WD plots will be for the analytic signals corresponding to the given real signals.

The volume under the WD is equal to the signal energy. Projection of the WD on the time axis is equal to the squared magnitude (instantaneous power) of the signal:

$$\int_{-\infty}^{\infty} W_z(t,f)df = |x(t)|^2 \tag{2}$$

The energy density spectrum can be obtained from the Wigner distribution as its projection onto the frequency axis:

$$\int_{-\infty}^{\infty} W_z(t,f)dt = |X(f)|^2 \tag{3}$$

Equations (2) and (3) define the marginals of the WD. The group delay and the instantaneous frequency of the signal can be recovered from the WD. The first local moment in the time variable gives the group delay as

$$\frac{\int_{-\infty}^{\infty} t\ W_z(t,f)dt}{|X(f)|^2} = \tau_g(f) \tag{4}$$

The instantaneous frequency, meaningfully defined only for the analytic signal

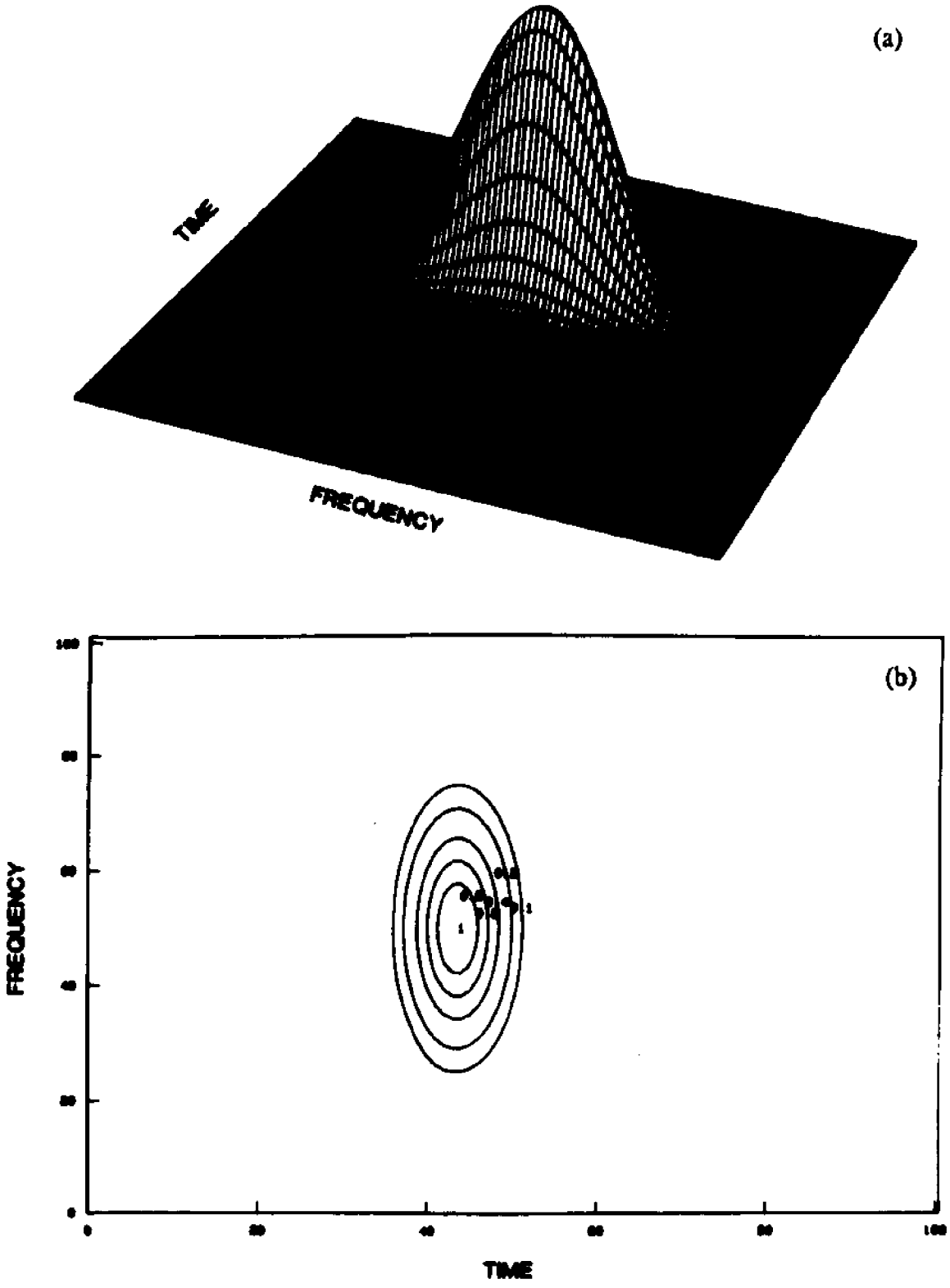

Figure 1. WD perspective and contour plots for the Gaussian pulse.

associated with a real bandpass signal, is the first local moment in the frequency variable of the WD of that analytic signal:

$$\frac{\int_{-\infty}^{\infty} f \; W_z(t,f)df}{|x(t)|^2} = f_i(t) \tag{5}$$

For an illustration of the properties described by Eqs. (2) - (5), refer to Figures 4.b and 4.c that display the marginals and moments of the WD shown on Figure 4.d.

Because of these properties, the WD is sometimes loosely called the "energy density" of the signal in the time-frequency plane. However, since the WD can have negative values, its interpretation as the pointwise energy density is inappropriate. A properly-weighted integral of the WD over a Heisenberg cell ($\Delta f \, \Delta t = 1/4\pi$, where Δf and Δt are rms widths in frequency and time of the weighting function) gives the signal energy in that cell [3]. Only in that sense the WD can be interpreted as the distribution of signal energy in the time-frequency plane.

As a bilinear signal representation, the WD exhibits cross-term effects[4]. For a signal that has two components spaced apart in the time-frequency plane, the Wigner distribution will contain positive auto-terms and an oscillatory cross-term that introduces negative values. The interfering oscillation will always be in the middle between the two auto-terms and perpendicular to a line drawn between their centers. The "spatial frequency" of these oscillations will be proportional to the spacing of these auto-terms. Two signals are disjoint if their WD supports do not overlap. However, the cross-term of disjoint signals gives zero contribution when averaged over the Heisenberg cell[4]. These effects are illustrated in Figure 2, where the WD perspective and contour plots for a signal composed of two complex Gaussian radio-frequency

pulses of different carrier frequencies are shown. One can observe the cross-term that oscillates from positive to negative values with relatively high "spatial frequency". In Figure 3, the pulses are closer, the cross-term partially overlaps the auto-terms, and the number of peaks and dips is smaller. If many components are present in the signal, there will be interfering cross-terms between each pair of corresponding auto-terms, and the WD picture will become obscure. However, for a signal with only a few components, the WD plot may be used for easy simultaneous visualization of such signal properties as the width in frequency, the group delay, the spread in time of different frequency components, the instantaneous frequency, and the energy concentration in the time-frequency plane.

There are several other relevant properties of the WD. For example, shifting the signal in time (or, equivalently, introducing a phase-shift in the f-domain) causes identical displacement of its WD in the time direction. Modulation of the signal by $\exp(j2\pi\alpha t)$ (or, equivalently, a shift in the f-domain by α) results in a displacement α of the WD in the frequency direction. Shifting in time followed by a modulation produces the corresponding displacements of the WD in the time and frequency direction. Multiplication of two signals in the time domain yields a one-dimensional convolution of their WD's in the frequency direction. The time convolution of two signals results in a one-dimensional convolution of their WD's in the time direction. This property makes the WD useful in the analysis of linear, time-invariant systems. The plot of the WD of the impulse response clearly characterizes the filtering action of the system. It identifies, in a qualitative manner, how much the individual frequency components of the input signal will be attenuated, delayed and spread in time. This time-spread information is not available in any other commonly used characterizations of linear, time-invariant systems. It is this

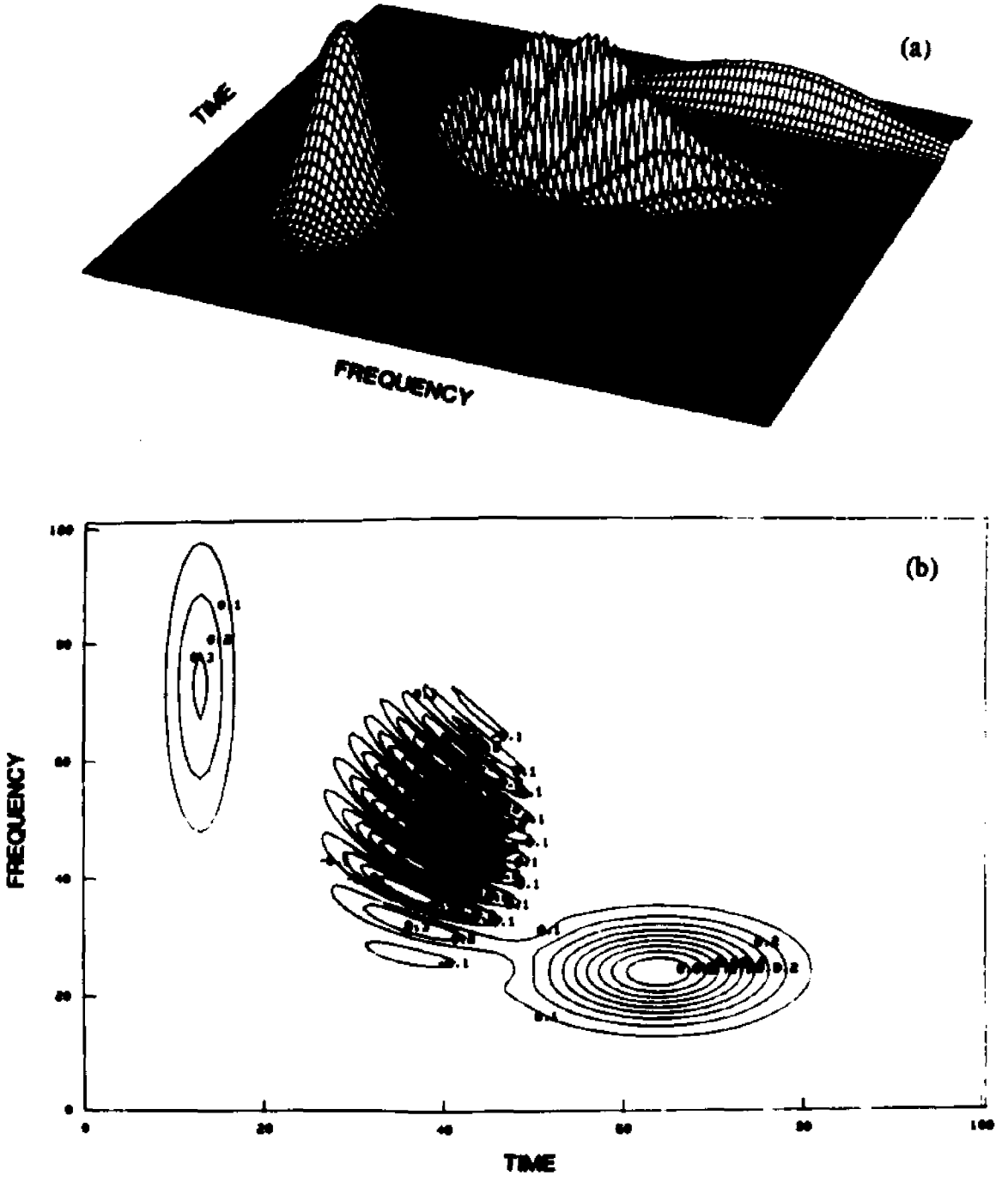

Figure 2. WD perspective and contour plots for two Gaussian pulses spaced apart in time and frequency. The oscillatory region in the middle illustrates the effect of interfering cross-terms.

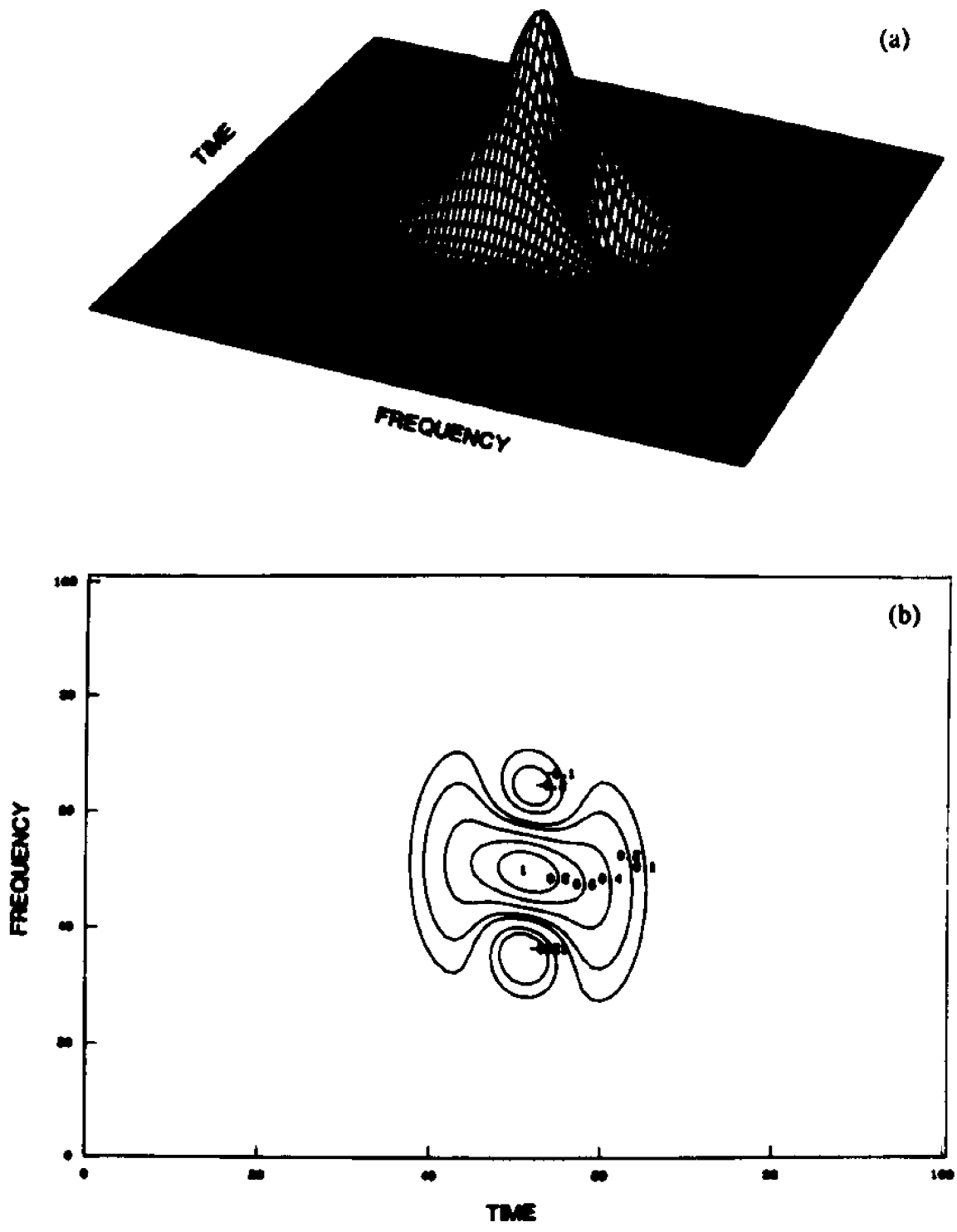

Figure 3. WD perspective and contour plots for two Gaussian pulses that are close in time and frequency. Notice how the cross-terms and auto-terms overlap obscuring the essential simplicity of the signal.

property that makes the WD especially convenient for characterization of ultrasonic transducers as linear filters.

3. Transducer Simulations

This section presents a WD analysis of simulated transducer impulse responses. The examples will show how the WD graphically depicts the essential features of the behavior of ultrasonic transducers. The simulations were done with an equivalent circuit implementation[5,6] of the one-dimensional Mason model for a piezoelectric transducer [7]. This implementation, an enhancement of the one developed at Stanford University [8,9], allows the specification of a complex transducer design, including electrical and mechanical losses in the piezoelectric, lossy matching layers, an electrical matching circuit, etc. Moreover, the impulse response can be optimized by varying the matching network components and the thickness and the impedance of the acoustic matching layers. All computer simulations used a nominal center frequency of 2.25 MHz and the piezoelectric materials parameters for the lead zirconate titanate PZT5A.

Figure 4.a shows the time-domain impulse response of a transducer with a quarter-wave thick matching layer whose acoustic impedance is chosen according to the cube-root rule[10] (cube of the matching layer acoustic impedance is equal to the product of the acoustic impedance of the transducer and the square of the acoustic load impedance). No electric matching network is introduced although the echo is band limited to twice the center frequency. This is a reasonable, though clearly not optimal, design; it is a "strawman" for contrasting improved designs. Figure 4.d shows the WD of this signal. Squared envelope and instantaneous frequency of this impulse response waveform are shown in Figure 4.b, and its spectrum and group delay in Figure 4.c. The

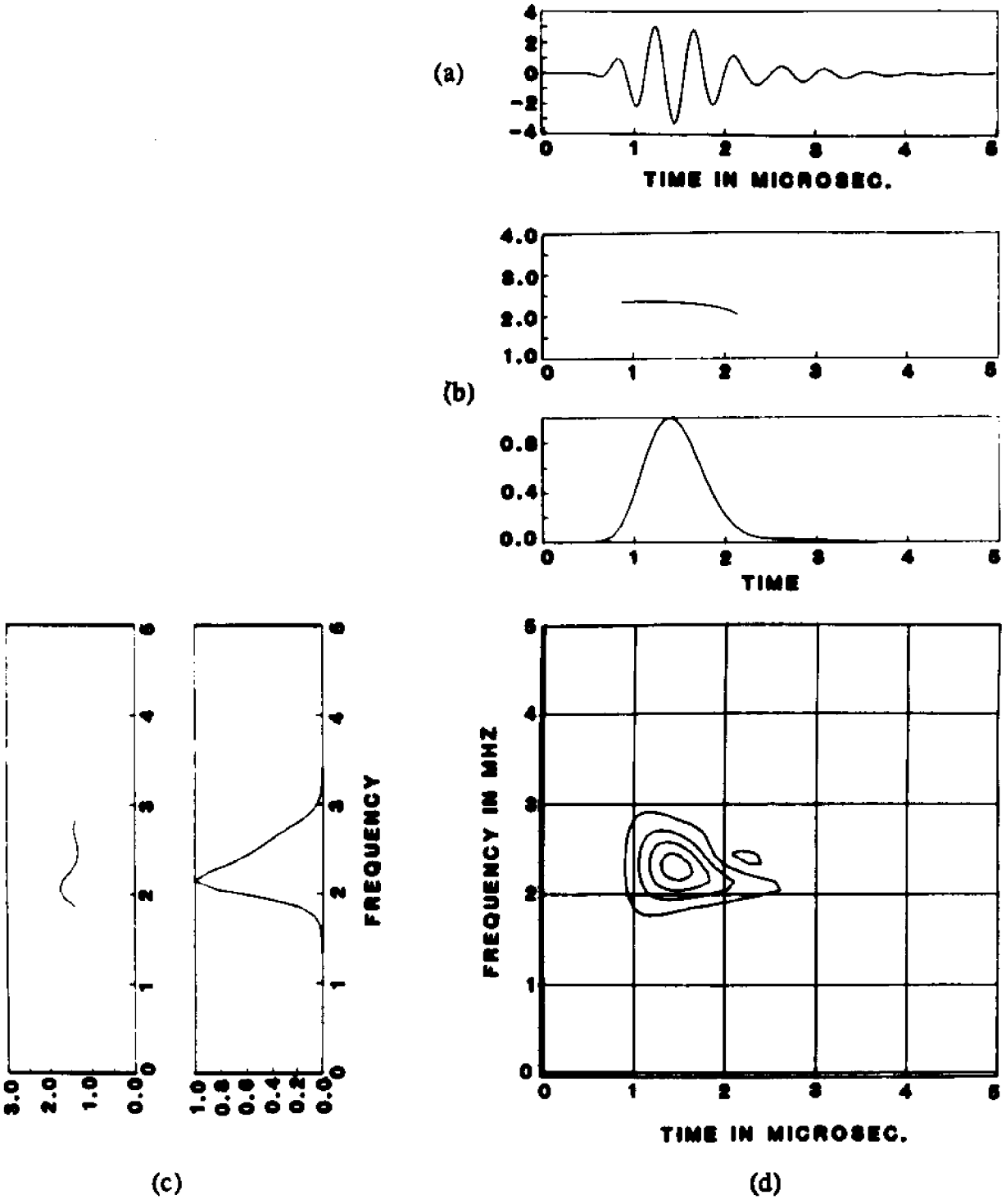

Figure 4. Analysis of the simulated impulse response of a transducer with a quarter-wave acoustical matching layer but no electric matching: (a) the time domain signal, (b) its envelope and instantaneous frequency, (c) its spectrum and group delay, and (d) a contour plot of its WD.

essential features of this impulse response are immediately apparent. Namely, while all the frequencies within the transducer bandwidth appear with the same initial delay, the low frequencies alone persist producing the long ring-down time. The persistence of the lower frequencies causes a shift in the instantaneous frequency - or chirp - over the duration of the pulse. Both aspects can be extracted separately from the frequency dependence of the group delay and from the time dependence of the instantaneous frequency, shown in Figures 4.b and 4.c. However, the WD plot thrusts them forward in a single picture. In addition, this plot displays how individual frequency components in the ultrasonic echo are distorted in passing through the transducer. None of the conventional characterizations describes the spreading of individual frequency components in transmission through the linear system, as the WD does. The transducer acts as a filter, and plot in Figure 4.d implies that, in both transmission and reception, the low-frequency components of the ultrasonic signal are delayed and spread more than the medium- and high-frequency ones. These are significant aspects of a transducer's performance, since such a transducer can introduce spurious frequency modulation in a medical ultrasound echo.

Figure 5.a shows the Wigner domain response of the same transducer incorporating, however, an optimized electrical matching network. This plot shows at a glance the improved performance. The bandwidth is wider, the pulse shortened and the chirp negligible. One salient feature of quarter-wave matching layers becomes prominent: they match optimally only at the center frequency. The high and low frequencies are spread more in time due to the "ears" shown in Figure 5.a. Optimizing the thickness and acoustic impedance of the matching layer will eliminate those "ears." Figure 5.b shows the impulse response from just such a fully optimized transducer. The Wigner

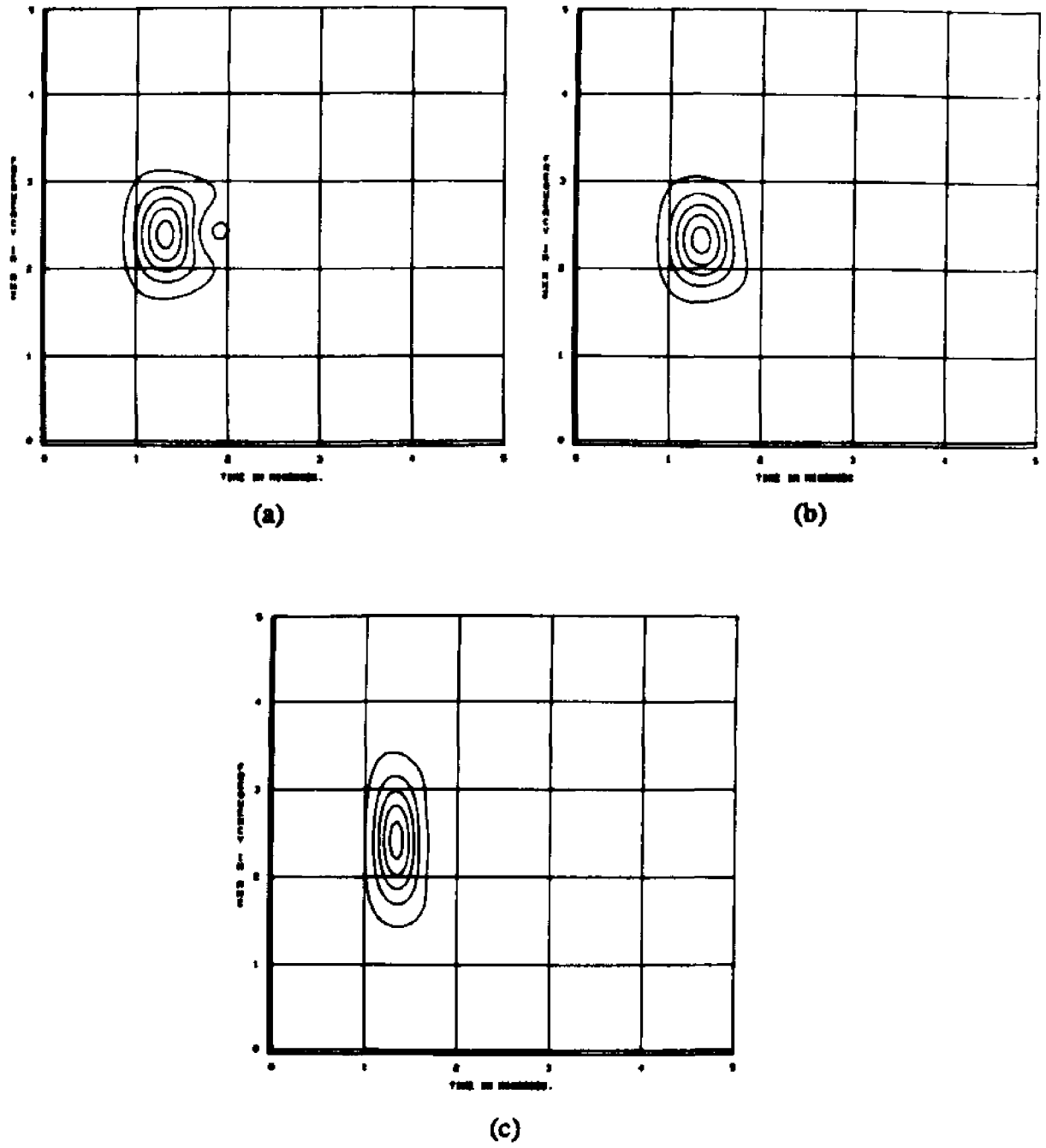

Figure 5. Contour plots of the WD's of simulated transducer impulse responses: (a) air-backed, quarter wave acoustic matching and optimized electric matching, (b) air-backed, optimized acoustic and electric matching, (c) matched backing, optimized acoustic and electric matching.

plot shows a nearly Gaussian-pulse character: symmetric in both time and frequency and compact in the time-frequency domain. Further improvement, broader bandwidth and shorter ring down, can be achieved - at the expense of sensitivity - by introducing a heavy backing. Figure 5.c shows how the response is stretched in frequency and squeezed in time for a fully optimized transducer with a matched backing. The area the signal occupies in the time-frequency domain cannot be reduced appreciably, but it can be squeezed into a different shape.

These examples show how the essential features of a transducer design can be perceived in a single WD plot of the impulse response.

4. Transducer Measurements

This section presents a WD analysis of three 3.5 MHz single-element commercial transducers. Their impulse response was measured in a water tank by recording the echo off a steel block in the focal plane. The transducers were driven with a Metrotek MP203 pulser which, when loaded with a 50 ohm resistor, produced voltage spikes whose amplitude spectrum was flat to within 1 dB up to 10 MHz. A Metrotek MR101 Receiver followed by a Metrotek MG701 Gate passed the echo to an HP5180A Waveform Recorder where it was digitized at 20 MHz sampling frequency.

Figures 6.a and 6.b show the WD of the impulse response for two highly sensitive transducers. According to the manufacturer, these transducers represent single and double matching layer designs, respectively. In Figure 6.a, the single matching layer design exhibits the characteristic "ears" seen in the simulation of a quarter-wave matched transducer above (Figure 5.a). In this case, however, the low frequencies are spread even more in time, producing a distinctive chirp over the pulse length. The WD of the two matching

layer design (Figure 6.b) is much broader in frequency and somewhat narrower in time. Again we see the low frequencies are delayed and spread out into a tail which introduces a significant chirp over the pulse length. The tilted orientation of the Wigner density in the time-frequency plane explains why the ring-down time of this transducer is almost as long as the ring-down time in the previous example, even though its bandwidth is much wider. Such tilts in the WD reveal a transducer which does not make optimal use of its bandwidth to produce shorter pulses.

Figure 6.c shows the time-frequency plot of a much less sensitive transducer; this suggests that the transducer has a backing that introduces damping. In this case, the bandwidth is large and the characteristic "ears" of quarter-wave matching appear - but are balanced in duration. This pulse exhibits negligible chirp.

In these three cases we see how the WD of the transducer's impulse response captures graphically the interrelationship between the frequency-dependent delay and time-dependent instantaneous frequency. In particular, a frequency dependence in the time-delay or time-spread modifies the evolution of the instantaneous frequency of the ultrasonic echo. A transducer should have a constant delay and uniform temporal spread over its entire bandwidth, if the phase variation information in an incident acoustic signal is to be accurately transduced into the electrical output.

5. Conclusions

The WD of a transducer's impulse response shows the essential transducer performance characteristics - and their interrelationships - in a single plot. It also provides additional information that is unavailable in more common characterizations - the spreading of individual frequency components of the signal

as it passes through the transducer. Therefore, the WD is a useful tool for characterization and evaluation of ultrasonic transducers. More generally, this is also true for any linear shift-invariant system.

References

1. T. A. C. M. Claasen and W. F. G. Mecklenbrauker, "The Wigner distribution - a tool for time-frequency signal analysis," *Philips J. Res.* 35, pp. 217-250, 276- 300, 372-389 (1980).

2. C. P. Janse and A. J. M. Kaizer, "Time-frequency distributions of loudspeakers: the application of the Wigner distribution" *J. Audio Eng. Soc.* 31, No. 4 (1983).

3. N. G. de Bruijn, "Uncertainty principles in Fourier analysis," in *Inequalities,* O. Shisha (ed.), Academic Press, pp. 57-71 (1967).

4. F. Hlawatsch, "Interference Terms in the Wigner Distribution," *Proc. Intl. Conf. Digital Signal Processing - 84,* North-Holland, pp. 363-367, (1984).

5. R. Krimholtz, D. Leedom and G. Matthaei, "New equivalent circuits for elementary piezoelectric transducers" *Electron. Lett.* 6, p. 398 (1970).

6. D. Leedom, R. Krimholtz, and G. Matthaei, "Equivalent circuits for transducers having arbitrary even- or odd-symmetry piezoelectric excitation", *IEEE Trans. Sonics Ultrasonics,* vol. SU-18, p. 128 (1971).

7. W. P. Mason, *Electromechanical Transducers and Wave Filters,* Second Edition, van Nostrand-Reinhold, Princeton, New Jersey, 1948.

8. A. R. Selfridge, "The Design and Fabrication of Ultrasonic Transducers and Transducer Arrays," Ph.D. Thesis, Stanford University, July 1982.

9. A. R. Selfridge, R. Baer, B. T. Khuri-Yakub and G. S. Kino, "Computer-Optimized Design of Quarter-Wave Acoustic Matching and Electrical Matching Networks for Acoustic Transducers," *Proc. 1981 IEEE Ultrasonics Symposium* 644 (1981).

10. C. S. DeSilets, J. D. Fraser, and G. S. Kino, "The Design of Efficient

Broadband Piezoelectric Transducers," *IEEE Trans. Sonics Ultrasonics*, vol. SU-25, p. 115 (1978).

Chapter 4

Scale-Invariant Wigner Distribution and Ambiguity Functions

1. Introduction

The conventional Wigner distribution (WD) and the ambiguity function (AF) belong to a class of two-dimensional (2-D) representations of one-dimensional signals. These 2-D functions encode important physical information about the signal. Since WD's projection on the frequency axis is the energy spectrum and its projection on the spatial (or time) axis is the local (or instantaneous) power of the signal[1,2], the WD may be viewed as a local frequency spectrum of the signal. On the other hand, the AF is a correlation function in Doppler and space (or time) shifts[3]. The two representations are not independent; they form a 2-D Fourier transform pair[1]. Both signal descriptions have a number of optical implementations (see Ref.4 for references).

An essential feature of these representations is their invariance to shifts in the signal. This property makes them appropriate for analysis and processing of signals in linear shift-invariant systems. However, there are many linear shift-variant optical and electronic systems with scale-invariance rather than shift-invariance as a desired property. Such systems, for example, are of interest whenever the detection or estimation of signals of unknown size has to be performed. In these applications, it is required that linear scaling of input signals has either no effect at all on the processing output, or gives rise to a shift in the processing output, or results in a linear scaling of that output. Inputs and outputs of such systems are often related through integral

transformations of the so called scale-convolution or scale-correlation type. An appropriate tool for the analysis of such systems is the Mellin transform which in this case plays the same role as does the Fourier transform in the case of linear shift-invariant systems[5]. A number of applications of scale-invariant signal processing techniques have been reported: in the restoration of images with spatially-variant degradations[6,7], in spectral analysis[8] and signal recovery[9], in the deformation invariant and scale-independent pattern recognition[10-12], in Doppler signal processing[13], in signal detection and estimation[14], in speech analysis[15], and in speech bandwidth compression and word recognition[16].

New two-dimensional signal representations are proposed here to extend the utility of WD and AF to scale-invariant systems. It is expected that these signal processing tools will open new possibilities for scale-invariant processing and characterization of not only one-dimensional but also two-dimensional signals and systems. The definition and the properties of the Mellin transform are reviewed in Section 2. This transform plays the central role because of its scale-invariant properties. In Sections 3 and 4, the scale-invariant Wigner distribution (SIWD) and the ambiguity function (SIAF) are defined, their properties are discussed, and the relationship between the two is revealed. The two representations are related to two-dimensional signals and systems in Sect. 5. It is shown how a two-dimensional system with circular symmetry and with a point-spread function which is a function of the radial variable only, can be characterized with SIWD and SIAF. Also, the two-dimensional signals that are separable into a product of radial and angular components can be analyzed via SIWD and SIAF in the radial direction and via WD and AF in the angular direction. This is shown to be true even in the general case using the circular harmonic expansion of a two-dimensional signal. Following this

discussion, optical implementations of SIWD and SIAF are proposed in Sect. 6, and a number of examples are given in Sect. 7. Finally, in Sect. 8, the implications of scale-invariance of these representations are summarized and are related to potential applications.

2. The Mellin Transform (MT)

For the given signal f(x), existing on the positive real axis $x \geq 0$, the Mellin transform is defined as[17,18]

$$F(p) = \int_0^\infty f(x)\, x^{p-1}\, dx \tag{1}$$

where p is a complex variable taking values from the region of convergence of the above integral. This transform has recently received attention in optics mainly because of its scale-invariant properties[6-14]. Its inverse is found to be[17,18]

$$f(x) = \frac{1}{2\pi j} \int_{c-j\infty}^{c+j\infty} F(p)\, x^{-p}\, dp \tag{2}$$

where c is chosen so that the line of integration lies in the region of convergence of the integral (1) in the complex p-plane. Properties of this transform pair are well documented in the literature[17,18].

For the purposes of the present discussion, however, it is advantageous to consider a Mellin transform evaluated on the imaginary axis $p = -js$:

$$\underline{F}(s) = \int_0^\infty f(x)\, x^{-j2\pi s-1}\, dx \tag{3}$$

$$f(x) = \frac{1}{2\pi} \int_{-\infty}^{\infty} \underline{F}(s)\, x^{-j2\pi s}\, ds \tag{4}$$

This form of the Mellin transform pair will exist if the integral (1) exists and the imaginary axis is in its region of convergence. If the change of variables

$x=e^t$ is made in (3), it follows that the Mellin transform of the imaginary argument equals the Fourier transform of the distorted function $f(e^t)$:

$$\underline{F}(s) = \int_{-\infty}^{\infty} f(e^t)\, e^{-j2\pi st}\, ds = F\{f(e^t)\} \tag{5}$$

Therefore, the integral (3) will exist and the integral (4) will converge in the least square sense if $f(e^t)$ is square-integrable, or, alternatively, if

$$\int_0^{\infty} |f(x)|^2 \frac{dx}{x} < \infty \tag{6}$$

It will be assumed in the rest of this chapter that these conditions are true for all signals of interest, and the terms Mellin transform (MT) and inverse Mellin transform will refer to Eqs. (3) and (4).

Many of the properties of the Mellin transform of imaginary argument follow from the orthogonality relations of its kernels[17,18]:

$$\int_0^{\infty} x^{j2\pi s} x^{-j2\pi\sigma-1} dx = \delta(s-\sigma) \tag{7}$$

$$\int_{-\infty}^{\infty} x^{j2\pi s} \gamma^{-j2\pi s-1} ds = \delta(x-\gamma) \tag{8}$$

Some basic properties of the MT, defined in Eq. (3), will be outlined here for reference purposes. The 'Parseval relation' for the MT is

$$\int_0^{\infty} f_1(x) f_2^*(x) \frac{dx}{x} = \int_{-\infty}^{\infty} \underline{F}_1(s) \underline{F}_2^* ds \tag{9}$$

Signal scaling results in a phase shift in the MT domain:

$$g(x) = f(ax) \quad \leftrightarrow \quad \underline{G}(s) = a^{j2\pi s} \underline{F}(s) \tag{10}$$

Complex modulation of the signal causes a shift in the MT domain:

$$g(x) = x^{-j2\pi\sigma} f(x) \quad \leftrightarrow \quad \underline{G}(s) = \underline{F}(s+\sigma) \tag{11}$$

Complex conjugation and change of sign have the following effects:

$$f^*(x) \leftrightarrow \underline{F}^*(-s) \tag{12}$$
$$f(x^{-1}) \leftrightarrow \underline{F}(-s) \tag{13}$$
$$f^*(x^{-1}) \leftrightarrow \underline{F}^*(s) \tag{14}$$

If f(x) is real, then $\underline{F}^*(s)=\underline{F}(-s)$. If $\underline{F}(s)$ is real, then $f^*(x)=f(x^{-1})$. The MT of the product of signals is the linear convolution of individual MT's:

$$g(x) = f_1(x)\, f_2(x) \quad \leftrightarrow \quad G(s) = \underline{F}_1(s) * \underline{F}_2(s) \tag{15}$$

where * denotes convolution. The following property is very useful for the analysis of scale invariant systems. It states that the scale convolution of two signals, defined as

$$g(x) = \int_0^\infty f_1(y) f_2(x/y) \frac{dy}{y} = f_1(x) \otimes f_2(x) \tag{16}$$

has MT equal to the product of individual MT's:

$$\underline{G}(s) = \underline{F}_1(s)\, \underline{F}_2(s) \tag{17}$$

There are many problems in physics and engineering where the scale convolution integral (16) appears, and in such cases MT is an appropriate tool for their solution[17,18].

The next property finds its application in scale-invariant pattern recognition. The MT of the scale correlation of two signals, defined as

$$\underline{R}_{12}(\eta) = \int_0^\infty f_1(x) f_2^*(x/\eta) \frac{dx}{x} = f_1(\eta) \oplus f_2(\eta) \tag{18}$$

is equal to

$$\underline{S}_{12}(s) = \underline{F}_1(s)\, \underline{F}_2^*(s) \tag{19}$$

The MT of the scale autocorrelation function, $\underline{S}_{11}(s)$, is called the Mellin "power" spectrum[8].

3. Scale-Invariant Wigner Distribution

The auto-Wigner distribution $W_f(x,u)$ is a quadratic transformation that is invariant to shifts in space and spatial frequency of a one-dimensional signal $f(x)$. This is a direct consequence of its definition

$$W_f(x,u) = \int_{-\infty}^{\infty} f(x+\frac{\xi}{2}) f^*(x-\frac{\xi}{2}) e^{-j2\pi u\xi} d\xi$$
$$= \int_{-\infty}^{\infty} F(u+\frac{\eta}{2}) F^*(u-\frac{\eta}{2}) e^{j2\pi x\eta} d\eta \qquad (20)$$

where $F(u)$ is the Fourier transform (FT) of $f(x)$:

$$F(u) = \int_{-\infty}^{\infty} f(x) e^{-j2\pi ux} dx \qquad (21)$$

The WD is obtained through the following sequence of steps:

(1) the signal is shifted in one, while its complex conjugate is shifted in the opposite direction by an equal amount, and their products are formed for all possible shifts;

(2) for every value of the spatial variable, the FT of the product is determined with respect to the shift variable.

It is the shift, performed in the first step, that causes the WD to be shift-invariant. Therefore, to construct a SIWD, in the first step, a scaling rather than a shifting operation should be performed. In the second step, the FT should be replaced by the MT. Consequently, the cross-SIWD of two signals $f_1(x)$, $f_2(x)$ is defined as:

$$\underline{W}_{12}(x,s) = \int_0^{\infty} f_1(\gamma^{1/2}x) f_2^*(\gamma^{-1/2}x) \gamma^{-j2\pi s-1} d\gamma \qquad (22)$$

With the change of variable $\gamma = e^{\lambda}$, an expression involving the FT is obtained:

$$\underline{W}_{12}(x,s) = \int_{-\infty}^{\infty} f_1(e^{\lambda/2}x) f_2^*(e^{-\lambda/2}x) e^{-j2\pi s\lambda} d\lambda \qquad (23)$$

where λ is an exponential scaling variable. Therefore, the SIWD can be obtained if the shifting and the Fourier transform in the aforementioned two-step procedure, are replaced by the linear scaling and the MT (as in (22)), or by the exponential scaling and the FT (as in (23)). With the help of the orthogonality relations for the MT kernels Eqs. (7) and (8), an alternative expression for the SIWD may be derived:

$$\underline{W}_{12}(x,s) = \int_{-\infty}^{\infty} \underline{F}_1(s+\frac{\sigma}{2})\underline{F}_2^*(s-\frac{\sigma}{2})x^{j2\pi s}\,d\sigma \tag{24}$$

This equation is analogous to the second part of (20) with the kernel of the inverse FT replaced by the kernel of the inverse MT.

Using the definition of the scale-invariant WD, the properties of the MT, and the ortnogonality relationships for the kernels of the MT, the following SIWD properties can be derived:

1) The scale-invariant auto-WD is real. For a real signal, it is also an even function of s. Moreover,

$$\underline{W}_{12}^*(x,s)=\underline{W}_{21}(x,s) \tag{25}$$

2) SIWD is bilinear. Namely, if

$$g(x) = f_1(x)+f_2(x), \quad h(x) = f_3(x)+f_4(x)$$

then

$$\underline{W}_{gh} = \underline{W}_{13}+\underline{W}_{14}+\underline{W}_{23}+\underline{W}_{24} \tag{26}$$

3) In the x-domain, scale-invariant WD has the same support as the signal, and in the s-domain, the same support as the MT of the signal.

4) Scaling in space (or, equivalently, phase-shift in s-domain) of both signals causes the same scaling of $\underline{W}$ in the space dimension. That is, if

$$g(x) = f_1(e^{\mu}x), \qquad h(x) = f_2(e^{\mu}x)$$

or, equivalently,

$$\underline{G}(s) = e^{j2\pi\mu s}\underline{F}_1(s), \qquad \underline{H}(s) = e^{j2\pi\mu s}\underline{F}_2(s),$$

then

$$\underline{W}_{gh}(x,s) = \underline{W}_{12}(e^{\mu}x,s) \tag{27}$$

5) Modulation in space by $x^{j2\pi\alpha}$ (or, equivalently, shift in the s-domain by α) of both signals results in the shift of $\underline{W}$ in the s-direction by α. That is, if

$$g(x) = x^{j2\pi\alpha}f_1(x), \qquad h(x) = x^{j2\pi\alpha}f_2(x)$$

or, equivalently,

$$\underline{G}(s) = \underline{F}_1(s-\alpha), \qquad \underline{H}(s) = \underline{F}_2(s-\alpha)$$

then

$$\underline{W}_{gh}(x,s) = \underline{W}_{12}(x,s-\alpha) \tag{28}$$

6) Scaling followed by modulation produces corresponding scaling of $\underline{W}$ in space and shift in s-domain. If

$$g(x) = x^{j2\pi\alpha}f_1(e^{\mu}x), \qquad h(x) = x^{j2\pi\alpha}f_2(e^{\mu}x)$$

then

$$\underline{W}_{gh}(x,s) = \underline{W}_{12}(e^{\mu}x,s-\alpha) \tag{29}$$

7) Taking the inverse Fourier transform of (23), or inverse MT of (22), and changing variables yields

$$\begin{aligned} f_1(x_1)f_2^*(x_2) &= \int_{-\infty}^{\infty} \underline{W}_{12}(\sqrt{x_1x_2},s)e^{j2\pi s\ln(x_1/x_2)}ds \\ &= \int_{-\infty}^{\infty} \underline{W}_{12}(\sqrt{x_1x_2},s)(x_1/x_2)^{j2\pi s}ds \end{aligned} \tag{30}$$

For $x_1=x_2=x$:

$$f_1(x)f_2^*(x) = \int_{-\infty}^{\infty} \underline{W}_{12}(x,s)ds \tag{31}$$

In the case of the scale-invariant auto-WD this reduces to

$$|f(x)|^2 = \int_{-\infty}^{\infty} \underline{W}_f(x,s)ds. \tag{32}$$

Eq. (32) can be used to extract the signal envelope. Integrating this expression over x yields the signal energy:

$$E = \int_0^{\infty} |f(x)|^2 dx = \int_0^{\infty}\int_{-\infty}^{\infty} \underline{W}_f(x,s)ds\ dx \tag{33}$$

If, on the other hand, $x_1=x$, $x_2=1$:

$$f_1(x)f_2^*(1) = \int_{-\infty}^{\infty} \underline{W}_{12}(\sqrt{x},s)x^{j2\pi s}\,ds. \tag{34}$$

Eq. (34) allows the signal $f_1(x)$ to be recovered within a complex non-zero multiplying constant from its scale-invariant WD at $\sqrt{x}$ using the inverse MT.

8) Applying MT on (24) and changing variables produces

$$\underline{F}_1(s_1)\underline{F}_2^*(s_2) = \int_0^{\infty} \underline{W}_{12}(x,\frac{s_1+s_2}{2})x^{-j2\pi(s_1-s_2)-1}dx \tag{35}$$

If $s_1=s_2=s$, then

$$\underline{F}_1(s)\underline{F}_2^*(s) = \int_0^{\infty} \underline{W}_{12}(x,s)\frac{dx}{x} \tag{36}$$

Expression on the left side of this equation is the MT of one form of the scale correlation function, Eq.(18). The Mellin spectrum, i.e. MT of the scale autocorrelation function, can be obtained from the scale-invariant

auto-WD as:

$$|\underline{F}(s)|^2 = \int_0^\infty \underline{W}_f(x,s)\frac{dx}{x} \tag{37}$$

Setting $s_1=s$, $s_2=0$ an inversion formula for the MT of the signal can be derived:

$$\underline{F}_1(s)\underline{F}_2^*(0) = \int_0^\infty \underline{W}_{12}(x,\frac{s}{2})x^{-j2\pi s-1}dx \tag{38}$$

9) Scale convolution in x-domain results in one-dimensional scale convolution of $\underline{W}$s in the direction of x axis. Let

$$g(x) = \int_0^\infty f_1(y)f_2(x/y)\frac{dy}{y} = f_1(x) \otimes f_2(x) \tag{39}$$

$$h(x) = \int_0^\infty f_3(y)f_4(x/y)\frac{dy}{y} = f_3(x) \otimes f_4(x) \tag{40}$$

Then

$$\underline{W}_{gh}(x,s) = \int_0^\infty \underline{W}_{12}(y,s)\underline{W}_{34}(x/y,s)\frac{dy}{y} = \underline{W}_{12}(x,s) \otimes_x \underline{W}_{34}(x,s) \tag{41}$$

10) Multiplication in x-domain yields one-dimensional linear convolution of $\underline{W}$s in the direction of s axis. If

$$g(x) = f_1(x)\, f_2(x), \qquad h(x) = f_3(x)\, f_4(x)$$

then

$$\underline{W}_{gh}(x,s) = \int_{-\infty}^\infty \underline{W}_{12}(x,\sigma)\underline{W}_{34}(x,s-\sigma)d\sigma = \underline{W}_{12}(x,s) *_s \underline{W}_{34}(x,s) \tag{42}$$

11) The first local moment of scale-invariant auto-WD in the s variable is

$$\frac{\int_{-\infty}^\infty s\underline{W}_f(x,s)ds}{\int_{-\infty}^\infty \underline{W}_f(x,s)ds} = x\ \mathrm{Im}\frac{f'(x)}{f(x)} \tag{43}$$

where $f'(x)$ is the first derivative of $f(x)$. If f(x) is analytic signal, Eq. (43) may be used to recover the local spatial frequency of the signal at a point.

4. Scale-Invariant Ambiguity Function

The radar ambiguity function (AF) is a correlation function in space shift and spatial frequency shift. It is defined in its symmetrical form[3] as:

$$A_f(\eta,\xi)=\int_{-\infty}^{\infty} f(x+\frac{\xi}{2})f^*(x-\frac{\xi}{2})e^{-j2\pi x\eta}dx=\int_{-\infty}^{\infty} F(u+\frac{\eta}{2})F^*(u-\frac{\eta}{2})e^{j2\pi u\xi}du \quad (44)$$

Since shifts in space and spatial frequency introduce only an additional phase factor in $A_f(\eta,\xi)$, the magnitude of the AF is shift-invariant. For the cross-AF, shifting of one signal with respect to the other results in a displacement of the correlation peak in η,ξ plane by the amount equal to the shifts. However, the shape of the magnitude of the cross-AF remains invariant. The AF is obtained through a sequence of similar steps as the WD. The only difference is that the FT of the product is performed with respect to the reference rather than the shift coordinate. The SIAF can be constructed by transforming the cross-product, used in the definition of the SIWD, with respect to the reference coordinate x. The MT as in Eq. (22) must be used, since x is a linear and not an exponential argument of f. Hence, the cross-SIAF is defined as

$$\underline{A}_{12}(\sigma,\lambda) = \int_0^{\infty} f_1(e^{\lambda/2}x)f_2^*(e^{-\lambda/2}x)x^{-j2\pi\sigma-1}dx \quad (45)$$

This expression can be transformed, by a change of variables $x=e^y$, into a more suitable form

$$\underline{A}_{12}(\sigma,\lambda) = \int_{-\infty}^{\infty} f_1(e^{y+\lambda/2})f_2^*(e^{y-\lambda/2})e^{-j2\pi\sigma y}dy \quad (46)$$

The following alternative representation of the SIAF, that also relies on the use of FT, may be obtained:

$$\underline{A}_{12}(\sigma,\lambda) = \int_{-\infty}^{\infty} \underline{F}_1(s+\frac{\sigma}{2})\underline{F}_2^*(s-\frac{\sigma}{2})e^{j2\pi\lambda s}\,ds \tag{47}$$

From the orthogonality relationships for kernels of the MT and of the FT, and from the definitions of the SIWD and of the SIAF, it follows that these new functions are related as

$$\begin{aligned}\underline{A}_{12}(\sigma,\lambda) &= \int_{-\infty}^{\infty}\int_{0}^{\infty} \underline{W}_{12}(x,s)e^{j2\pi\lambda s}x^{-j2\pi\sigma-1}dx\;ds \\ &= \int_{-\infty}^{\infty}\int_{-\infty}^{\infty} \underline{W}_{12}(e^y,s)e^{j2\pi(\lambda s-y\sigma)}dy\;ds\end{aligned} \tag{48}$$

and

$$\underline{W}_{12}(x,s) = \int_{-\infty}^{\infty}\int_{-\infty}^{\infty} \underline{A}_{12}(\sigma,\lambda)x^{j2\pi\sigma}e^{-j2\pi\lambda s}\,d\sigma\,d\lambda \tag{49}$$

$$\underline{W}_{12}(e^y,s) = \int_{-\infty}^{\infty}\int_{-\infty}^{\infty} \underline{A}_{12}(\sigma,\lambda)e^{j2\pi(y\sigma-\lambda s)}\,d\sigma\,d\lambda \tag{50}$$

Therefore, $\underline{A}_{12}(\sigma,\lambda)$ and $\underline{W}_{12}(e^y,s)$ represent a two-dimensional FT pair, while $\underline{A}_{12}(\sigma,\lambda)$ and $\underline{W}_{12}(x,s)$ constitute mixed two-dimensional transform pair with MT as the mapping between x and σ axis and Fourier transform as the mapping between λ and s axis.

From the definition of the scale-invariant AF, the properties of the MT, and from the Eqs. (7) and (8), it follows:

1) The magnitude of the scale-invariant auto-AF is symmetric with respect to the origin. Moreover,

$$\underline{A}_{12}^*(\sigma,\lambda) = \underline{A}_{21}(-\sigma,-\lambda) \tag{51}$$

2) $\underline{A}_{12}$ is bilinear. Namely, if

$$g(x) = f_1(x)+f_2(x), \quad h(x) = f_3(x)+f_4(x)$$

then

$$\underline{A}_{gh} = \underline{A}_{13}+\underline{A}_{14}+\underline{A}_{23}+\underline{A}_{24} \tag{52}$$

3) Scaling in space (or, equivalently, phase-shift in s-domain) of both signals introduces only a phase factor into $\underline{A}$. The magnitude of $\underline{A}$ is invariant to this scaling. If

$$g(x) = f_1(e^{\mu}x), \qquad h(x) = f_2(e^{\mu}x)$$

or, equivalently,

$$\underline{G}(s) = e^{j2\pi\mu s}\underline{F}_1(s), \qquad \underline{H}(s) = e^{j2\pi\mu s}\underline{F}_2(s),$$

then

$$\underline{A}_{gh}(\sigma,\lambda) = e^{j2\pi\sigma\mu}\underline{A}_{12}(\sigma,\lambda) \tag{53}$$

If one signal is scaled with respect to the other, a phase factor is introduced and the correlation peak is shifted in the λ direction by a proportional amount:

$$\begin{gathered} g(x) = f_1(e^{\mu}x), \qquad h(x) = f_2(x) \\ \underline{A}_{gh}(\sigma,\lambda) = e^{j\pi\sigma\mu}\underline{A}_{12}(\sigma,\lambda+\mu) \end{gathered} \tag{54}$$

4) Modulation in space by $x^{j2\pi\alpha}$ (or, equivalently, shift in the s-domain by α) of both signals results in an additional phase factor only. If

$$g(x) = x^{j2\pi\alpha}f_1(x), \qquad h(x) = x^{j2\pi\alpha}f_2(x)$$

or, equivalently,

$$\underline{G}(s) = \underline{F}_1(s-\alpha), \qquad \underline{H}(s) = \underline{F}_2(s-\alpha)$$

then

$$\underline{A}_{gh}(\sigma,\lambda) = e^{-j2\pi\lambda a}\underline{A}_{12}(\sigma,\lambda) \tag{55}$$

Hence, magnitude of the scale-invariant AF is invariant to shifts in the s-domain. If, however, only one signal is modulated, a phase factor is created and the correlation peak is shifted in the σ direction by a proportional amount:

$$\begin{gathered} g(x) = x^{j2\pi a} f_1(x), \qquad h(x) = f_2(x) \\ \underline{A}_{gh}(\sigma,\lambda) = e^{-j\pi\lambda a}\underline{A}_{12}(\sigma-\alpha,\lambda) \end{gathered} \tag{56}$$

5) Scaling, followed by modulation, of both signals produces composite phase factor in $\underline{A}$, while magnitude remains invariant:

$$\begin{gathered} g(x) = x^{j2\pi a} f_1(e^{\mu}x), \qquad h(x) = x^{j2\pi a} f_2(e^{\mu}x) \\ \underline{A}_{gh}(\sigma,\lambda) = e^{j2\pi(\sigma\mu-\lambda a)}\underline{A}_{12}(\sigma,\lambda) \end{gathered} \tag{57}$$

If only one of the signals is scaled and modulated, a composite phase factor is generated. In this case the correlation peak is displaced off both axis:

$$\begin{gathered} g(x) = x^{j2\pi a} f_1(e^{\mu}x), \qquad h(x) = f_2(x) \\ \underline{A}_{gh}(\sigma,\lambda) = e^{j\pi(\sigma\mu-\lambda a)}\underline{A}_{12}(\sigma-\alpha,\lambda+\mu) \end{gathered} \tag{58}$$

Eq. (58) demonstrates the scale invariance property of the newly defined SIAF.

6) Performing the inverse MT of (45), and changing variables yields:

$$f_1(x_1)f_2^*(x_2) = \int_{-\infty}^{\infty} \underline{A}_{12}(\sigma, ln\frac{x_1}{x_2})(x_1x_2)^{j\pi\sigma}d\sigma \tag{59}$$

For $x_1=x_2=x$:

$$f_1(x)f_2^*(x) = \int_{-\infty}^{\infty} \underline{A}_{12}(\sigma,0)x^{j\pi\sigma}d\sigma \tag{60}$$

In the case of the scale-invariant auto-AD this reduces to

$$|f(x)|^2 = \int_{-\infty}^{\infty} \underline{A}_f(\sigma,0)x^{j\pi\sigma}d\sigma \tag{61}$$

Eq. (61) can be used to extract the signal envelope. On the other hand, if $x_1=x$, $x_2=1$:

$$f_1(x)f_2^*(1) = \int_{-\infty}^{\infty} \underline{A}_{12}(\sigma,\ln x)x^{j\pi\sigma}d\sigma \tag{62}$$

Eq. (62) allows the signal $f_1(x)$ to be recovered within complex non-zero multiplying constant from its scale-invariant AF at $\ln x$ using the inverse MT.

7) Applying the Fourier transform to Eq. (47) and changing variables produces

$$\underline{F}_1(s_1)\underline{F}_2^*(s_2) = \int_{-\infty}^{\infty} \underline{A}_{12}(s_1-s_2,\lambda)e^{-j\pi(s_1+s_2)\lambda}d\lambda \tag{63}$$

If $s_1=s_2=s$, then

$$\underline{F}_1(s)\underline{F}_2^*(s) = \int_{-\infty}^{\infty} \underline{A}_{12}(0,\lambda)e^{-j2\pi s\lambda}d\lambda \tag{64}$$

The function $\underline{A}_{12}(0,\lambda)$ represents another form of the scale correlation function between $f_1(x)$ and $f_2(x)$. It is related to the product on the left side through the Fourier transform[8]:

$$\underline{A}_{12}(0,\lambda) = \int_0^{\infty} f_1(e^{\frac{\lambda}{2}}x)f_2^*(e^{-\frac{\lambda}{2}}x)\frac{dx}{x} = \int_0^{\infty} f_1(x)f_2^*(e^{-\lambda}x)\frac{dx}{x} \tag{65}$$

The change of variables $\xi=e^{\lambda}$ may be used to transform the first form of the scale correlation, Eq. (18), into the second form, Eq (65). The Mellin spectrum is the Fourier transform of the scale autocorrelation function defined as above[8]:

$$|\underline{F}(s)|^2 = \int_{-\infty}^{\infty} \underline{A}_f(0,\lambda) e^{-j2\pi s\lambda} d\lambda \tag{66}$$

Setting $s_1=s$, $s_2=0$ an inversion formula for the MT of the signal can be derived:

$$\underline{F}_1(s)\underline{F}_2^*(0) = \int_{-\infty}^{\infty} \underline{A}_{12}(s,\lambda) e^{-j\pi s\lambda} dx \tag{67}$$

8) Scale convolution in x-domain results in a one-dimensional linear convolution of $\underline{A}$'s in the direction of λ-axis. Let

$$g(x) = \int_0^{\infty} f_1(y) f_2(x/y) \frac{dy}{y} \equiv f_1(x) \otimes f_2(x) \tag{68}$$

$$h(x) = \int_0^{\infty} f_3(y) f_4(x/y) \frac{dy}{y} \equiv f_3(x) \otimes f_4(x) \tag{69}$$

then

$$\underline{A}_{gh}(\sigma,\lambda) = \int_{-\infty}^{\infty} \underline{A}_{12}(\sigma,\eta) \underline{A}_{34}(\sigma,\lambda-\eta) d\eta \equiv \underline{A}_{12}(\sigma,\lambda) *_{\lambda} \underline{A}_{34}(\sigma,\lambda) \tag{70}$$

9) Multiplication in x-domain yields one-dimensional linear convolution of $\underline{A}$'s in the direction of the σ axis. If

$$g(x) = f_1(x)\, f_2(x), \qquad h(x) = f_3(x)\, f_4(x)$$

then

$$\underline{A}_{gh}(\sigma,\lambda) = \int_{-\infty}^{\infty} \underline{A}_{12}(\xi,\lambda) \underline{A}_{34}(\sigma-\xi,\lambda) d\xi \equiv \underline{A}_{12}(\sigma,\lambda) *_{s} \underline{A}_{34}(\sigma,\lambda) \tag{71}$$

10) Let the squared magnitude of the auto-SIAF be called scale-invariant ambiguity surface (SIAS). The SIAS peaks at the origin:

$$|\underline{A}_{11}(\sigma,\lambda)|^2 \leq \underline{A}_{11}^2(0,0) \tag{72}$$

where

$$\underline{A}_{11}(0,0) = \int_0^\infty |f_1(x)|^2 \frac{dx}{x} = \int_{-\infty}^\infty |\underline{F}_1(s)|^2 ds \tag{73}$$

11) The products of the cross-SIAF's are related through the two-dimensional Fourier transform:

$$\int_{-\infty}^\infty \int_{-\infty}^\infty \underline{A}_{12}(\sigma,\lambda)\underline{A}_{34}^*(\sigma,\lambda)e^{j2\pi(\lambda\xi-\sigma\eta)}d\lambda d\sigma = \underline{A}_{13}(\xi,\eta)\underline{A}_{24}^*(\xi,\eta) \tag{74}$$

Two special cases of this relationship are of interest. If $f_1(x)=f_3(x)$ and $f_2(x)=f_4(x)$, it follows that the 2-D Fourier transform of the magnitude of the cross-SIAF equals the product of the individual auto-SIAF's:

$$\int_{-\infty}^\infty \int_{-\infty}^\infty |\underline{A}_{12}(\sigma,\lambda)|^2 e^{j2\pi(\lambda\xi-\sigma\eta)}d\lambda d\sigma = \underline{A}_{11}(\xi,\eta)\underline{A}_{22}^*(\xi,\eta) \tag{75}$$

In addition, the SIAS is its own 2-D Fourier transform. This follows if $f_1(x)=f_2(x)$ is put in the equation above.

$$\int_{-\infty}^\infty \int_{-\infty}^\infty |\underline{A}_{11}(\sigma,\lambda)|^2 e^{j2\pi(\lambda\xi-\sigma\eta)}d\lambda d\sigma = |\underline{A}_{11}(\xi,\eta)|^2 \tag{76}$$

From the property 10 and Eq. (76), the volume under the SIAS is

$$\int_{-\infty}^\infty \int_{-\infty}^\infty |\underline{A}_{11}(\sigma,\lambda)|^2 d\lambda d\sigma = |\underline{A}_{11}(0,0)|^2 = [\int_0^\infty |f_1(x)|^2 \frac{dx}{x}]^2 = [\int_{-\infty}^\infty |\underline{F}_1(s)|^2 ds]^2 \tag{77}$$

12) The property that the SIAS is its own 2-D Fourier transform, Eq. (76), imposes a constraint on the distribution of the volume under the SIAS in the σ and λ directions. The marginal distribution in the σ-direction of the volume under the SIAS is determined by the values of the SIAS on the λ-axis, and, from the property 7, that means by the shape of the Mellin spectrum.

$$\int_{-\infty}^\infty |\underline{A}_{11}(\sigma,\lambda)|^2 d\lambda = \int_{-\infty}^\infty |\underline{A}_{11}(0,\lambda)|^2 e^{j2\pi\lambda\sigma} d\lambda \tag{78}$$

Similarly, the marginal distribution in the λ-direction of the volume under the SIAS is determined by the values of the SIAS on the σ-axis, and, from the property 6, that means by the shape of the signal envelope.

$$\int_{-\infty}^{\infty} |\underline{A}_{11}(\sigma,\lambda)|^2 d\lambda = \int_{-\infty}^{\infty} |\underline{A}_{11}(0,\lambda)|^2 e^{j2\pi\lambda\sigma} d\lambda \tag{79}$$

The last two equations imply that, if the SIAS central peak is squeezed along the σ axis, the volume under the SIAS must spread out in the λ direction, and vice versa.

5. Two-Dimensional Signals and Systems

In principle, one may define four-dimensional scale-invariant WD and AF as generalizations of Eqs. (22) and (45), and then derive their analogous sets of properties. However, in this chapter, attention will be focused on SIWD and SIAF as defined above. Although they are two-dimensional representations of one-dimensional signals, they could be useful for the analysis and characterization of some two-dimensional signals and systems such as the signals and systems with circular symmetry. The point-spread function of such systems is a function of radial variable only. If the input to such a system has circular symmetry so does its output. It may be shown that these systems are scale-invariant[18,19]. Therefore, scale-invariant analysis and characterization of these one-dimensional functions can be performed via SIWD and SIAF.

For example, consider the projection of a circularly symmetric signal $f(r,\theta)=f(r)$ at angle ϕ. Because of circular symmetry, the projection doesn't vary with ϕ. The collection of these projections for all values of ϕ is the Radon transform of $f(r,\theta)=f(r)$. It is, in this case, independent of ϕ and it is equal to the Abel transform of f(r) denoted as $f_A(p)$ [18]. The Abel transform is defined as a scale convolution type integral[18]. Therefore, the SIWD (or

SIAF) of $f_A(p)$ can be obtained through the one-dimensional scale-convolution of the SIWD (SIAF) of the transform kernel with the SIWD (SIAF) of f(r) according to Eq. (41) (Eq. (70)).

As another example, consider a general two dimensional signal as a function of polar coordinates, $f(r,\theta)$. In this case, based on the discussion above, it seems natural to define a four-dimensional WD or AF by taking the MT in the radial direction and the Fourier transform in the angular direction:

$$\overline{W}_f(r,\theta;s,\phi) = \int_0^{\infty}\int_0^{2\pi} f(\gamma^{1/2}r,\theta+\frac{\alpha}{2}) f^*(\gamma^{-1/2}r,\theta-\frac{\alpha}{2}) \gamma^{-j2\pi s-1} e^{-j2\pi\alpha\phi}\, d\alpha d\gamma \quad (80)$$

$$\overline{A}_f(\sigma,\psi;\lambda,\alpha) = \int_0^{\infty}\int_0^{2\pi} f(e^{\lambda/2}r,\theta+\frac{\alpha}{2}) f^*(e^{-\lambda/2}r,\theta-\frac{\alpha}{2}) r^{-j2\pi\sigma-1} e^{-j2\pi\theta\psi}\, d\theta dr \quad (81)$$

where angular addition is modulo-2π. If the signal is separable into radial and angular components, i.e.

$$f(r,\theta) = a(r)\,\Psi(\theta) \quad (82)$$

then the particular mixed four-dimensional WD and AF, defined above, also separate into products of two-dimensional SIWD with WD (see Eq. (80)) and two-dimensional SIAF with AF (see Eq. (81))

$$\overline{W}_f(r,\theta;s,\phi) = \underline{W}_a(r,s)\; W_\Psi(\theta,\phi) \quad (83)$$

$$\overline{A}_f(\sigma,\psi;\lambda,\alpha) = \underline{A}_a(\sigma,\lambda)\; A_\Psi(\psi,\alpha) \quad (84)$$

Hence, the separable signals, Eq. (82), can be analyzed in the radial direction via SIWD and SIAF, and in the angular direction via WD and AF.

In a more general case, $f(r,\theta)$ can always be expanded as a sum of circular harmonic separable functions[19]:

$$f(x,y) = f(r\cos\theta, r\sin\theta) = \sum_{n=-\infty}^{\infty} a_n(r) e^{jn\theta} \quad (85)$$

The mixed four-dimensional WD (or AF) of $f(r,\theta)$ in this case decomposes into

a sum of four-dimensional auto-WD's and cross-WD's (auto-AF's and cross-AF's) of individual expansion terms:

$$\overline{W}_f(r,\theta;s,\phi) = \sum_{n=-\infty}^{\infty}\sum_{k=-\infty}^{\infty} \overline{W}_{nk}(r,\theta;s,\phi) \tag{86}$$

$$\overline{A}_f(\sigma,\psi;\lambda,\alpha) = \sum_{n=-\infty}^{\infty}\sum_{k=-\infty}^{\infty} \overline{A}_{nk}(\sigma,\psi;\lambda,\alpha) \tag{87}$$

Here, $\overline{W}_{nk}(r,\theta;s,\phi)$ and $\overline{A}_{nk}(\sigma,\psi;\lambda,\alpha)$ are four-dimensional cross-WD and cross-AF relating n-th and k-th terms in the expansion (85). As in (83) and (84), each of the elements in sums (86) and (87), however, is separable.

SIWD's (or SIAF's) of the inputs and outputs of various two-dimensional systems can be also related using the properties given in Sec. 3 (or Sec. 4). For example, the output of the two-dimensional Fourier transformer admits the circular harmonic expansion[19]:

$$F(u,v) = F(\omega\cos\nu,\omega\sin\nu) = \sum_{n=-\infty}^{\infty} \overline{a}_{nn}(\omega)\, e^{-jn\nu} \tag{88}$$

where the output expansion coefficients $\overline{a}_{nn}(\omega)$ are n-th order Hankel transforms of the input expansion coefficients $a_n(r)$. The four-dimensional WD of $F(u,v)$ is the sum of the auto-terms and the cross-terms of the form (86). Each of the terms in this sum is separable, as in (83), into a product of a radial SIWD and an angular WD. The n-th order Hankel transform is an example of the Mellin-type scale convolution. Hence, using the property (41), each SIWD term in the output four-dimensional WD can be related to its corresponding SIWD term in the input four-dimensional WD. Corresponding statements can be made about SIAF terms in the input and output mixed four-dimensional AF.

Similarly, the output $f_R(p,\phi)$ of the Radon transformer admits a circular harmonic expansion[20]:

$$f_R(p,\phi) = \sum_{n=-\infty}^{\infty} a_{Gn}(p)\, e^{jn\phi} \tag{89}$$

where the output expansion coefficients $a_{Gn}(p)$ are Gegenbauer transforms of the input expansion coefficients $a_n(r)$. The four-dimensional WD of $f_R(p,\phi)$ is the sum of the auto-terms and the cross-terms in the form of (86). Each of the terms in this sum is separable, as in (83), into a product of a radial SIWD and an angular WD. Since the Gegenbauer transform[20] is another example of the Mellin-type scale convolution, the input SIWD terms and the output SIWD terms can be related using the corresponding property (41).

The scale convolution appears also in some imaging systems that suffer from shift-variant distortions like coma aberrations and tilt of the imaging plane out of focal plane for a cylindrical lens system[6]. The SIWD's and SIAF's of inputs and outputs in such systems can also be related in a manner outlined above.

6. Optical Implementation

There are many optical implementations of the WD and the AF (see Ref.4 for references), geometric optical transformations[21,22] and the MT[23-25]. These realizations may be used as building blocks for the optical implementation of the SIWD and SIAF.

A convenient way of producing the SIWD is based on Eq.(23). The realization is illustrated on Fig. 1. The signals are first subjected to logarithmic coordinate transformation, then the WD of such pre-distorted signals is generated, and finally the post-distortion by exponential transformation of spatial (time) coordinate of WD is performed.

The optical realization of the SIAF, illustrated on Fig. 2 and based on Eq.(46), is even simpler. Logarithmic coordinate transformation is first

performed on the signals, followed by generation of the optical ambiguity function of the pre-distorted signal.

7. Numerical Examples

In the examples that follow, numerical evaluations of SIWD an SIAF were based on Eqs. (23) and (46) to take advantage of the fast algorithms for the Fourier transform calculation. Necessary coordinate transformations were done using the standard cubic spline interpolation. The fast Fourier transform was used to generate the WD and the AF. Resulting SIWD and SIAF for a sinusoid signal modulated by the Gaussian pulse and for a rectangular chirp signal are presented in Figs. 3 and 4. In each case, for comparison, both the WD and the AF of the signal are also given. Figs. 3.a and 4.a show the input signals, Figs. 3.b and 4.b show the corresponding WD's, and in Figs. 3.c and 4.c the SIWD's are depicted. The AF's of these signals are presented on Figs. 3.d and 4.d, and their SIAF's on 3.e and 4.e. In these examples, one can observe that the space (time) - bandwidth product is larger in the domains of scale-invariant representations. However, this is not true in general. For example, if the frequency of the chirp is decreasing instead, the space (time) - bandwidth products would be reduced in the domains of scale-invariant representations. These effects can be used advantageously in radar, spread spectrum communication and pattern recognition systems.

8. Discussion and Conclusion

Performance of shift-invariant signal processing systems is known to deteriorate rapidly with small scale changes of the signal being processed. Many problems of this type have been resolved by the nonlinear (logarithmic) coordinate transformation followed by linear shift-invariant processing, or by use of the scale invariant linear integral transformation (MT)[6-14]. The

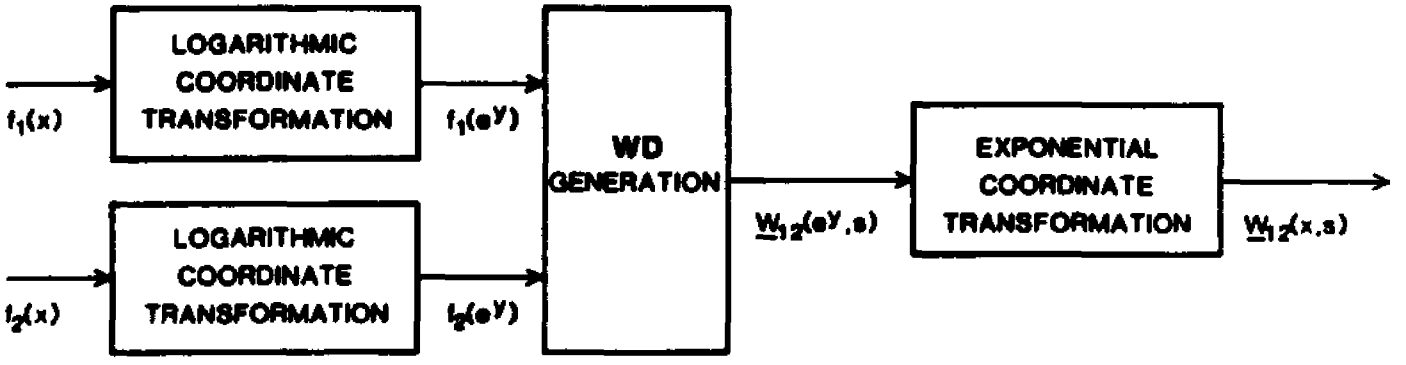

Figure 1 Block diagram of an optical realisation of SIWD.

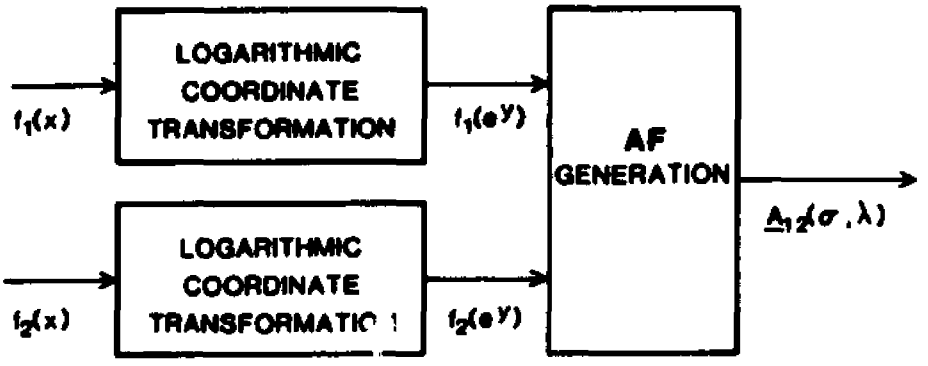

Figure 2 Block diagram of an optical realisation of SIAF.

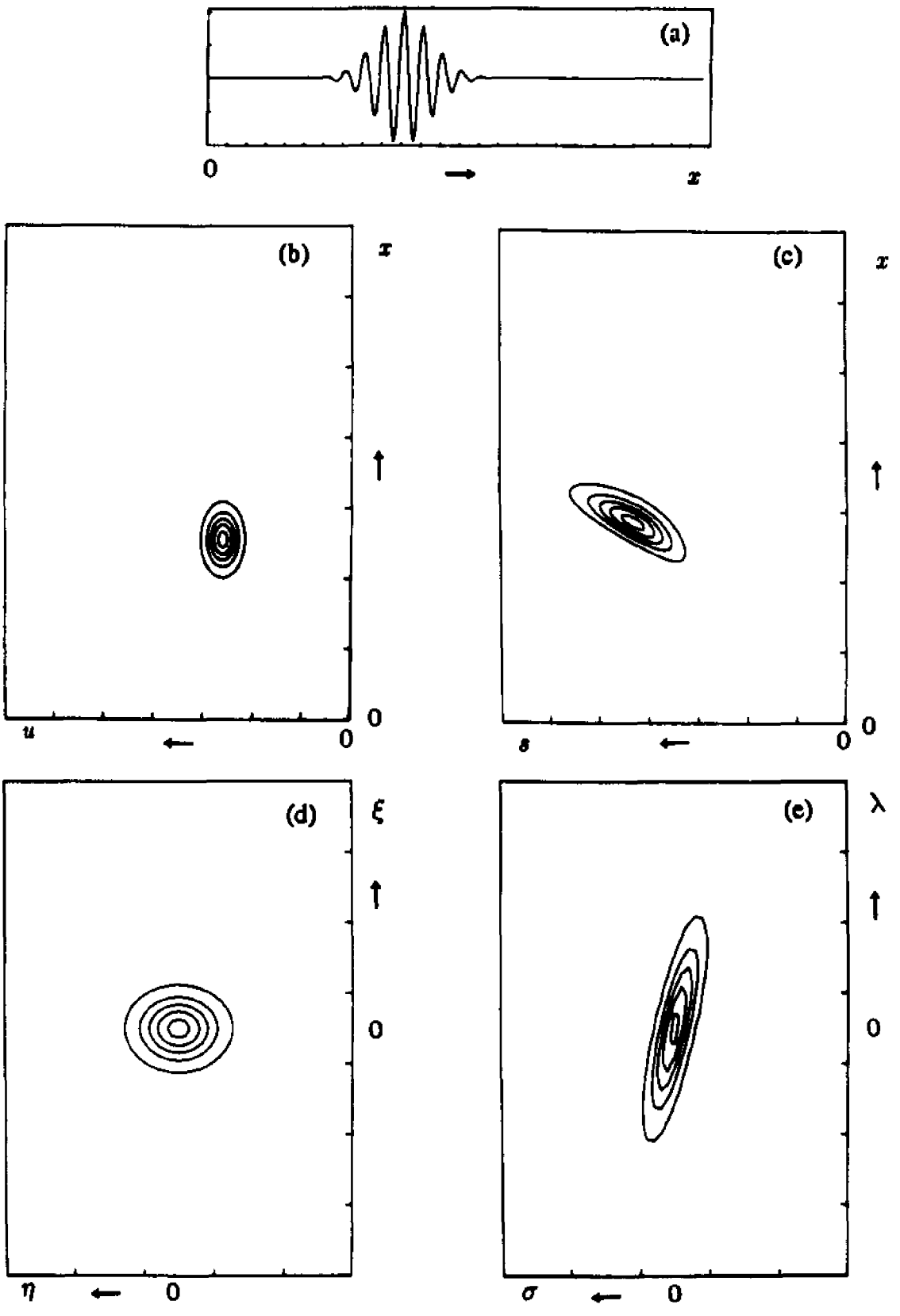

Figure 3 (a) Gaussian RF chirp signal. (b) Conventional WD. (c) Scale-invariant WD. (d) Conventional AF. (e) Scale-invariant AF.

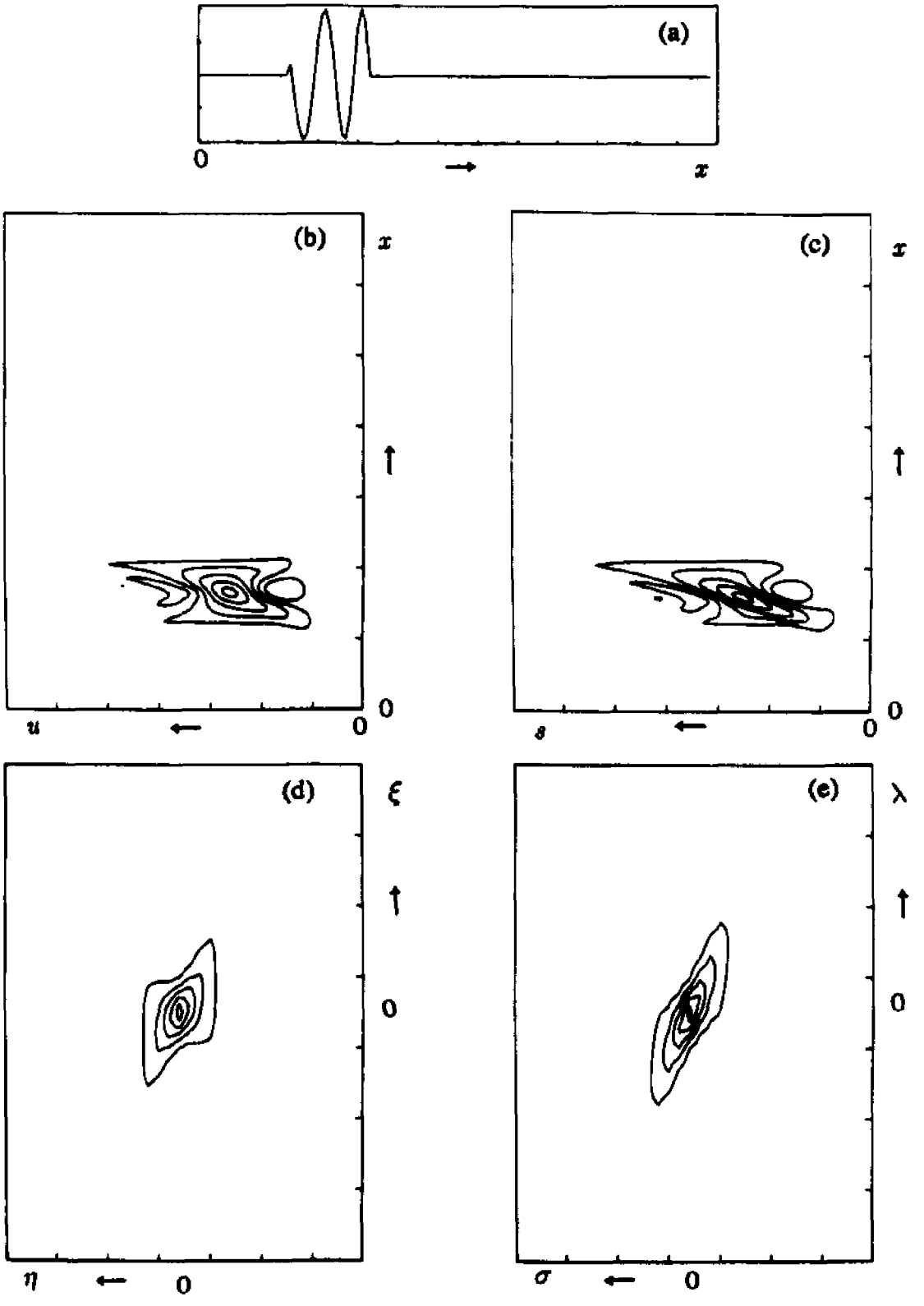

Figure 4 (a) Rectangular RF chirp signal. (b) Conventional WD. (c) Scale-invariant WD. (d) Conventional AF. (e) Scale-invariant AF.

SIWD and SIAF could be used at least in those scale-invariant applications that correspond to shift-invariant applications in which WD and AF are used.

The Wigner distribution has been applied to analysis and characterization of space (time) invariant electronic and optical systems[2,26-28]. It has been also used for shift-invariant parameter estimation and feature extraction[26-28]. Similarly, scale-invariant WD may be used for analysis and characterization of space variant, scale invariant systems like interpolators, decimators and magnifiers. Its immunity to scale changes in the signal should make it useful for a range of parameter estimation and feature extraction problems that have not been tackled before. Applications of the ambiguity function have been mainly in the radar and communication signal processing and design, and also in pattern recognition. Since Doppler frequency shifts are equivalent to signal scaling, scale-invariant processing preserves Doppler invariance[13]. This implies that scale-invariant ambiguity function should be useful in radar and communications, e.g. for the synthesis and optimal processing of non-linear spread spectrum codes[13] that are created by coordinate transformation of linear codes. Scale independent pattern recognition is another possible application of SIAF.

References

1. T. A. C. M. Claasen and W. F. G. Mecklenbrauker, "The Wigner distribution - a tool for time-frequency signal analysis," parts I, II and III, *Philips J. Res.* 35, 1980, 217-250, 276-300, 372-389.

2. M. J. Bastiaans, "Signal description by means of a local frequency spectrum," *Proc. SPIE* 373, 1981, 49-62.

3. A. W. Rihaczek, *Principles of High Resolution Radar,* McGraw-Hill, 1969.

4. G. Eichmann and B. Z. Dong, "Two-dimensional optical filtering of 1-D signals," *Appl. Opt.* 21, no. 17, Sept. 1982, 3152-3156.

5. P. Baudelaire, "Linear stretch-invariant systems," *Proc. IEEE* 62, Apr. 1974, 467-468.

6. G. M. Robbins and T. S. Huang, "Inverse filtering for linear shift-variant imaging systems," *Proc. IEEE* 60, July 1972, 862-872.

7. A. Sawchuk, "Space invariant image restoration by coordinate transformations," *J. Opt. Soc. Am.* 64, Feb. 1974, 138-144.

8. H. E. Moses and A. F. Quesada, "The power spectrum of the Mellin transformation with applications to scaling of physical quantities," *J. Math. Phys.* 15, June 1974, 748-752.

9. H. E. Moses and B. T. Prosser, "Phases of complex functions from the amplitudes of the functions and the amplitudes of the Fourier and Mellin transforms," *J. Opt. Soc. Am.* 73, Nov. 1983, 1451-1454.

10. D. Casasent and D. Psaltis, "Deformation invariant, space-variant optical pattern recognition," in *Progress in Optics XVI* (ed. E. Wolf), North-Holand, 1978, 289-356.

11. C. Braccini, G. Gambardella and A. Grattarola, "Digital image processing

by means of generalized scale-invariant filters," in *Issues in Acoustic Signal-Image Processing and Recognition* (ed. C. H. Chen), NATO ASI Series, Springer-Verlag, 1983, 315-329.

12. R. A. Messner and H. H. Szu, "Simultaneous image processing and feature extraction for two-dimensional non-uniform sensors," *Proc. SPIE* 449, Nov. 1983, 693-710.

13. D. Psaltis, D. Casasent, and A. Sexton, "Optical signal processing of non-linear coded waveforms," *Proc. IEEE* 1978 Opt. Comp. Symp. 1978, 80-85.

14. C. Braccini, G. Gambardella, "Signal detection and estimation techniques based on linear shift-variant filtering and short-space frequency variant spectral analysis," *Proc. of the Workshop Italy-USA on Digital Signal Processing*, Portovenere, Italy, Aug. 1981, 157-170.

15. R. A. Altes, "The Fourier-Mellin transform and mammalian hearing," *J. Acoust. Soc. Am.* 63, no. 1, Jan. 1978, 174-183.

16. D. Malah, "Time-domain algorithms for harmonic bandwidth reduction and time scaling of speech signals," *IEEE Trans. ASSP*, vol. 27, no.2, Apr. 1979, 121-133.

17. I. N. Sneddon, *The use of integral transforms*, McGraw-Hill, 1972.

18. R. N. Bracewell, *The Fourier transform and its applications*, second ed., McGraw-Hill, 1978.

19. A. Papoulis, *Systems and transforms with applications in optics*, McGraw-Hill, 1968.

20. S. R. Deans, *The Radon transform and some of its applications*, J. Wiley, 1983.

21. O. Bryngdahl, "Geometrical transformations in optics," *J. Opt. Soc. Amer.*

64, 1974, 1092-1099.

22. J. W. Goodman, P. Kellman, E. W. Hansen, "Linear space-variant optical processing of 1-D signals," *Appl. Opt.* 16, Mar. 1977, 733-738.

23. D. Casasent and C. Szczutkowski, "Optical Mellin transforms using computer generated holograms," *Opt. Commun.* 19, Nov. 1976, 217-222.

24. J. W. Goodman, "Linear space-variant optical processing," in *Optical Data Processing, Fundamentals* (ed. S. Lee), Springer-Verlag, 1980.

25. J. F. Walkup, "Space-variant coherent optical processing", *Opt. Eng.* 19, 1980, 339.

26. P. Flandrin and W. Martin, "Pseudo-Wigner Estimators for the Analysis of Non-Stationary Processes," *Proc. ASSP Spectrum Estimation Workshop II*, pp. 181-185, Tampa, 1983.

27. G. F. Boudreaux-Bartells and T. W. Parks, "Signal Estimation Using Modified Wigner Distributions," *Proc. ICASSP 84*, pp. 22.3.1-4, San Diego, 1984.

28. B. Bouachache and F. Rodriguez, "Recognition of Time-Varying Signals in the Time-Frequency Domain by Means of the Wigner Distribution," *Proc. ICASSP 84*, pp. 22.5.1-4, San Diego, 1984.

Chapter 5

Outer Product Expansion of Time-Frequency Signal Representations

1. Introduction

Among bilinear joint time-frequency representations of finite energy signals and harmonizable random signals the Wigner distribution (WD) is optimal in many respects[1-5].The following problems are encountered in applications[6]: WD sensitivity to noise, abundance of redundant information in the WD (like undesirable interfering cross-terms in the WD of multicomponent signals), and smearing caused by the use of windows for signals of long duration.

Any square-integrable function of two variables, regarded as the kernel of on an integral operator on Hilbert spaces, is determined by its singular system[7-9]. This system is defined by three sets: the set of singular values, and two sets of corresponding biorthogonal singular functions. In this chapter, an outer product expansion of the WD in terms of its singular values and singular functions is proposed. Its use to alleviate aforementioned problems is illustrated by examples with synthetic and experimental data. The corresponding expansion of the ambiguity function has the same expansion coefficients and most of the discussion is directly applicable there.

The Wigner distribution $W_s(t,f)$ of a finite-energy signal $s(t)$, that has the Fourier transform (FT) $S(f)$, is defined as [1]

$$W_s(t,f) = \int_{-\infty}^{\infty} s(t+\tau/2)\, s^*(t-\tau/2)\, e^{-j2\pi f\tau} d\tau$$
$$= \int_{-\infty}^{\infty} S(f+\nu/2)\, S^*(f-\nu/2)\, e^{j2\pi t\nu} d\nu \qquad (1)$$

In applications of the WD several problems are encountered. First, there is a lot of redundancy in the WD since it is a 2-D representation of a 1-D signal. In order to use the WD successfully in applications like pattern recognition and signal detection, it would be desirable to find a data reduction method for the WD. Secondly, for many applications, such as parameter estimation, the noise sensitivity of the WD should be reduced. Because the WD is a quadratic signal representation, the WD of a signal contaminated by noise will contain two noise-induced components. One of them, the quadratic noise component, is uncorrelated with signal. The other, linear noise component, is correlated with the signal. Therefore, dependence of the signal-to-noise ratio (SNR) in the WD on input SNR exhibits a threshold effect: for high input SNR it is linear, for low input SNR it is quadratic. In the case of multicomponent signals, the presence of oscillatory cross-terms caused by the bilinear nature of the WD may obscure the picture of auto-terms. This may prohibit successful use of the WD with multicomponent signals of complex structure. Two techniques have been presented so far that address the last two problems[5,6]. One possibility[5] is to smooth the WD independently in time and frequency direction by windowing. The other[6] is to perform 2-D filtering of the WD relying on the separability of the auto-terms and the cross-terms in the ambiguity function domain. However, both methods fail to successfully suppress cross-terms from closely spaced signal components. By 2-D smearing of the WD, they also introduce distortion that limits their noise suppression effectiveness.

To address these issues, an outer product expansion, based on the singular value decomposition (SVD) of the Wigner distribution, will be used. This is an application of the basic idea from the theory of Hilbert spaces that allows the use of the SVD as a series expansion of compact, non-normal

operators[7,8]. This expansion has found many different applications in science and engineering. One of the earliest was in the analysis of integral equations with general, non-symmetric kernels[9]. The well-known special cases are the Karhunen-Loeve expansion[10] and the expansion of time- and band-limited signals in terms of prolate spheroidal wave functions[11]. Another important application is in solution of over-determined, under-determined or ill-conditioned systems of linear equations[12,13]. More recently, SVD has been used in image processing for data compression and restoration of images[14], in non-linear spectral estimation for noise suppression[15,16], and in signal extrapolation[17].

2. Outer Product Expansion - Continuous Case

Any square integrable function of two variables, such as the Wigner distribution or ambiguity function, can be expanded into a series of outer products. Many such expansions are possible, but the most interesting are the ones that provide acceptable approximation with a minimum number of expansion terms. The Hilbert space theory provides the most general framework to study this problem.

Let $K(x,y)$ be a function that belongs to the Hilbert space of square integrable functions, $K(x,y) \in L^2(R \times R)$, where R is the set of real numbers. Let the sets $\{\phi_i(x)\}$ and $\{\psi_j(y)\}$ be two orthonormal bases of the Hilbert space $L^2(R)$. Consider a problem of finding a series expansion for $K(x,y)$ in terms of these orthonormal bases

$$K(x,y) = \sum_i \sum_j \alpha_{ij} \phi_i(x) \psi_j^*(y) \tag{2}$$

Here, equality means "almost everywhere" (everywhere, except possibly on a set of measure zero) and the series is mean convergent (L^2-norm tends to

zero). The expansion coefficients are bilinear forms

$$\alpha_{ij} = \langle K\psi_j, \phi_i \rangle = \int_{-\infty}^{\infty} \phi_i^*(x) \int_{-\infty}^{\infty} K(x,y)\psi_j(y)dy\ dx \tag{3}$$

In this equation, angle brackets denote the inner product and $K\psi$ denotes the integral transform:

$$\theta(x) = \int_{-\infty}^{\infty} K(x,y)\psi(y)dy \equiv K\psi \tag{4}$$

$K(x,y)$ is the kernel of the linear operator K and $K^\dagger(x,y)=K^*(y,x)$ is its adjoint.

The Hilbert space $L^2(R)$ is separable and, therefore, its orthonormal bases and the corresponding matrix of coefficients α_{ij} are countably infinite. Depending on the choice of the bases, this matrix can have different forms. The most interesting is a particular choice of the bases $\{\phi_i\}$ and $\{\psi_j\}$ that will produce the diagonal coefficient matrix.

To find such bases, consider the two compositions of kernel $K(x,y)$ and its adjoint $K^\dagger(x,y)$ that define integral operators $KK^\dagger$ and $K^\dagger K$, respectively:

$$\int_{-\infty}^{\infty} K(x,y)K^*(y,x')dy \equiv K_l(x,x') \tag{5}$$

$$\int_{-\infty}^{\infty} K^*(y,x)K(x,y')dx \equiv K_r(y,y') \tag{6}$$

These two kernels, K_l and K_r, are non-negative definite and Hermitian. As such, they have full sets of eigenvalues and associated orthonormal eigenfunctions[9]. It can be shown (see Ref. [9]) that the eigenvalues of kernels K_l and K_r are identical (and non-negative):

$$KK^\dagger\phi_i(x) = \sigma_i^2\phi_i(x), \qquad i=1,\ldots,\infty \tag{7}$$

$$K^\dagger K\psi_i(y) = \sigma_i^2\psi_i(y), \qquad i=1,\ldots,\infty \tag{8}$$

while their eigenfunctions $\phi_i(x)$ and $\psi_j(y)$ are biorthogonal with respect to K

$$K\psi_i = \sigma_i\phi_i, \qquad K^\dagger\phi_i = \sigma_i\psi_i, \qquad i=1,\ldots,\infty \tag{9}$$

The eigenfunctions ϕ_i and ψ_i are the singular functions of $K(x,y)$ belonging to the singular value σ_i. The set $\{\phi_i(x),\psi_i(y);\sigma_i\}$ is the singular system of $K(x,y)$. The elements of this set are indexed in such an order that the singular values in the sequence $\{\sigma_i\}$ are non-increasing.

Substituting $K\psi_j$, from Eq. (9), into Eqs. (3) and (2), an outer product expansion in terms of the singular system of $K(x,y)$, with diagonal coefficient matrix, is obtained as

$$K(x,y) = \sum_{i=1}^{\infty}\sigma_i\phi_i(x)\psi_i^*(y) \tag{10}$$

The equality above means "almost everywhere" and the series is mean convergent. Moreover, the squared L^2-norm of $K(x,y)$ is equal to the sum of the squared singular values:

$$\| K(x,y) \|^2 = \sum_{i=1}^{\infty}\sigma_i^2 \tag{11}$$

The best least squares approximation of $K(x,y)$ by the kernel of the finite rank n is [9]

$$K_n(x,y) = \sum_{i=1}^{n}\sigma_i\phi_i(x)\psi_i^*(y) \tag{12}$$

with the least squares error

$$\| K(x,y) - K_n(x,y) \|^2 = \sum_{i=n+1}^{\infty}\sigma_i^2 \tag{13}$$

The outer product expansion (12) is the optimum one, in a sense that, for a prescribed approximation error, it requires the minimum number of expansion terms[9]. Any integral transform with $K(x,y)$ or its adjoint as the kernel can

also be expanded in terms of the singular system $\{\phi_i,\psi_i;\sigma_i\}$. For every $a,b\in L^2(R)$:

$$p(x) = Ka = \int_{-\infty}^{\infty} K(x,y)a(y)dy = \sum_{i=1}^{\infty}\sigma_i\langle a,\psi_i\rangle\phi_i(x) \tag{14}$$

$$q(y) = K^{\dagger}b = \int_{-\infty}^{\infty} K^{*}(y,x)b(x)dx = \sum_{i=1}^{\infty}\sigma_i\langle b,\phi_i\rangle\psi_i(y) \tag{15}$$

Also, for every $f,b\in L^2(R)$,

$$\langle Ka,b\rangle = \sum_{i=1}^{\infty}\sigma_i\langle a,\psi_i\rangle\langle\phi_i,b\rangle \tag{16}$$

If $K(x,y)$ is a continuous function, the convergence in Eqs. (10), (14), (15) and (16) is uniform and absolute.

3. Outer Product Expansion of the Sampled Wigner Distribution

As a square-integrable function of two variables, the WD admits expansion (10) in the series of outer products of its singular functions weighted by corresponding singular values σ_i. Since the WD is real-valued, so are its singular functions. Moreover, the marginals and local moments of WD, being integral transforms with WD as a kernel, have orthonormal expansions in terms of one or the other set of singular functions, as in (14) and (15). In most practical cases, however, one deals with discrete approximations to the WD. Therefore, the optimum outer product expansion of the WD will be given, in this section, in the framework of finite-dimensional vector spaces.

In order to numerically evaluate the WD, the signal has to be sampled and, if necessary, time-limited. From N data samples a discrete approximation to the WD of the continuous signal can be calculated in one of the several ways[1,4,18]. One of the procedures most often used for this, achieves computational efficiency through the use of the FFT but also requires either over-

sampling by a factor of 2 or use of analytic signal to avoid aliasing[1]. However, regardless of the method used, the result is an $N \times M$ matrix W of samples of the continuous WD. In the discrete case, the singular system is generated by the singular value decomposition of this matrix of the WD samples[12-14]. Singular functions are replaced by singular vectors, outer products in the expansion are unit rank matrices, the number of terms in the expansions is finite, and there are no convergence problems. Then, the singular system $\{u_i, v_i; \sigma_i\}$ of the WD matrix is defined by

$$WW^T u_i = \sigma_i^2 u_i, \qquad i=1,\ldots,N \tag{17}$$

$$W^T W v_i = \sigma_i^2 v_i, \qquad i=1,\ldots,N \tag{18}$$

$$Wv_i = \sigma_i u_i, \qquad W^T u_i = \sigma_i v_i, \qquad i=1,\ldots,N \tag{19}$$

The SVD of the discrete WD is

$$W = \sum_{i=1}^{N} \sigma_i u_i v_i^T, \qquad \| W \|_F^2 = \sum_{i=1}^{N} \sigma_i^2 \tag{20}$$

where $\|W\|_F$ is the Frobenius matrix norm. As a consequence of the properties of the WD, the volume under the surface that corresponds to a particular expansion term is equal to the signal energy contained in that term. The fraction of signal energy contained in i-th term is denoted ϵ_i. The best least squares approximation of W by the matrix of the lower rank $K < N$ is

$$W_K = \sum_{i=1}^{K} \sigma_i u_i v_i^T \tag{21}$$

with least squares error

$$\| W - W_K \|_F^2 = \sum_{i=K+1}^{N} \sigma_i^2 \tag{22}$$

In addition, the linear transformations, with W or W^T as the transformation matrices, admit expansions as

$$p = Wa = \sum_{i=1}^{N} \sigma_i (v_i^T a) u_i \tag{23}$$

$$q = W^T b = \sum_{i=1}^{N} \sigma_i (u_i^T b) v_i \tag{24}$$

$$a^T W^T b = \sum_{i=1}^{N} \sigma_i (a^T v_i)(u_i^T b) \tag{25}$$

The proposed expansion, Eq. (20), can also be regarded as a non-linear and non-unitary transformation of the signal, with $\{\sigma_i\}$ as its generalized "spectrum". The singular value (s.v.) spectrum $\{\sigma_i\}$ exhibits several interesting properties. If $T(\delta)$ and $B(\delta)$ are essential time- and band-limit of the signal defined so that only δ fraction of its energy lies outside, the essential dimensionality of this signal is $2T(\delta)B(\delta)$ [11]. In the processing of synthetic noiseless monocomponent signals, it has been observed that with $K(\delta) = 2\ T(\delta)\ B(\delta)$ in Eq. (21), the fractional approximation error is $\Delta \approx 2\delta$. For example, chirped raised-cosine pulse, shown in Fig. 1.a, has $TB = 4$ with $\delta = 0.01$. Contour plot of the WD of this signal is depicted on Fig. 1.b, and its singular values on Fig. 1.c. For this signal $K = 8$, and error in the approximation (21) is 2%. The dependence of the singular value spectrum on the time-bandwidth product of the signal is displayed on Fig. 2 for $TB = 1, 4, 6, 17$. Observe how the s.v. spectrum spreads with increase in the time-bandwidth product of the signal. It is also noticeable that the number of significant, non-zero singular values that determines the width of the s.v. spectrum is equal to signal dimensionality $2TB$. The exact shape of the s.v. spectra is dependent on the actual frequency vs. time dependence within the signal.

Permutations of rows and columns or unitary transformations of W lead to similarity transformations of WW^T and $W^T W$. Consequently, the s.v.'s of W remain the same. The s.v.'s of W are invariant to time and frequency shifts of the signal since these correspond to permutations of rows and columns

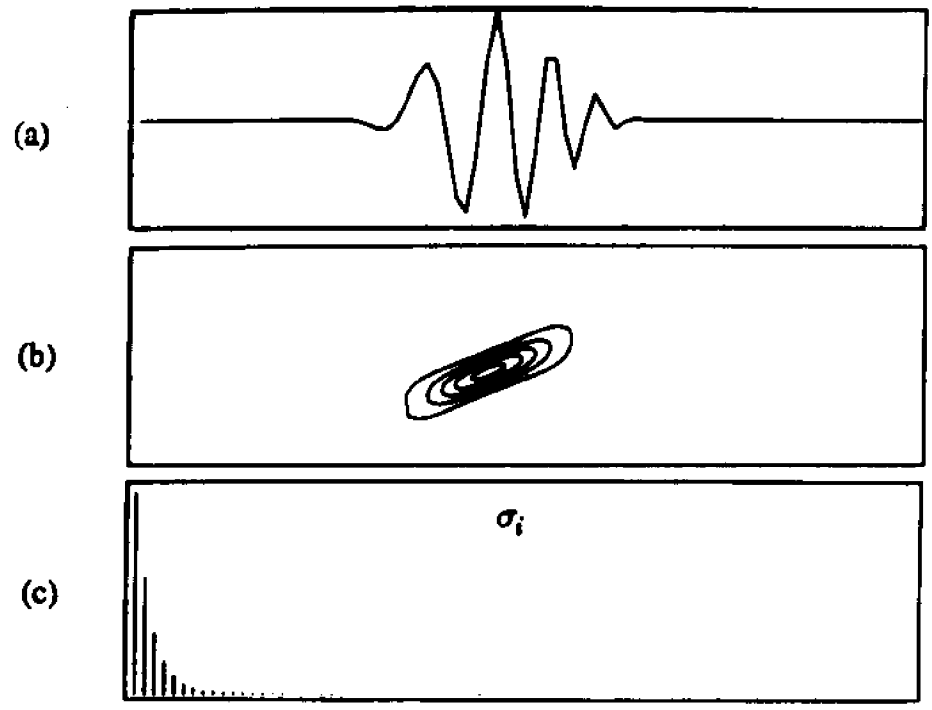

Figure 1. Chirped RF raised cosine pulse (TB = 4) - (a) waveform, (b) WD contour plot, (c) WD's singular values.

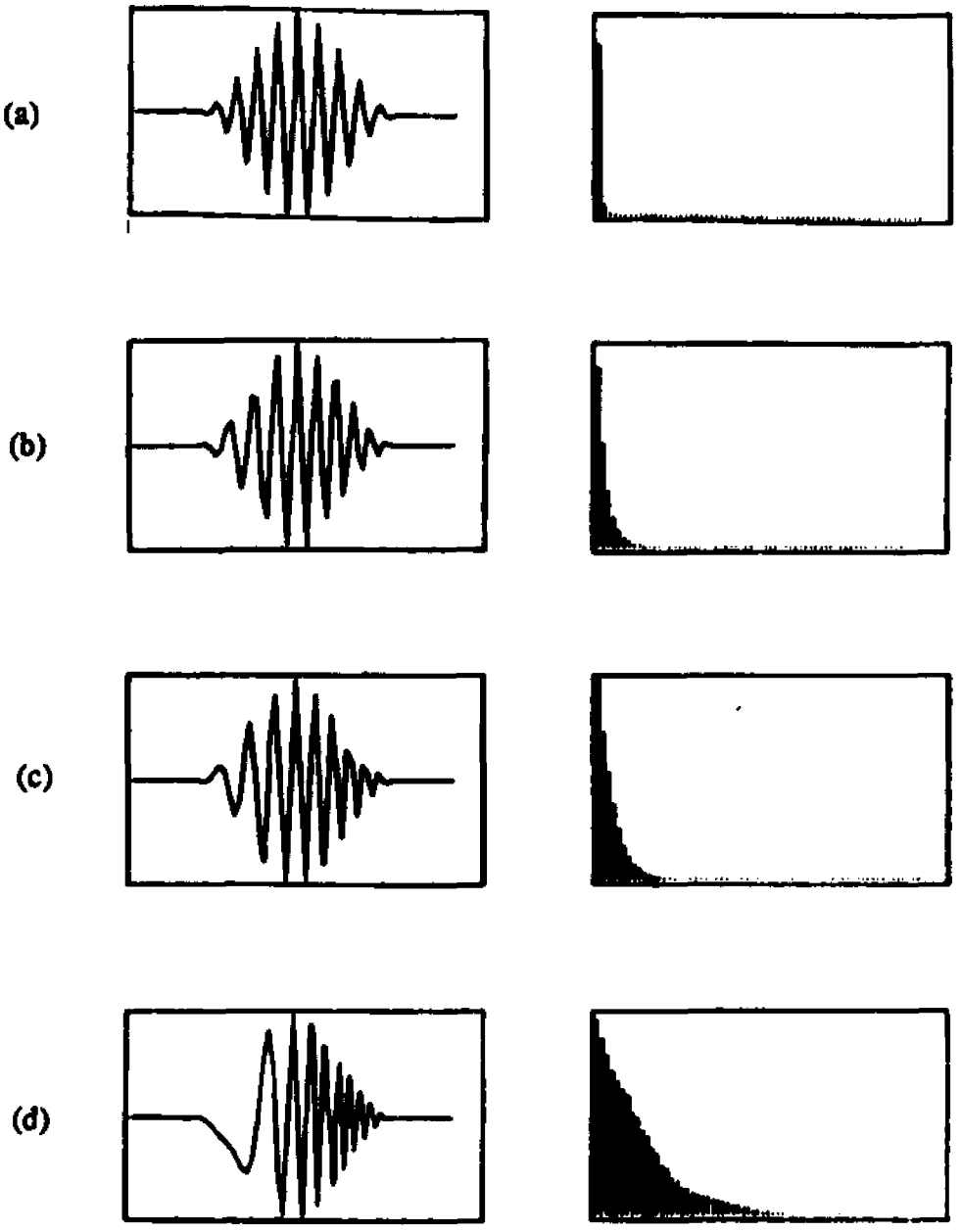

Figure 2. waveforms and s.v. spectra for chirped RF raised cosine pulses of different chirp rate - (a) TB = 1, (b) TB = 4, (c) TB = 6, (d) TB = 17.

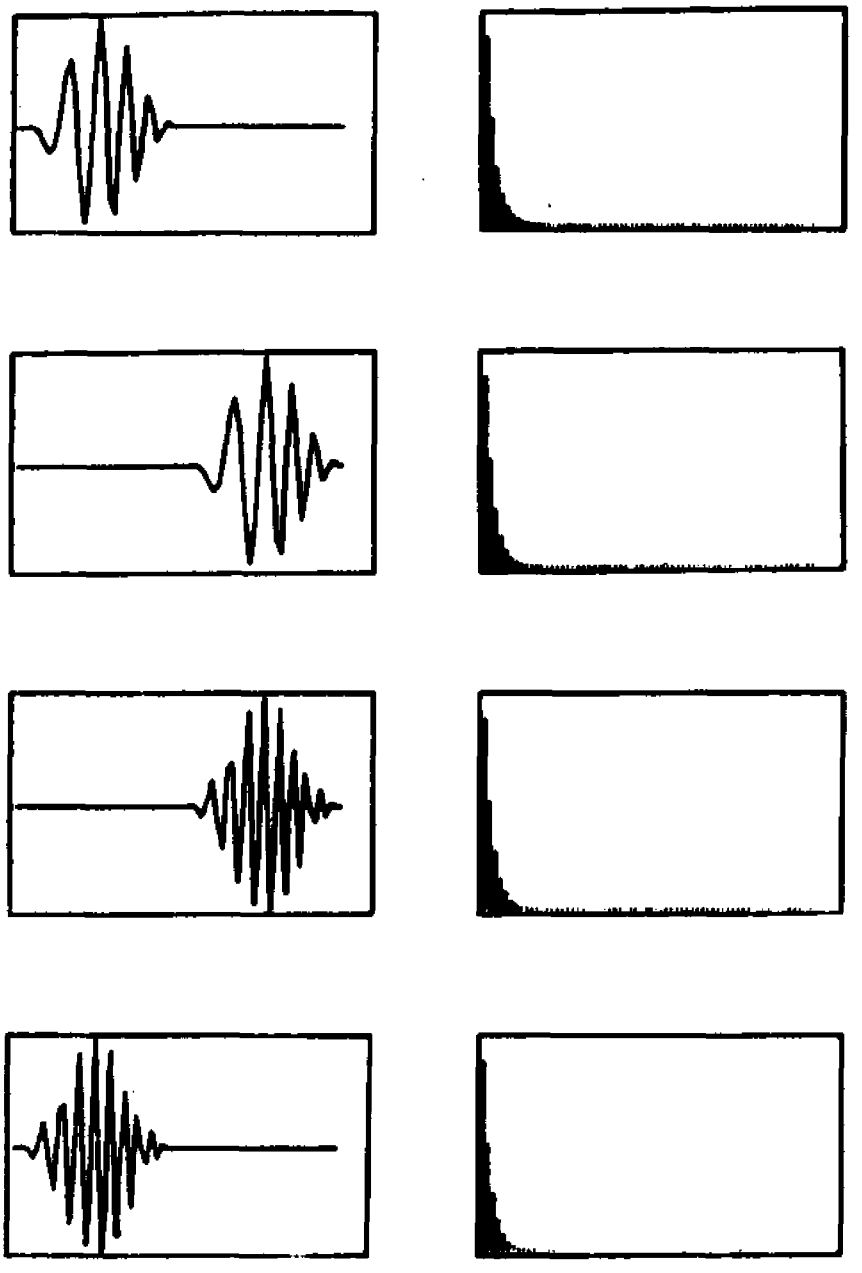

Figure 3. Waveforms and s.v. spectra for chirped RF raised cosine pulses of different central frequencies and delays with the same chirp rate, TB = 4.

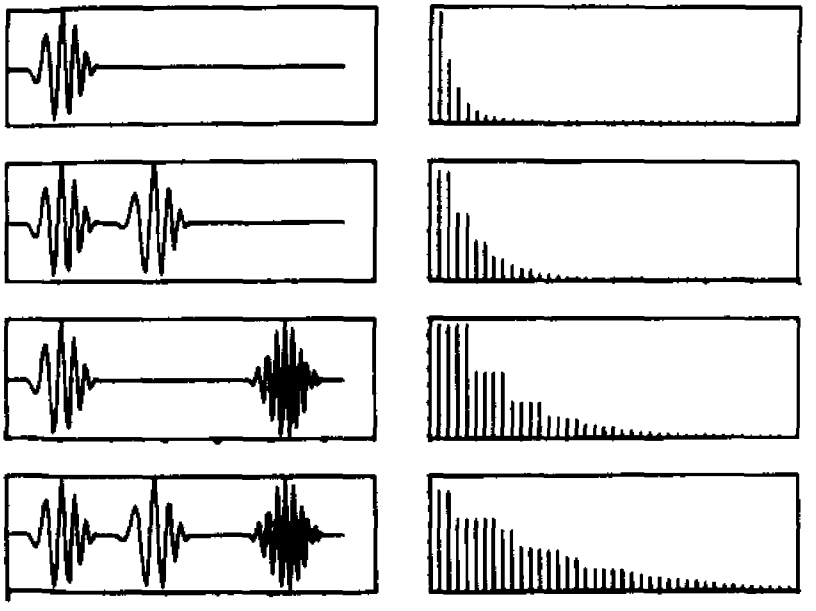

Figure 4. Waveforms and s.v. spectra for different multicomponent signals. Individual components have identical chirp rate and TB = 4.

of W. This is demonstrated in Fig. 3, where four signals with the same time-bandwidth product ($TB = 4$) but with different central frequency and position in time are shown to have identical s.v. spectra. The ambiguity function has the same s.v.'s as its 2-D Fourier transform, the WD. Other time-frequency signal representations that can be obtained from the WD by unitary transformations (such as the Rihaczek distribution) possess the same s.v.'s also.

For a multicomponent signal, containing M similar components displaced in the time-frequency plane, the s.v. spectrum changes as a function of the number of components and their spacing. Fig. 4 illustrates this effect. Each component of the signals in the Figure has $TB = 4$. Notice how the width of the s.v. spectrum increases and its shape changes as the number of components is increased. Also, with the same number of components, the width and shape of the spectrum depend on the spacing between the components in time-frequency plane.

The singular value spectrum has a high data reduction potential. It encodes the following signal features: time-bandwidth product, frequency vs. time dependence, number of signal components and their spacing. The spectrum is invariant to shifts of the signal in time and frequency. It can be obtained by SVD either from the Wigner distribution (which is real-valued), from the ambiguity function (which is complex-valued), or from any other time-frequency representation that is related to WD and AF through a unitary transformation (such as the Rihaczek distribution). Consequently, the s.v. spectrum seems to be well suited for pattern recognition and signal detection tasks. This fact will be demonstrated in subsequent Chapters. In the next section, the potential of the SVD for noise and interference suppression in the Wigner distribution are explored.

4. Enhancement of the Wigner Distribution

The SVD may be used to suppress noise in the WD without smearing it in any direction, thus preserving its resolution. As an example, consider a signal of very low dimensionality, such as the Gaussian high frequency pulse shown in Fig. 5a. The WD of this signal is shown in Fig. 5b and its s.v. spectrum in Fig. 5c. When the same signal is corrupted by noise, $SNR=6dB$, as shown in Fig. 6a, its WD and s.v. spectrum are perturbed as displayed in Figs. 6b and 6c. The amount of noise in the WD is proportional to the noise energy and hence to the observation time. The noise contributions, having larger time-bandwidth product than the signal, are distributed over the larger number of expansion terms than those of the signal. Consequently, by proper truncation of the outer product expansion (20), most of the signal contributions will be retained, while a significant fraction of the noise contributions will be rejected. From the s.v. spectrum shown in Fig. 5c, we see that it is sufficient, in this example, to take only the first expansion term as an approximation of the signal WD. Comparing Fig. 6d with Fig. 5b (ignore the change of scale), the strong noise suppression effect is noticeable. However, for a signal with larger time-bandwidth product this noise suppression gain is smaller. In such a case, the fraction of expansion terms that has to be retained is larger, and so is the amount of noise. As a rule, the smaller the dimensionality of the signal compared to the dimensionality of the noise that falls in the observation interval, the greater the noise reduction potential of this technique. If the number of terms retained after truncation is less than the signal dimensionality, even better noise suppression can be achieved at the expense of some WD distortion. The amount of distortion is proportional to the least squares error (see Eq. (22)).

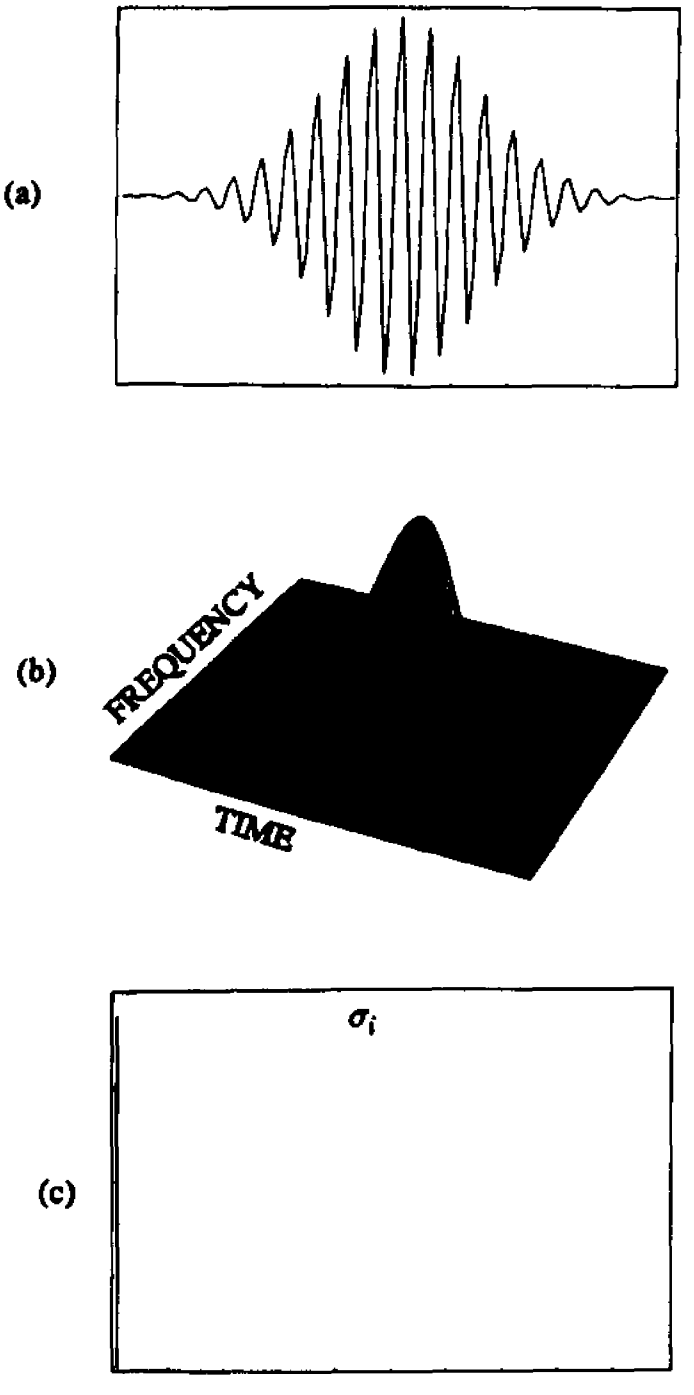

Figure 5. Gaussian RF pulse - (a) waveform, (b) WD perspective plot, (c) s.v. spectrum.

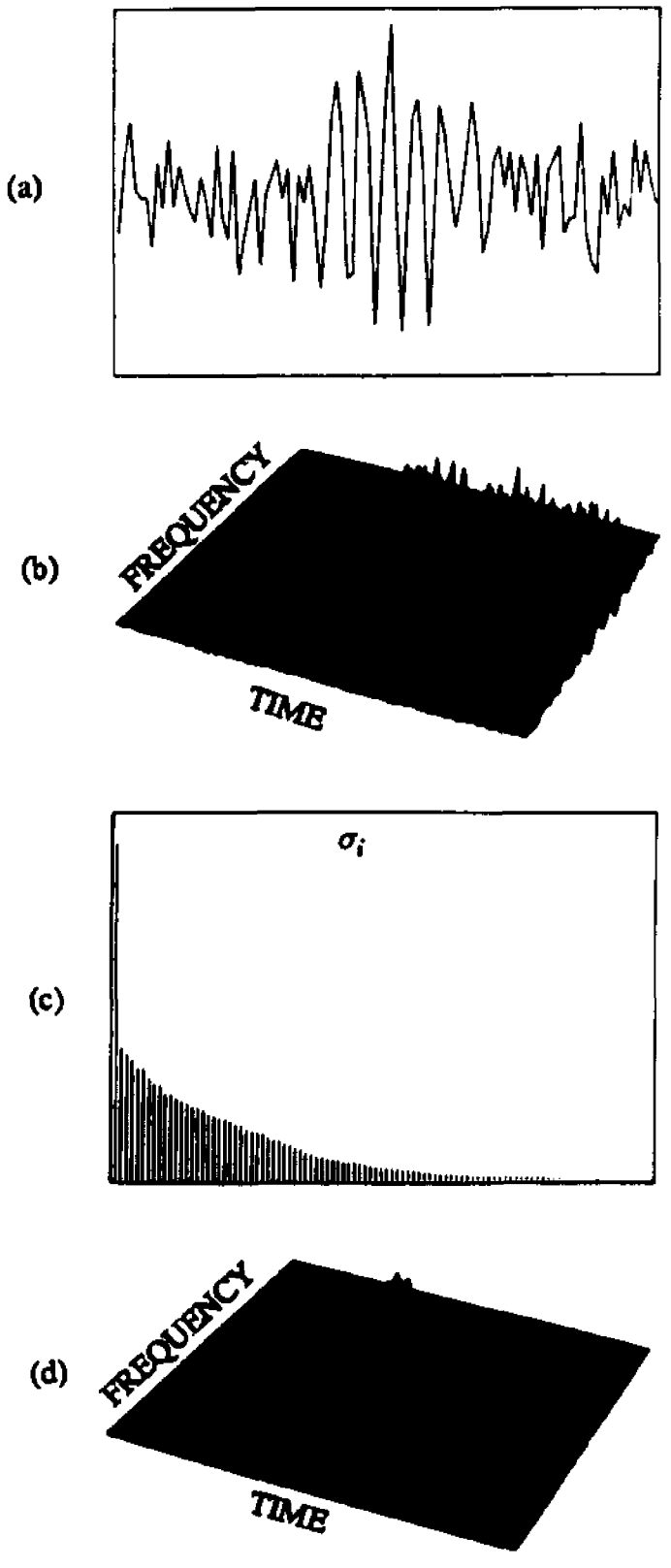

Figure 6. Gaussian RF pulse in noise (S/N = 6dB) - (a) waveform, (b) WD perspective plot, (c) s.v. spectrum, (d) enhanced WD.

The same method may be applied to improve estimates of various signal characteristics that may be obtained from the WD. For example, the squared envelope of the signal and its energy density spectrum, being simple integral transformations of the WD of the signal[1], have series expansions like (23) and (24). To reduce noise effects, these expansions can be truncated as explained above.

All these observations carry over to the case of multicomponent signals. One such signal, that consists of components with low TB product, is depicted on Fig. 7.a. It is an experimentally measured series of ultrasonic echoes in noise, $SNR=15dB$. They were obtained with broadband, Gaussian-like RF driving pulse of $TB<1$. The singular value spectrum of the measured signal is shown in Fig. 7b. Perspective plot of the WD of this signal is shown on Fig. 8.a, together with the first five outer product expansion terms. There are four echoes in the signal on Fig 7.a, so the WD is reconstructed with $K=4$ as the truncation point, and the result is presented on Fig. 8.b. Observe how the noise is almost completely suppressed, and the complex structure of the WD of the multicomponent signal is clearly visible. The signal envelope estimate from the WD on Fig. 8.a is shown on Fig. 9.a, and its improvement obtained with truncation at Fig. 9.b. However, even more could be done for multicomponent signals to separate auto-terms from cross-terms in the WD. The outer products dominated by the auto-terms contain significant fraction of signal energy ϵ_i. Therefore, they are characterized by large σ_i and ϵ_i. Products dominated by the cross-terms exhibit contain very little or no signal energy; the corresponding σ_i are large and ϵ_i are small. Finally, small σ_i and ϵ_i characterize noise dominated expansion terms. Based on these facts, the cross-terms in the WD may be suppressed. Fig. 10.a shows the distribution of energy over the terms of expansion (20) for the signal in Fig. 7a. Notice that

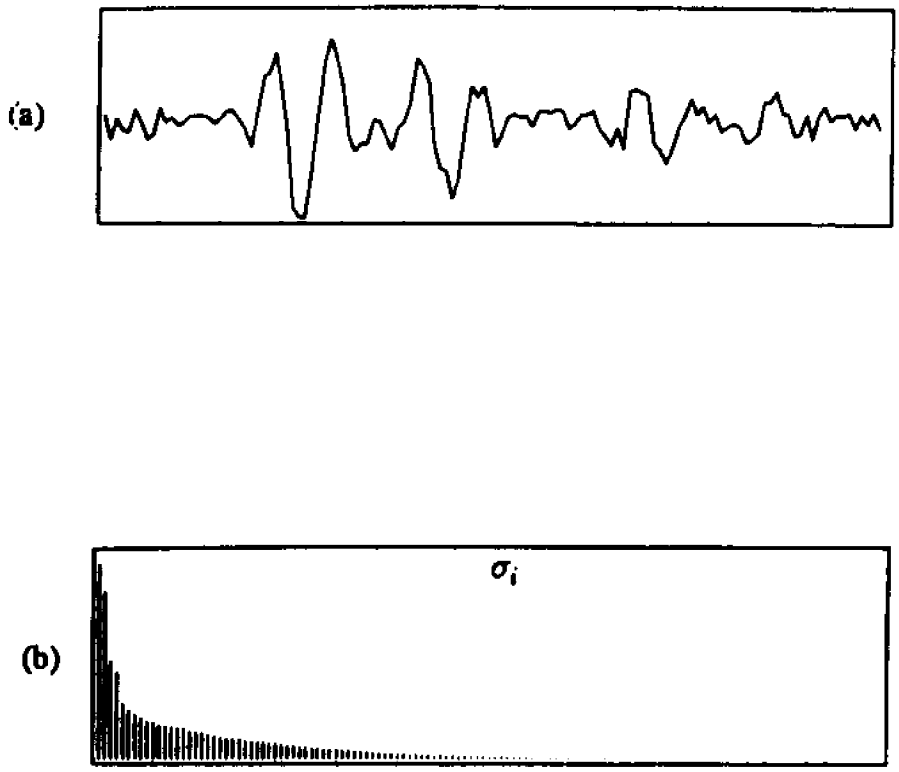

Figure 7. Series of ultrasonic echoes in noise - (a) waveform, (b) s.v. spectrum.

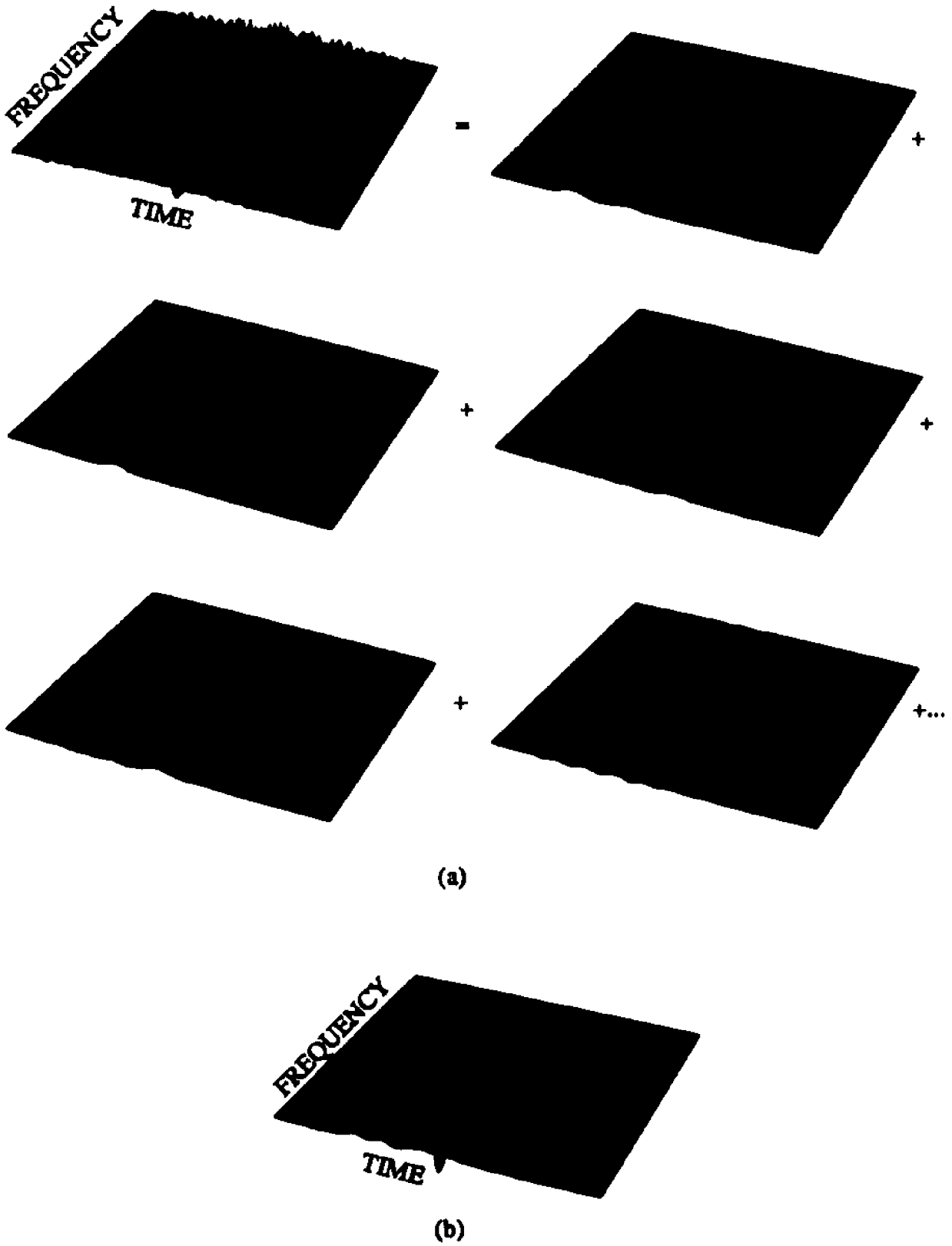

Figure 8. WD perspective plots for the signal in Fig. 7.a - (a) outer product expansion, (b) enhanced WD.

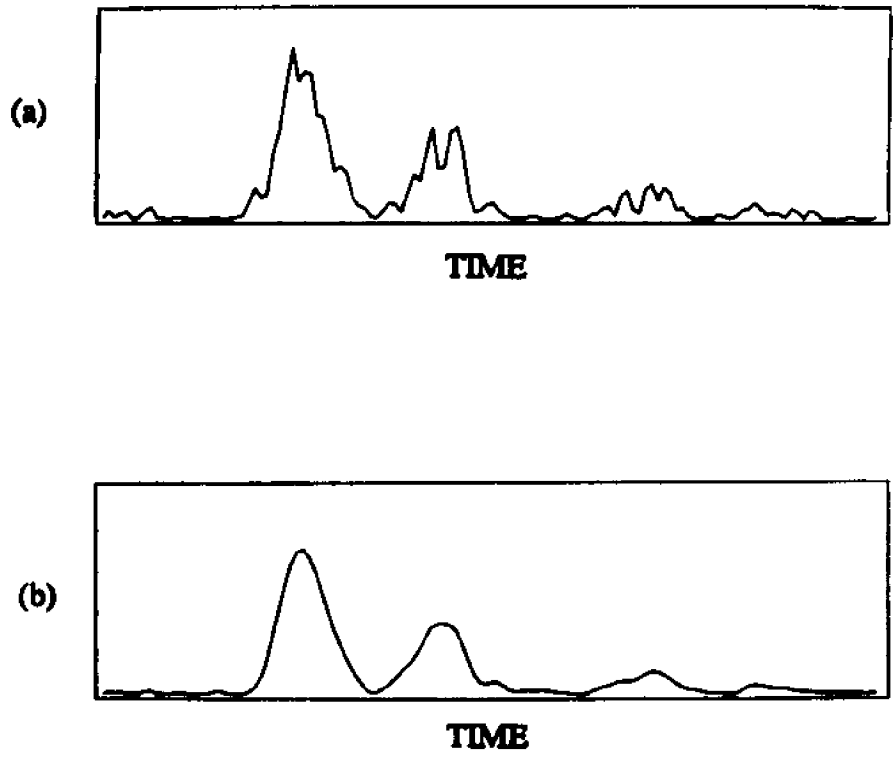

Figure 9. Envelope estimates for the signal in Fig. 7.a - (a) from the original WD on Fig. 8.a, (b) from the enhanced WD on Fig. 8.b.

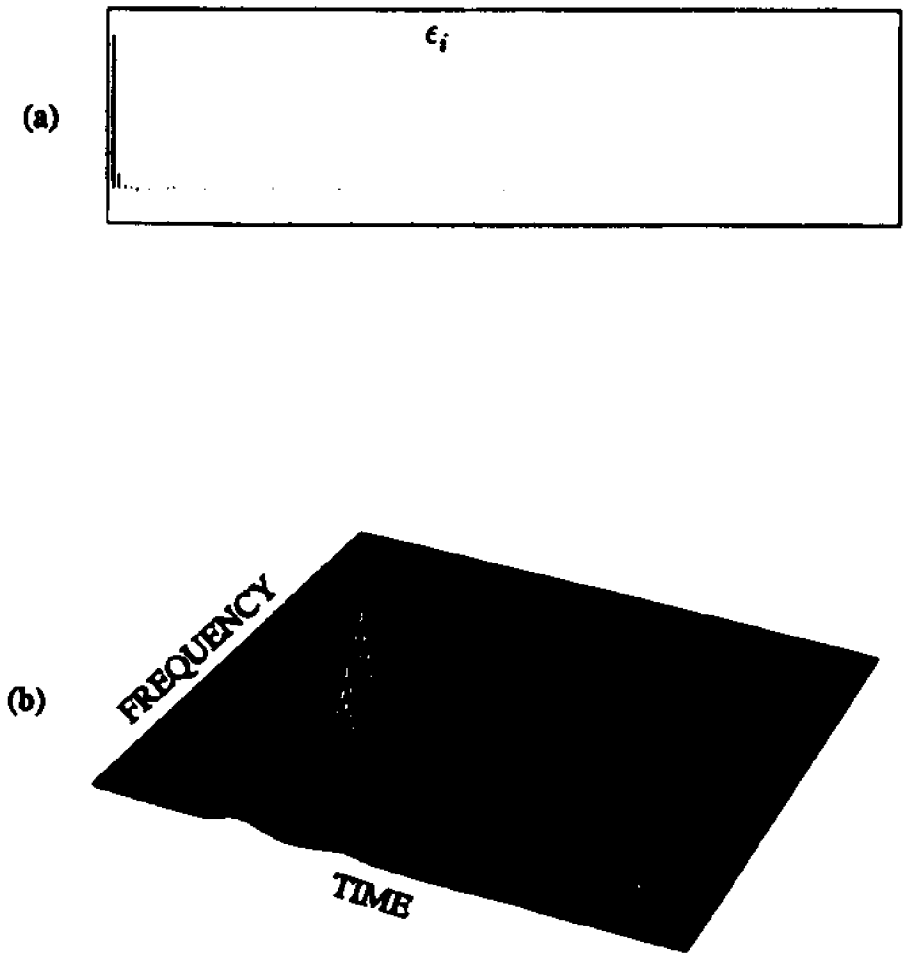

Figure 10. (a) Distribution of energy over the expansion terms. (b) Restored WD auto-terms only.

the auto-terms are mostly concentrated in the first term of the expansion. Using this as the criterion for the truncation of the outer product expansion of the WD, cross-terms were suppressed as shown on Fig. 10.b.

We see that the suppression of both noise and interfering cross-terms is possible using the SVD of the Wigner distribution. The resulting enhancement of the Wigner distribution may be important in situations where a signal has wide dynamic range and low level components in its Wigner distribution are corrupted by noise.

5. Conclusions

The proposed outer product expansion of the WD has high data compression and interference suppression potential, especially for low time-bandwidth signals. Examples involving synthetic and experimental data in noise demonstrate possible enhancement of WD by the proposed method which makes various post-processing techniques potentially more effective. For example, improved estimates of signal parameters can be obtained from the enhanced WD. Also, better performance signal detection and recognition in WD domain is possible.

References

1. T. A. C. M. Claasen and W. F. G. Mecklenbraüker, "The Wigner Distribution - A Tool for Time-Frequency Signal Analysis", *Philips J. Res.* 35, pp. 217-250, 276-300, 372-389, 1980.

2. W. Martin, "Time-Frequency Analysis of Random Signals", *Proc. ICASSP 82*, pp. 1325-1328, Paris, 1982.

3. T. A. C. M. Claasen and W. F. G. Mecklenbraüker, "On the Time-Frequency Discrimination of Energy Distributions: Can They Look Sharper Then Heisenberg?", *Proc. ICASSP 84*, pp. 41B.7.1-4, San Diego, 1984.

4. G. F. Boudreaux-Bartels, "Time Frequency Signal Processing Algorithms: Analysis and Synthesis Using Wigner Distributions", Ph.D. Thesis, Rice University, Houston, 1983.

5. P. Flandrin and W. Martin, "Pseudo-Wigner Estimators for the Analysis of Non-Stationary Processes", *Proc. ASSP Spectrum Estimation Workshop II*, pp. 181-185, Tampa, 1983.

6. P. Flandrin, "Some Features of Time-Frequency Representations of Multicomponent Signals", *Proc. ICASSP 84*, pp. 41B.4.1-4, San Diego, 1984.

7. A. W. Naylor and G. R. Sell, *Linear Operator Theory in Engineering and Science*, Springer-Verlag, 1983.

8. L. E. Franks, *Signal Theory*, Prentice-Hall, 1969.

9. F. Smithies, *Integral Equations*, Cambridge Univ. Press, 1958.

10. K. Fukunaga, *Introduction to Statistical Pattern Recognition*, Academic Press, 1972.

11. H. J. Landau and H. O. Pollak, "Prolate Spheroidal Wave Functions,

Fourier Analysis and Uncertainty - III: The Dimension of the Space Of Essentially Time- and Band-Limited Signals", *BSTJ* Vol. 41, No. 4, pp. 1295-1336, July 1962.

12. C. L. Lawson and R. J. Hanson, *Solving Least Squares Problems*, Prentice-Hall, 1974.

13. G. H. Golub and C. F. van Loan, *Matrix Computations* The Johns Hopkins University Press, 1983.

14. H. C. Andrews and B. R. Hunt, *Digital Image Restoration*, Prentice-Hall, 1977.

15. D. W. Tufts and R. Kumaresan, "Estimation of Frequencies of Multiple Sinusoids: Making Linear Prediction Perform Like Maximum Likelihood", *Proc. IEEE* Vol. 70, No. 9, pp. 975-989, Sept. 1982.

16. J. A. Cadzow, "Spectral Estimation: An Over-Determined Rational Model Equation Approach", *Proc. IEEE* Vol. 70, No. 9, pp. 907-938, Sept. 1982.

17. B. J. Sullivan and B. Liu, "On the Use of Singular Value Decomposition and Decimation in Discrete-Time Band-Limited Signal Extrapolation" *IEEE Trans. Acoust., Speech, Signal Processing*, vol. ASSP-32, no. 6, pp. 1201-1212, Dec. 1984.

18. T. A. C. M. Claasen and W. F. G. Mecklenbraüker, "The Aliasing Problem in Discrete-Time Wigner Distributions," *IEEE Trans. Acoust. Speech, Signal Processing*, vol. ASSP-31, pp. 1067-1072, Oct. 1983.

Chapter 6

Two-Dimensional Shape Description

1. Introduction

Object classification and recognition are among the most fundamental and important problems in computer vision. The significance of shape for object recognition by a human visual system is well understood. Shape is invariant to many variations in the imaging process, such as the changes in lighting conditions, the dynamic range, the signal to noise ratio, the sensor resolution, the detector sensitivity, etc. The problem of shape description, in addition to scene analysis for computer vision, also arises in cell classification in biology and medicine, in chromosome classification in genetics, in the interpretation of X-ray images in radiology, in radar and sonar target identification, etc. [1-10].

In image analysis, for the purpose of classification, an object's boundary extracted from the image represents the shape of the object. Boundary data compression is achieved through the extraction of geometrically invariant features that are used as shape descriptors. A variety of such shape description techniques are available for object classification and recognition[1,2]. They can be called either external, if they rely on local boundary followers that trace the boundary only, or internal, if they rely on global boundary followers that also examine the interior. Alternatively, classification into either scalar transform or space domain techniques is possible. The former produce an array of scalar features used as an input to statistical pattern classifiers, while the latter transform an image into another image to be used as an input to subsequent syntactic pattern classifiers. Depending on whether it is possible

to reconstruct the boundary from the descriptors or not, the distinction can be made between information preserving and non-preserving techniques.

Shape descriptors must be invariant to scaling, to rotation, to translation of the boundary, to change of the starting point and to the direction of boundary tracing. Recognition of both the similarities and the differences between shapes should be facilitated. Significant dimensionality reduction, equivalent to data compression, should be achieved. Descriptors should be sensitive to local boundary variations while insensitive to noise and fuzziness in the boundary description.

There are several boundary representations employed with external scalar transform techniques. For example, Cartesian coordinates as functions of arc length have been suggested[3,4,5]. Other parametrizations, such as local tangent angle, cumulative angular bend[5,6], or relative angular bend[7] as functions of arc length have been employed also. Alternatively, the curvature or the radius of the curvature as functions of arc length have been preferred sometimes[8]. For a restricted class of boundaries, polar coordinates can be chosen[9]. More recently, the radius as a function of arc length has been used[10]. While some of these representations are inherently shape invariant, others may require normalization. However, all of the above representations are parametrizations of the boundary as a periodic function of single independent variable.

Standard scalar transform methods are based either on the method of moments[1], or on the Fourier analysis of some function derived from the boundary[3-8], or on the circular auto-regressive (CAR) modeling of the boundary[9,10]. The major drawback of the moment method is that the first few moments carry significant information only for simple but not for more compli-

cated objects[1]. The problem with the other two methods is their relative insensitivity to local shape variations[1].

This paper presents a novel shape description method that is based on the representation of a boundary in space - spatial frequency domain. It combines two signal processing tools - the Wigner distribution (WD) and the singular value decomposition (SVD). It is expected that the method will be useful in applications where boundaries need to be classified according to their signature in the space - spatial frequency plane. For shape classification, one of the many 1-D representations of the 2-D contours is employed. Boundary features, or shape descriptors, are obtained using singular value decomposition of the WD. The rationale for this approach lies in the properties of WD singular values - they encode certain shape features such as the space-bandwidth product, the shape complexity in terms of number of components and their spacing, and the spatial frequency vs. the space dependence. The singular values of the boundary WD possess all the properties required of good shape descriptors. To illustrate the effectiveness of these descriptors in shape classification, a number of examples are presented. The proposed method is useful, more generally, for robust classification of any 1-D waveforms.

2. Boundary Representation in Space - Spatial Frequency Domain

For a case of a periodic function of spatial variable, such as the boundary of an object, the boundary WD (BWD) is defined as

$$W_f(x,m) = \frac{1}{S}\int_{-S/2}^{S/2} f(x+\sigma/2)f^*(x-\sigma/2)\, e^{-j\frac{2\pi m}{S}\sigma}\, d\sigma, \qquad 0\leq x\leq S \qquad (1)$$

where S is the spatial period.

For the numerical evaluation of the BWD, the boundary is sampled at N points and $N\times M$ matrix $W(n,m)$ of BWD samples is obtained as outlined in

earlier chapters. Because the BWD is a 2-D representation of a 1-D signal, it is a redundant representation. To reduce the BWD redundancy, the SVD is used, as explained in Chapter 5:

$$W(n,m) = U\ D\ V^T = \sum_{i=1}^{N} \sigma_i u(n)_i v^T(m)_i, \quad \|W\|^2 = \sum_{i=1}^{N} \sigma_i^2 \tag{2}$$

where T denotes a transpose, and $D = diag(\sigma_1, \sigma_2, \ldots, \sigma_N)$. The numbers $\sigma_1 \geq \sigma_2 \geq \cdots \geq \sigma_N$ are the singular values (s.v.) of the BWD with following properties (Chapter 5). Permutations of the rows (columns), or unitary transformations of W, lead to similarity transformations on WW^T and $W^T W$. Consequently, the s.v.'s are invariant to these transformations. The s.v.'s are also invariant to spatial shifts of the signal (and also to spatial frequency shifts of the analytic signal) since these shifts correspond to permutations of rows (columns) of W. If S and B are the essential space- and band-limits of the signal defined such that only δ fraction of its energy lies outside, the essential dimensionality of this signal is $2BS$. For a monocomponent signal, in the absence of noise, the number of significant expansion terms that contain $(1 - \delta)$ fraction of the signal energy is approximately equal to the dimensionality of the signal $K(\delta) = 2B(\delta)S(\delta)$.

As shown in Chapter 5, the s.v.'s of the WD encode certain invariant features of the signal such as the space-bandwidth product, the signal complexity in terms of number of components and their spacing, and the spatial frequency vs. space dependence. Therefore, the s.v.'s of the BWD are proposed for descriptors of shape.

3. The singular value shape descriptors

Let the boundary be represented by the circular sequence $r(n)$. The sequence $r(n)$ can be any of the various representations for 2-D shape boun-

daries. We next evaluate its WD and perform a SVD of the result. The set of singular values, thus obtained, represents the desired feature vector that describes the boundary shape. We term these singular values as the singular value descriptors (s.v.d.'s).

The s.v.d.'s satisfy all shape description requirements. For boundary rotation, or for change in the starting point, $r(n)$ shifts circularly resulting in row permutation of the WD matrix. A change of the direction of tracing results in a reflection of $r(n)$ which is another row permutation of W. These row permutations do not change the s.v.d.'s. The translation and scaling of the image do not change $r(n)$, and hence the s.v. descriptors are invariant. Even if the boundary representation is not scale invariant, the complexity of the signal, the nature of spatial frequency vs. space dependence and the space-bandwidth product remain the same, and the s.v.d.'s do not change. Therefore, none of the invariance properties of the s.v.d.'s, except translation invariance, depend on the particular choice of the boundary representation. Since all of the standard representations are translation invariant, any one of them can be used to produce a particular set of s.v.d.'s. The number of essentially non-zero s.v.d.'s is equal to the space-bandwidth product of $r(n)$ which, in general, is not large. In the examples that follow, it will be demonstrated that only a few dominant s.v.d.'s are sufficient for successful shape classification. This means that s.v.d.'s achieve a high degree of data compression. The noise induced perturbations are distributed almost uniformly over all s.v.d.'s resulting in a high signal-to-noise ratio for the dominant s.v.d's (see Chapter 5). This property provides for the good noise immunity of these descriptors. Using different examples, other properties of s.v.d.'s, such as the tolerance to within-class variations, good between-class separation, and a sensitivity to local shape variations will also be demonstrated.

4. Classification of shapes

In the examples that follow, the boundary is represented by a 1-D sequence of radial distances measured from the centroid to each of N equidistant points on the boundary, $r(n)$ It can be shown that the circular sequence $r(n)$ is scale, rotation and translation invariant, and provides an unambiguous representation of arbitrarily complex boundaries[9-10]. It is rather insensitive to noise. Because of the nonlinear nature of the feature extraction process, these properties do not propagate directly into the s.v.d's. As explained above, however, the corresponding s.v.d.'s properties are not induced by the particular choice of boundary representation.

Several examples are used to illustrate the classification potential of the s.v. descriptors. In all of the examples, the contours have been hand digitized using a digitizing tablet, the samples were interpolated, and then resampled to obtain a set of equidistant points. This process introduces a substantial amount of boundary noise, or uncertainty. However, it will be seen that this does not impair the classification performance of the s.v.d.'s.

The contour in Fig 1.a has been geometrically transformed in several ways as shown on Figs. 1.b, 1.c, and 1.d. Both the starting point and the direction of boundary tracing are indicated on the figures. Boundaries were sampled at 128 equidistant points. Fig. 2 shows the resulting representations $r(n)$. Noticeable are the ripples introduced by the digitizing process. The WD of the contour in Fig. 1.a, and twenty largest s.v. descriptors are displayed in Figs. 3.a and 3.b. The relative scatter among the feature vectors, caused by the imperfection of digitizing process, is less then 2% illustrating the invariance property of the s.v.d.'s.

In Figure 4. two classes of shapes are presented. A significant degree of

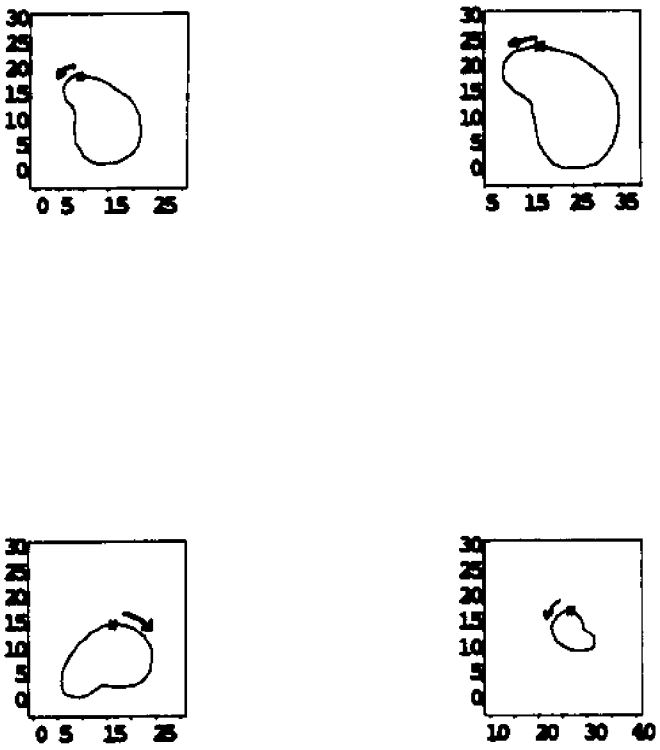

Figure 1. Geometrical transformations of the boundary.

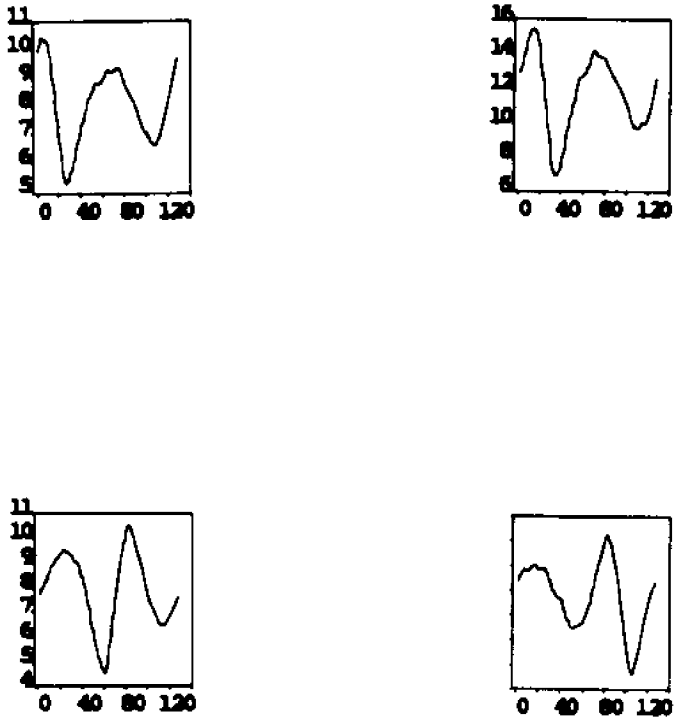

Figure 2. Boundary representations of shapes on Fig. 1.

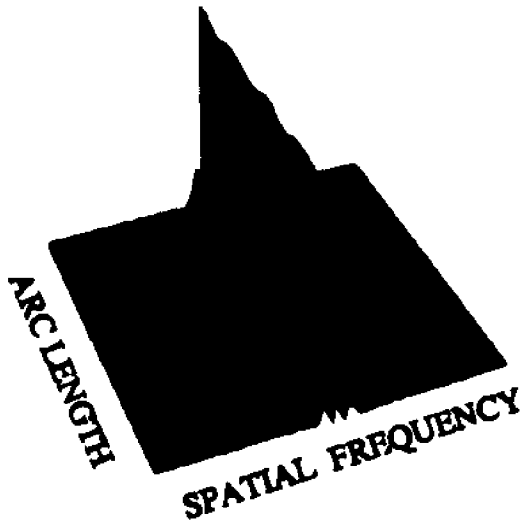

(a)

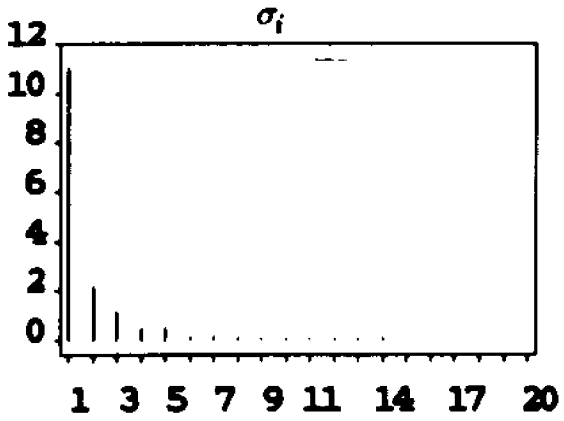

(b)

Figure 3. (a) The WD of the boundary on Fig. 2.a. (b) The singular values of the distribution on Fig. 3.a.

variability exists within each class. The boundaries were sampled at 128 equidistant points. The largest twenty s.v. descriptors for typical members of each class, A0 and B0, are shown in Fig. 5.a. Fig. 5.b displays a scatter plot of the pairs of dominant s.v.d.'s. Noticeable is the tight clustering of shapes within each class and the good separation between the clusters. This demonstrates the high tolerance to intra-class variability and good inter-class separability provided by the s.v.d.'s. Moreover, this result was achieved using only two of the largest s.v.d.'s, demonstrating the high data compression property of the descriptors.

To show the sensitivity of the s.v.d.'s to local shape variations, even with large intra-class variations, forty hand printed Roman characters B and D, collected in Fig. 6, were analyzed. The characters were represented by their outer boundary sampled at 32 points. The notch in the boundary of B, represents the localized shape variation that distinguishes it from the boundary of D. Using four dominant s.v.d.'s as a feature vector, boundaries were classified using standard hierarchical clustering based on the simple Euclidean distance measure[11]. Fig. 7.a shows the resulting clustering tree. In this diagram, the vertical spacing between the nodes indicates the separation between the classes. Two well separated clusters are noticeable, one containing the B's and the other containing the D's. As shown on the scattering diagram of Fig. 7.b, clear separation exists even if only two dominant s.v.d.'s are used.

The digitized boundaries of six aircrafts, displayed in Fig. 8.a, were used to show that the s.v.d.'s are also appropriate for complex shapes. The clustering diagram of Fig. 8.b is obtained using four largest s.v.d.'s, while Fig. 8.c displays the scatter plot of two dominant s.v.d.'s. It is clear that the s.v.d.'s provide high degree of data compression.

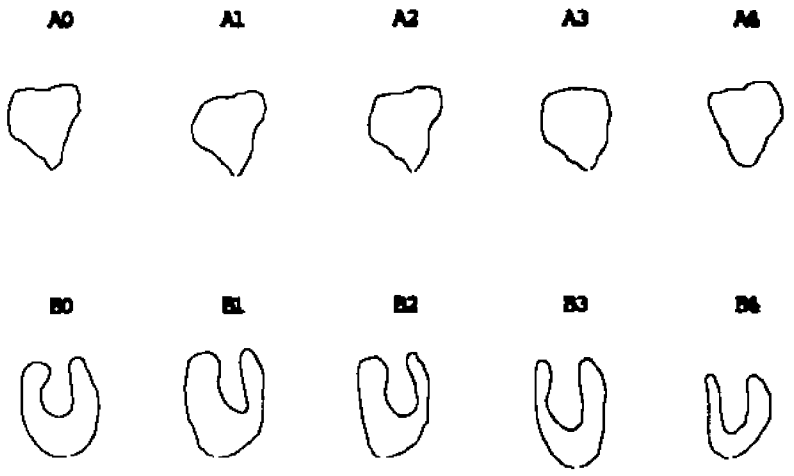

Figure 4. Two classes of shapes with substantial intra- class variation.

(a)

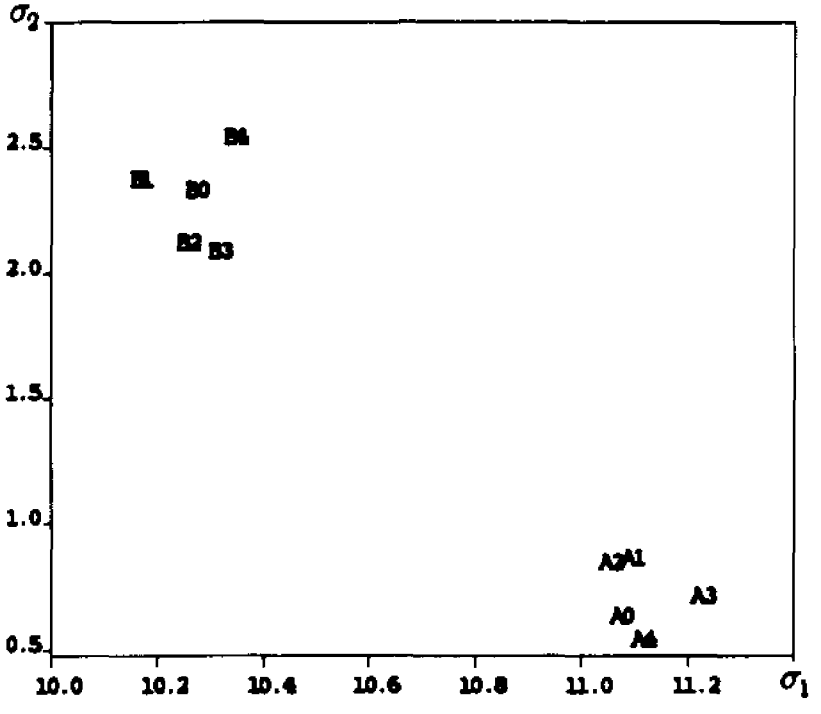

(b)

Figure 5. (a) The twenty dominant s.v.d.'s for shapes A0 and B0. (b) Scatter plot of the two dominant s.v.d.'s for shapes in Fig. 4.

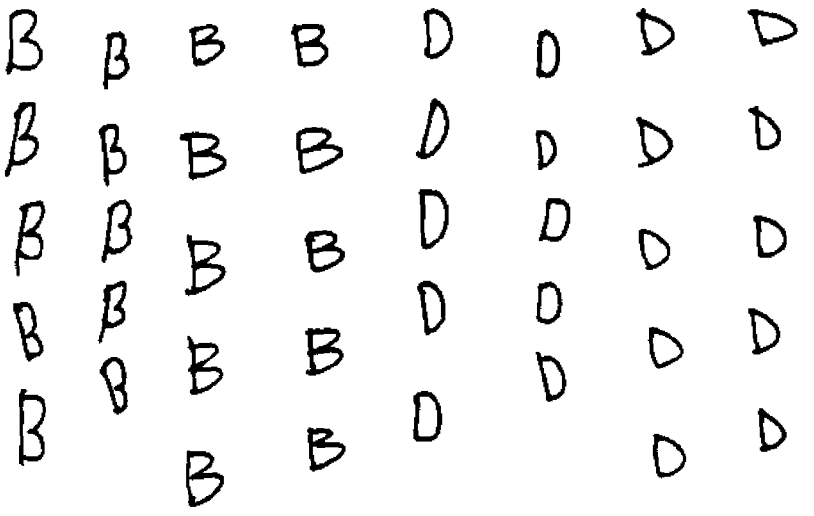

Figure 6. Hand-printed character set.

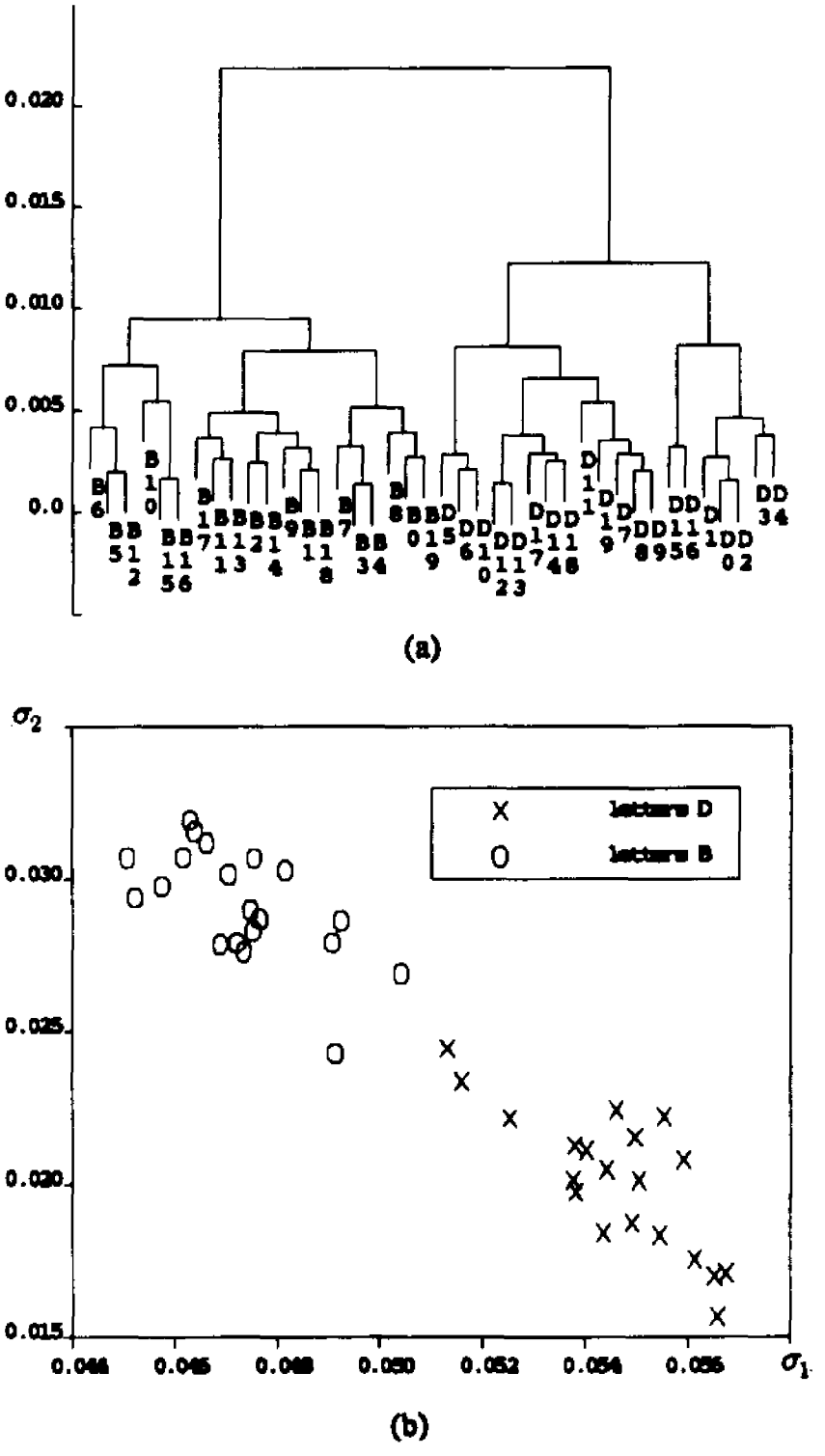

Figure 7. (a) The clustering tree obtained using first four s.v.d.'s for letters in Fig. 6. (b) Scatter plot of the first two s.v.d.'s for the same letters as in (a).

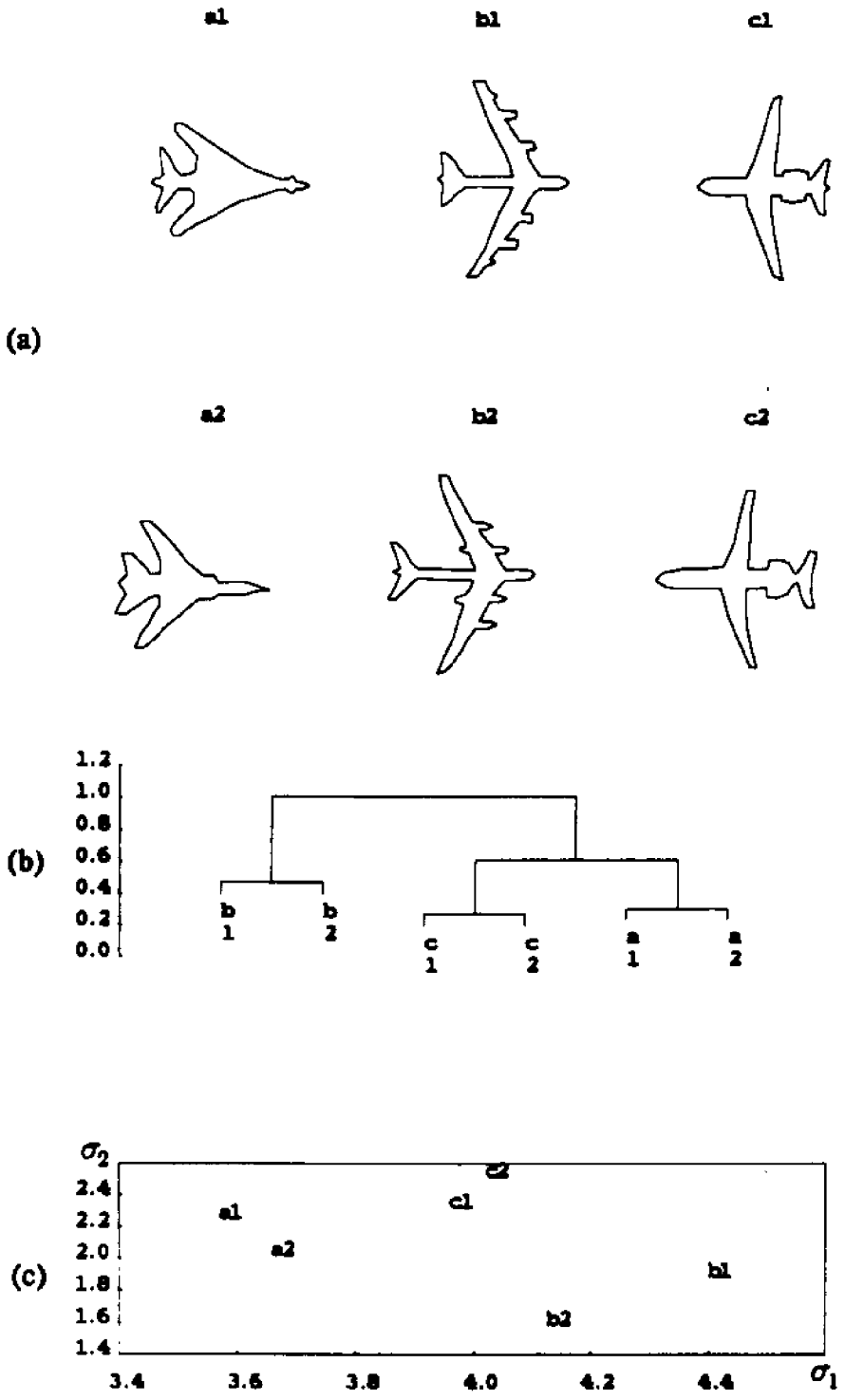

Figure 8. (a) Set of aircraft boundaries. (b) The clustering tree obtained with four dominant s.v.d.'s. (c) Scatter plot of the two dominant s.v.d.'s for shapes in (a).

Due to the ordering of the s.v.'s, increasing the number of s.v.d.'s used for classification would only improve the resolution of the classifiers in all of the above examples. It should be underscored that the above results were obtained using a non-optimal classification procedure. Further performance improvement can be achieved if more sophisticated, optimal and other sub-optimal procedures, are used. For example, the Fukunaga-Koontz or the Foley-Sammon transformation of the feature vector can be performed to maximize the inter-class separation[12].

5. Conclusions

The singular values of the boundary WD are proposed as shape descriptors. They possess all the shape descriptors properties. The singular values are invariant to all geometrical transformations of shapes normally encountered during imaging, segmentation and boundary tracing. They provide a high degree of data compression and good noise immunity. Small changes in the object result in small changes in the descriptors. Tolerance to intra-class variations is significant, while good inter-class separability is maintained. The singular value descriptors are also sensitive to local shape variations. In spite of the increased computational complexity associated with the calculation of the WD and the SVD, it is hoped that the s.v. descriptors will find applications in shape classification primarily due to their robustness, high data compression and other properties described above. More generally, the singular values of the WD should also be useful for classification of arbitrary 1-D patterns.

References

1. T. Pavlidis, "A Review of Algorithms for Shape Analysis," *Computer Graphics and Image Processing*, vol. 7, pp. 243-258, Apr. 1978.

2. T. Pavlidis, "Algorithms for Shape Analysis of Contours and Waveforms," *IEEE Trans. Pattern Anal. Machine Intell.*, vol. PAMI-2, no. 4, pp. 301-312, July 1980.

3. G. H. Granlund, "Fourier Preprocessing for Hand Print Character Recognition," *IEEE Trans. Comput.*, vol. C-21, pp. 195-201, Feb. 1972.

4. C. W. Richard and H. Hemami, "Identification of Three-Dimensional Objects Using Fourier Descriptors of the Boundary Curve," *IEEE Trans. Syst., Man, Cybern.*, vol. SMC-4, pp. 371-378, July 1974.

5. E. Persoon and K. S. Fu, "Shape Discrimination Using Fourier Descriptors," *IEEE Trans. Syst., Man, Cybern.*, vol. SMC-7, pp. 170-179, March 1977.

6. C. T. Zahn and R. Z. Roskies, "Fourier Descriptors for Plane Closed Curves," *IEEE Trans. Comput.*, vol. C-21, pp. 269-281, March 1972.

7. A. Oliviero and G. Scarpetta, "A New Approach to Contour Coding," *Computer Graphics and Image Processing*, vol. 15, pp. 87-92, Feb. 1981.

8. D. H. Ballard and C. M. Brown, *Computer Vision*, Prentice-Hall, Englewood Cliffs, 1982.

9. R. L. Kashyap and R. Chellappa, "Stochastic Models for Closed Boundary Analysis: Representation and Reconstruction," *IEEE Trans. Inform. Theory*, vol. IT-27, no. 5, pp. 627-637, Sept. 1981.

10. P. F. Singer and R. Chellappa, "Classification of Boundaries on the Plane Using Stochastic Models," *Proc. CVPR-83*, pp. 146-147, June 1983.

11. K. Fukunaga, *Introduction to Statistical Pattern Recognition,* Academic Press, 1972.

12. D. Casasent and V. Sharma, "Feature extractors for distortion-invariant robot vision", *Optical Engineering,* vol. 23, no. 5, pp. 492-498, Sept./Oct. 1984.

Chapter 7

Tissue Characterisation

1. Introduction

Estimation of the ultrasound attenuation of tissue is an important area for research in medical ultrasonics. This tissue parameter, once properly measured, promises to be useful for tissue characterization, in general, and for discriminating diffuse liver diseases, in particular [1,2]. Many techniques have been advanced to determine the tissue attenuation from the echo signal of the broadband ultrasonic pulse used in forming conventional medical ultrasonic images. In this setting, while the transducer is rotated over a limited angular segment, a radio-frequency (RF) ultrasonic pulse is transmitted periodicly and an echo signal is received. In this way, an area in the tissue can be effectively scanned. An echo signal received from a single angular direction during the scanning process is called an A-line.

One useful approach to tissue characterization exploits the empirical observation that ultrasonic attenuation in tissue increases roughly in proportion to frequency [3,4]. The mean frequency of a broadband pulse steadily decreases as the pulse propagates through tissue since its high frequency components are attenuated more strongly than its low frequency components. The downward shift in mean frequency with depth in a train of ultrasonic echos, then, provides a direct measure of the slope of attenuation versus frequency.

In extracting the attenuation from the frequency variation one must take into account a number of important physical effects, such as the initial pulse spectrum, the transducer diffraction and the precise form of the frequency dependence of the attenuation. However, an accurate estimate of the

frequency variation with depth is the key element required in this approach. The commonly used methods for evaluating this frequency shift require averaging of the estimates from a large number of A-lines in order to suppress noise-like variations in the local frequency caused by interference effects [4,5]. In this chapter, an efficient technique is presented for the estimation of intrinsic frequency variation from an ultrasonic A-line with little or no averaging between the lines. By identifying echo segments corrupted by interference-induced noise, we eliminate the need for averaging large amounts of data. These segments are rejected in evaluating the local frequency. The identification is achieved using the singular value decomposition (SVD) on the Wigner distribution (WD) of the signal. The method essentially performs a non-linear filtering of the echo signal to reduce greatly the interference effects between overlapping echoes - both the correlated noise, as well as the uncorrelated electronic noise. Then, the local frequency is evaluated both accurately (i.e. without bias by noise) and efficiently (i.e. with a small data set). This analysis is carried out on the Wigner time-frequency function calculated from a segment of echo data. With the help of the singular value decomposition of the Wigner distribution, echo segments corrupted by interference and noise are rejected. In this way, correlated interference is suppressed much more efficiently than by averaging. This method is then applied on the traditional problem of estimating the attenuation slope from the downward shift in mean frequency with depth. Analysis of simulated echoes shows that accurate estimates can be obtained from a single A-line. Moreover, the correct answer is obtained with two orders of magnitude less data than the conventional Fourier approach. The resulting savings in data acquisition time and computation time are substantial.

2. The SVD of the Ultrasonic Echo's Wigner Distribution

Among joint time-frequency representations of finite energy signals, periodic signals and harmonizable random signals, the Wigner distribution is optimal in many respects[6-7]. It encodes important physical information about the signal in the form of a local frequency "spectrum". Ultrasonic echo is a bandpass signal. When dealing with such signals, it is more convenient to work with the WD of the corresponding analytic signal.

The WD properties were discussed in earlier chapters. Only the most pertinent results will be repeated here. We shall assume that the signal is analytic. For finite energy signals, the volume under the WD is equal to the signal energy or, for finite power signals, to the signal power. Projection of the WD on the time axis is equal to the squared magnitude (instantaneous power) of the signal:

$$\int_{-\infty}^{\infty} W_z(t,f)df = |x(t)|^2 \tag{1}$$

The energy density spectrum can be obtained as the projection onto the frequency axis:

$$\int_{-\infty}^{\infty} W_z(t,f)dt = |X(f)|^2 \tag{2}$$

The instantaneous frequency, which is meaningfully defined only on the analytic signal associated with a real bandpass signal, is the first local moment in the frequency variable of the WD of that analytic signal:

$$f_i(t) = \frac{\int_{-\infty}^{\infty} f\ W_z(t,f)df}{|x(t)|^2} \tag{3}$$

For the numerical evaluation of the WD, the signal is sampled. From the N data samples, a discrete approximation of the continuous signal WD is calculated. There are several procedures to evaluate sampled WD[8]. Regardless of the method used, the result is an $N \times M$ matrix W(n,m) of WD samples. Because the WD is a 2-D representation of a 1-D signal, it is a redundant representation. For the redundancy suppression and the enhancement of the WD, the singular value decomposition (SVD), introduced in Chapter 5, can be used. With this technique, improved signal parameter estimates are obtained from the WD.

In finite dimensional linear spaces, the singular value decomposition is essentially a generalization of the eigen-analysis to non-symmetric and even non-rectangular matrices. The sampled WD matrix W(n,m) is an example of such a matrix, and its decomposition, given in Chapter 5, is:

$$W(n,m) = U\ D\ V^T = \sum_{i=1}^{N} \sigma_i u_i(n) v_i^T(m), \qquad \|W\|^2 = \sum_{i=1}^{N} \sigma_i^2 \tag{4}$$

where T denotes a transpose, and D is the diagonal matrix, $D = diag(\sigma_1, \sigma_2, \ldots, \sigma_N)$. The numbers $\sigma_1 \geq \sigma_2 \geq \cdots \geq \sigma_N$ are the positive square roots of the eigenvalues of the square matrix WW^T (and $W^T W$ also), and are called the singular values (s.v.) of the matrix W. The columns of U (or V) are orthonormal eigenvectors u_i (or v_i) of WW^T (or $W^T W$). The set $\{u_i, v_i; \sigma_i\}$ is called the singular system of the matrix W. The singular vectors u_i are functions of the sampled time variable - n, while v_i are functions of the sampled frequency variable - m. As shown in Chapter 5, any linear transformation, with W as the transformation matrix, can be expanded in terms of one or the other set of singular vectors. Specifically, the sampled squared envelope of the signal, Eq. (1), and the sampled energy density spec-

trum, Eq. (2), admit orthogonal expansions:

$$|x(n)|^2 = We = \sum_{i=1}^{N} \sigma_i (e^T v_i) u_i(n) \tag{5}$$

$$|X(m)|^2 = W^T e = \sum_{i=1}^{N} \sigma_i (e^T u_i) v_i(m) \tag{6}$$

where $e = [1\ 1\ 1\ \cdots\ 1]^T$, and expression in parenthesis represents the inner product of vectors. Similarly, if $p = [0\ 1\ 2\ 3\ \cdots\ N-1]^T$, it follows that the vector Wp has the expansion

$$Wp = \sum_{i=1}^{N} \sigma_i (p^T v_i) u_i(n) \tag{7}$$

Therefore, sampled instantaneous frequency, Eq. (3), can be expressed as

$$f_i(n) = f_s \frac{\sum_{i=1}^{N} \sigma_i (p^T v) u_i(n)}{\sum_{i=1}^{N} \sigma_i (e^T v_i) u_i(n)} \tag{8}$$

where f_s is the sampling frequency.

It has been shown in Chapter 5 that the low order expansion terms carry gross information about the signal, while the higher order expansion terms reveal the fine structure in the signal. If all but K s.v.'s are close to zero, the above expansions (4)-(8) can be truncated to K terms, resulting in the best least squares approximation of W by a matrix of the lower rank $K < N$. The least squares error is equal to the sum of the squares of the deleted singular values. In the presence of noise, we can enhance the Wigner distribution and improve signal parameter estimates by properly truncating the expansions in Eqs. (4)-(8).

As explained in Chapter 5, the s.v. "spectrum" of the Wigner distribution encodes certain invariant features of the signal such as the time-bandwidth

(TB) product, the signal complexity in terms of the number of components and their spacing, and the frequency vs. time dependence. These features in an ultrasonic echo reflect the attenuation and the scattering characteristics of the medium. Therefore, using the s.v. spectrum it is possible to separate those segments of an ultrasonic A-line that have stable local frequency (small TB-product) from the ones with unstable local frequency variation (large TB-product).

3. Estimation of the Frequency Shift in Tissues - the Method

To illustrate the idea behind the method, consider the example shown in Fig. 1. The signal in Fig. 1.a is composed of four Gaussian RF pulses, two of which overlap - a composition similar to a typical ultrasonic A-line segment. In constructing this signal, prior to the superposition of pulses, the frequency within each pulse is chirped and the central frequency is shifted down going from the first to the last pulse. The resulting built-in frequency trend is indicated in Fig. 1.b by the dotted line. The instantaneous frequency in the composite signal, calculated using Eq. (3), exhibits a different variation with time as displayed in Fig. 1.b by the solid line. The transient effects, shown in Fig. 1.b, are a consequence of the phase differences between the adjacent pulses.

We are interested in estimation of the local frequency variation trend, not in the transients that obscure it. The standard approach is to extract a signal segment by windowing, calculate its Fourier spectrum, and determine the spectral centroid. This process is repeated for different positions of the sliding window. The shift in the spectral centroid delineates the local frequency variation trend. Typically, window lengths between one and eight pulse lengths are used. However, when the sliding window extracts the two randomly spaced overlapping pulses, the mean frequency of the corresponding spectrum

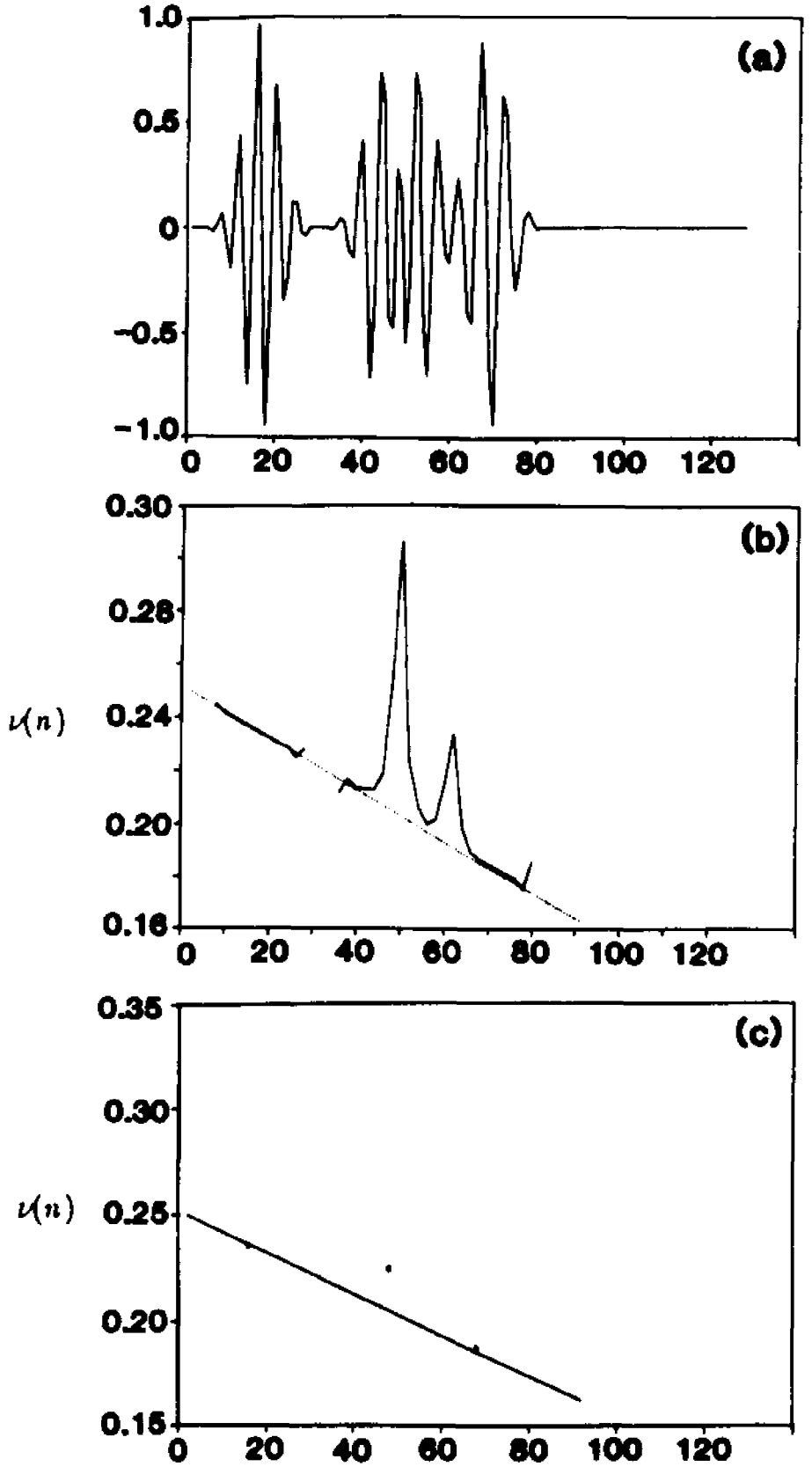

Figure 1. (a) Four partially overlapping Gaussian RF pulses. (b) Instantaneous frequency (solid line) and the built-in trend (dashed line) for the signal in (a).. (c) Short-time FT centroid estimates (points) and the built-in trend.

is a random variable. This random variable can significantly deviate from the overall trend. Fig. 1.c shows the centroid frequency estimates (points), obtained with this standard procedure, for three adjacent, non-overlapped positions of the 32-point rectangular window. Notice the significant deviation from the reference trend (solid line) at the middle window position. This noise-like deviation of the centroid frequency results from interference between randomly spaced overlapping pulses, and is thus correlated with the signal (unlike thermal noise). In the centroid frequency estimation from an ultrasonic echo signal, the conventional remedy is to use longer windows for smoothing along an A-line, and to average many lines. However, since the interference is correlated with the signal, and adjacent lines are correlated with each other, effective suppression of this type of noise requires averaging of excessive amounts of data. To use independent A-lines only, data should be taken from large tissue regions. As a result, genuine differences of trends between individual A-lines, that are due to the tissue characteristics, may also be averaged out in the process.

A much more efficient approach is to discard the noisy segments using the SVD of the WD. We can discriminate the stable from the unstable (noisy) local frequency points using the s.v. spectrum. Fig. 2 shows three sets of the WD s.v.'s obtained from the same windowed data as used in Fig. 1.c. To insure that the s.v. spectra are insensitive to pulse amplitude variations, prior to application of the SVD, the WD's are normalized to unit energy. The first window contains an isolated Gaussian RF chirp pulse resulting in the narrowest s.v. spectrum. The second window contains two pulses. Strong transient effect that exists between the two pulses (see Fig. 1.a) substantially increases the TB product of the extracted signal segment. Therefore, its s.v. spectrum is wide. In the last window (see Fig. 1.a), there is a slight overlap

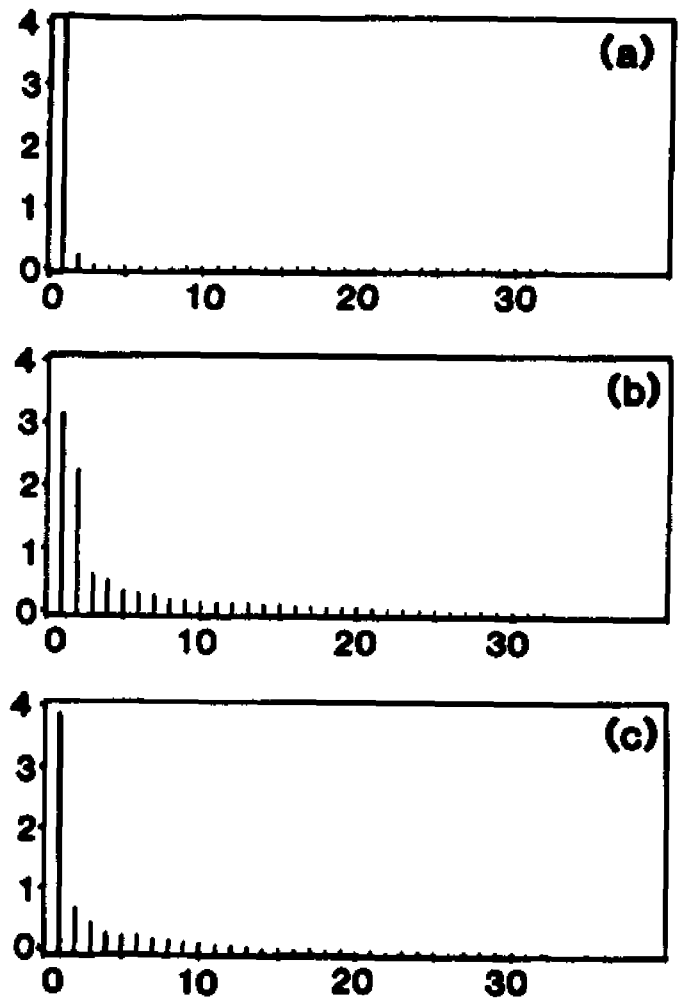

Figure 2. Singular values of the WD for the first (a), second (b), and third (c) 32-point segment of the signal in Fig. 1.a.

between the tails of the third and fourth pulse in. Here, the transient effect is not as pronounced as in the previous case; as a result, the s.v. spectrum is only slightly differs from the first case. Observe that, the magnitude of the dominant s.v. is low whenever the s.v. spectrum is wide and vice versa. The dependence, however, is not exactly inverse proportional. Namely, athough the signal energy is normalized, the sum of the s.v.'s need not necessarily be a constant.

Notice that the data windows characterized by stable local frequency possess the most compact s.v. spectra with the largest dominant s.v. On the other hand, wide s.v. spectra and smaller dominant s.v. imply that the local frequency in the data window is unstable. Using this fact we can separate the stable from the unstable frequency points. These conclusions remain true even in the presence of substantial uncorrelated thermal noise (see Fig. 3). Noise, in general, increases the TB-product of the data in the window and perturbs the s.v. spectrum (decreasing the dominant s.v.). The dominant s.v.'s have the best signal-to-noise ratio, and, therefore, are used for noise and interference discrimination.

The centroid frequency, as a gross signal feature, can be estimated using the first frequency singular vector as an approximation to the signal spectrum. This corresponds to the truncation of the expansion (6) to a single term, K=1. Such a sharp truncation of the expansion is acceptable because the TB-product of a clean ultrasonic RF pulse is low, and therefore the gross information is contained in the dominant first term while the remaining terms represent second order effects.

The following procedure is proposed for estimating the intrinsic frequency variation trend. As a first step, the A-line is partitioned into overlapping seg-

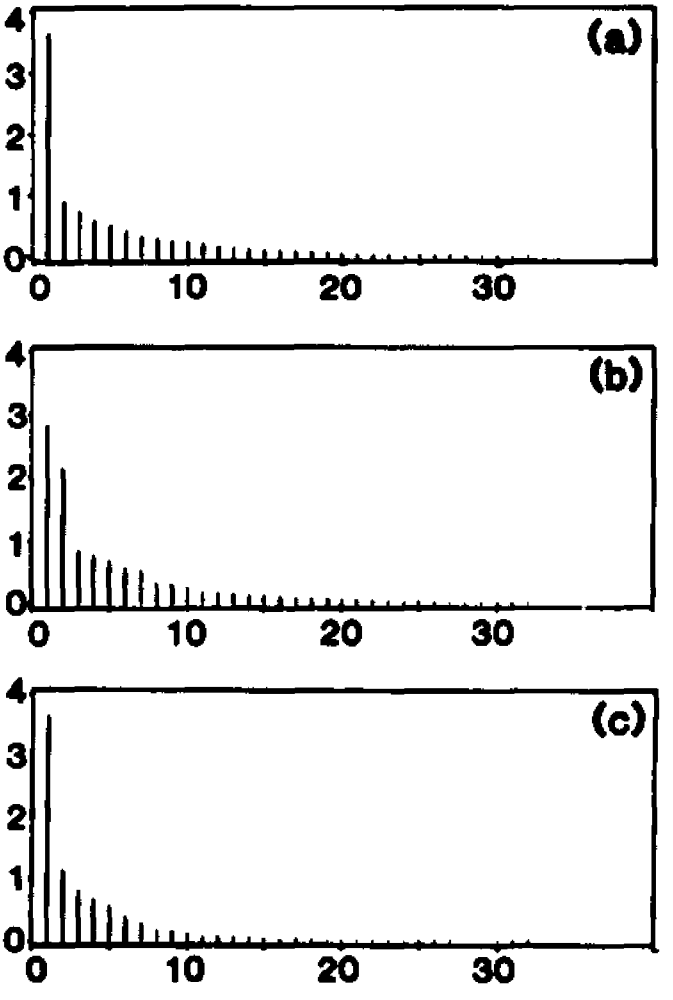

Figure 3. Singular values of the WD for the first (a), second (b), and third (c) 32-point segment of the signal in Fig. 1.a, corrupted by noise, S/N = 18dB.

ments using any standard window, e.g. Hamming window. On each data segment the WD is calculated and normalized. Then, the dominant s.v. of the WD and the corresponding frequency singular vector are determined. Data segments with stable frequency are identified by comparing their dominant singular value to a predetermined threshold. The local frequency is then the centroid of the dominant singular vector for each well-behaved data segment. The success of this technique is illustrated on the examples in the next section.

4. Frequency Estimation - Examples

Simulated ultrasonic RF A-lines are used to evaluate the performance of the proposed technique and to compare it with the standard, short-time Fourier transform based, technique. One such A-line is shown in Fig. 4.a. The RF pulse at the beginning of the A-line has 60% relative 6dB bandwidth and its central frequency is 1/4 of the sampling frequency (relative frequency $\nu_0 = f_0/f_s = 0.25$). In all the simulations, the A-line length is 256 wavelengths and a linear, 15% downward frequency shift along the A-line is present. Reflectors are randomly distributed along the A-line, resulting in random variations of the instantaneous frequency. Fig. 4.b shows the local frequency variation along the A-line from Fig. 4.a, estimated with the standard approach using 32-point (two pulse lengths) Hamming window with 75% overlap. Averaging of the estimates from many A-lines is needed to suppress the substantial amount of correlated random deviation from the linear trend. For comparison, the result obtained with the new method using the same data is shown in Fig. 4.c. Hardly any additional averaging is needed in this case.

The result in Fig. 4.c was obtained through the following procedure. We have found that half of the pulse length (8 points) is nearly the optimum window size. An A-line is segmented employing 8-point Hamming window with

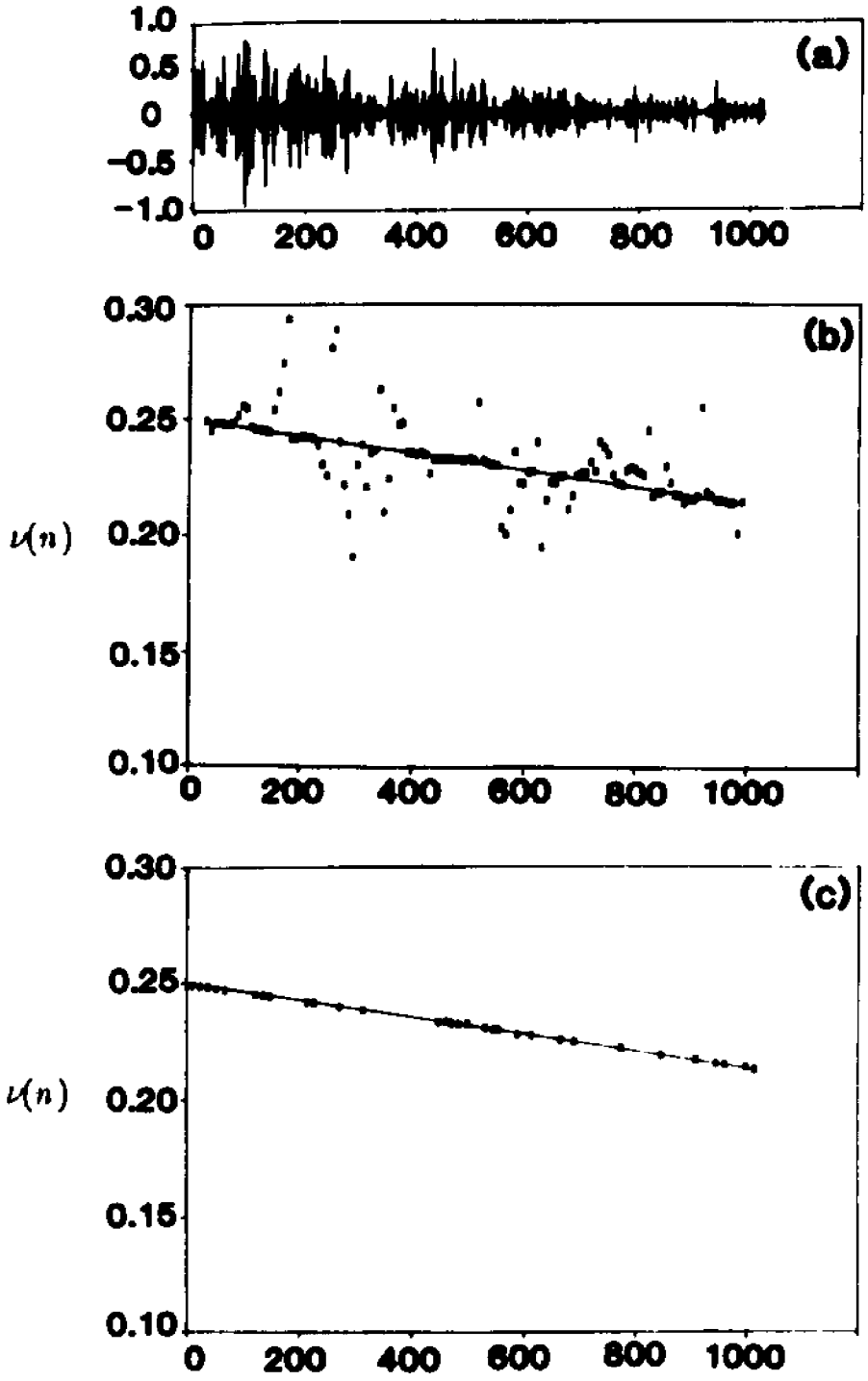

Figure 4. (a) Simulated ultrasonic A-line. (b) Standard, short-time Fourier transform centroid estimates using 32-point windows with 75% overlap. (c) Wigner distribution based centroid estimates using 8-point windows with 75% overlap.

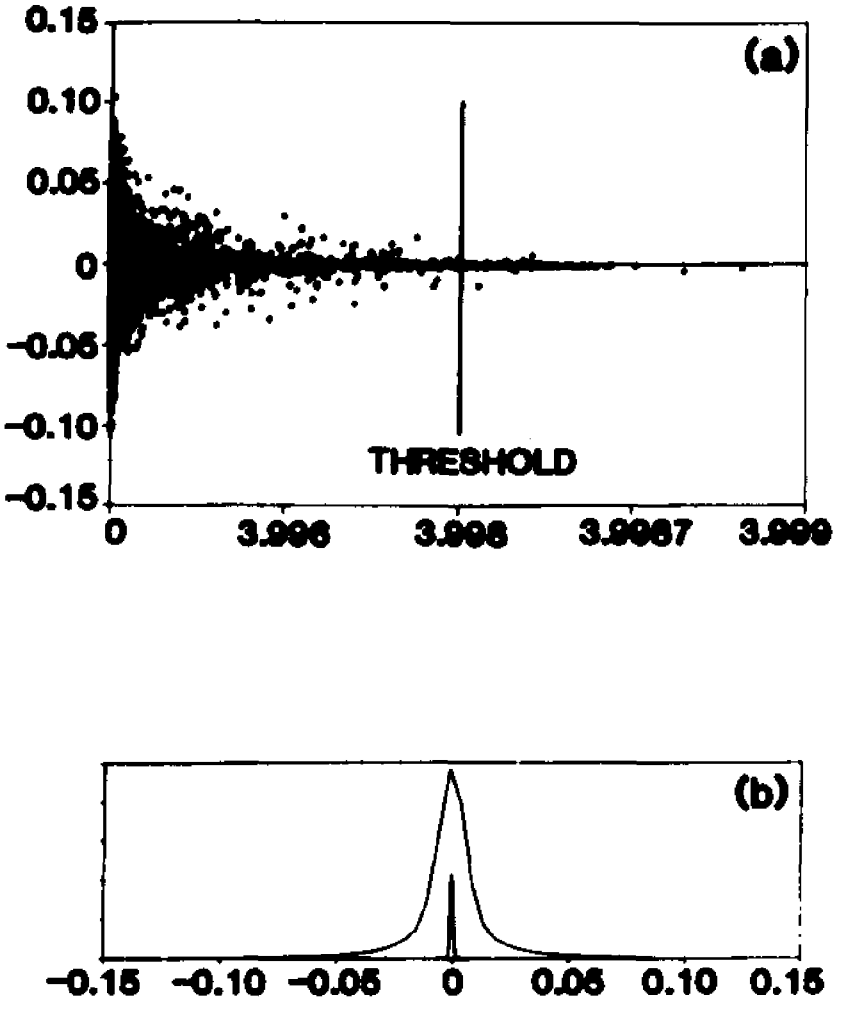

Figure 5. (a) Deviation of the centroid estimates from the built-in frequency trend (normalized to the sampling frequency) vs. magnitude of the corresponding dominant singular value. (b) Probability density of the linear regression residuals for short-time Fourier analysis method (wide spread) and for Wigner analysis method (narrow spread).

75% overlap. The dominant singular value, the corresponding frequency singular vector and its centroid are calculated for each data segment. The thrust of the method is that in the data segments characterized with largest dominant s.v.'s, the frequency is stable and therefore deviates very little from the actual frequency trend. The actual correlation of the frequency error and the magnitude of the dominant s.v.'s is shown in Fig. 5.a using the data from twelve simulated A-lines. The largest dominant s.v.'s correspond to smallest frequency estimation error; the threshold is set as shown in the Figure. By selecting only the frequency estimates from the data segments whose dominant s.v. is greater than the threshold, the plot shown in Fig. 4.c is obtained. Linear regression analysis of the data shown in Fig. 4.c produces a slope estimate deviating only 0.75% from the true value. Clearly, accurate frequency estimation on a single A-line is possible with this method.

The improvement over the standard short-time Fourier transform based technique becomes obvious when the plots shown in Figs. 4.b and 4.c are compared. To quantify this, the estimates of the frequency estimation error probability densities for the two methods were obtained as shown in Fig. 5.b. The standard error with the conventional approach is 23 times greater than with the new method. This implies that, for the same accuracy, about 500 times more data needs to be averaged with the standard technique. Strictly speaking, this is true only for the data with high signal to noise ratio. However, this is the case in conventional ultrasonic imaging.

When a substantial amount of white noise is added to the A-line in Fig. 4.a, so that the signal to noise ratio is only 18dB, the performance of both methods is impaired. Local frequency estimates obtained from a single A-line with conventional and WD based techniques are shown in Fig. 6. To compensate for noise effects, some between line averaging in the WD based method

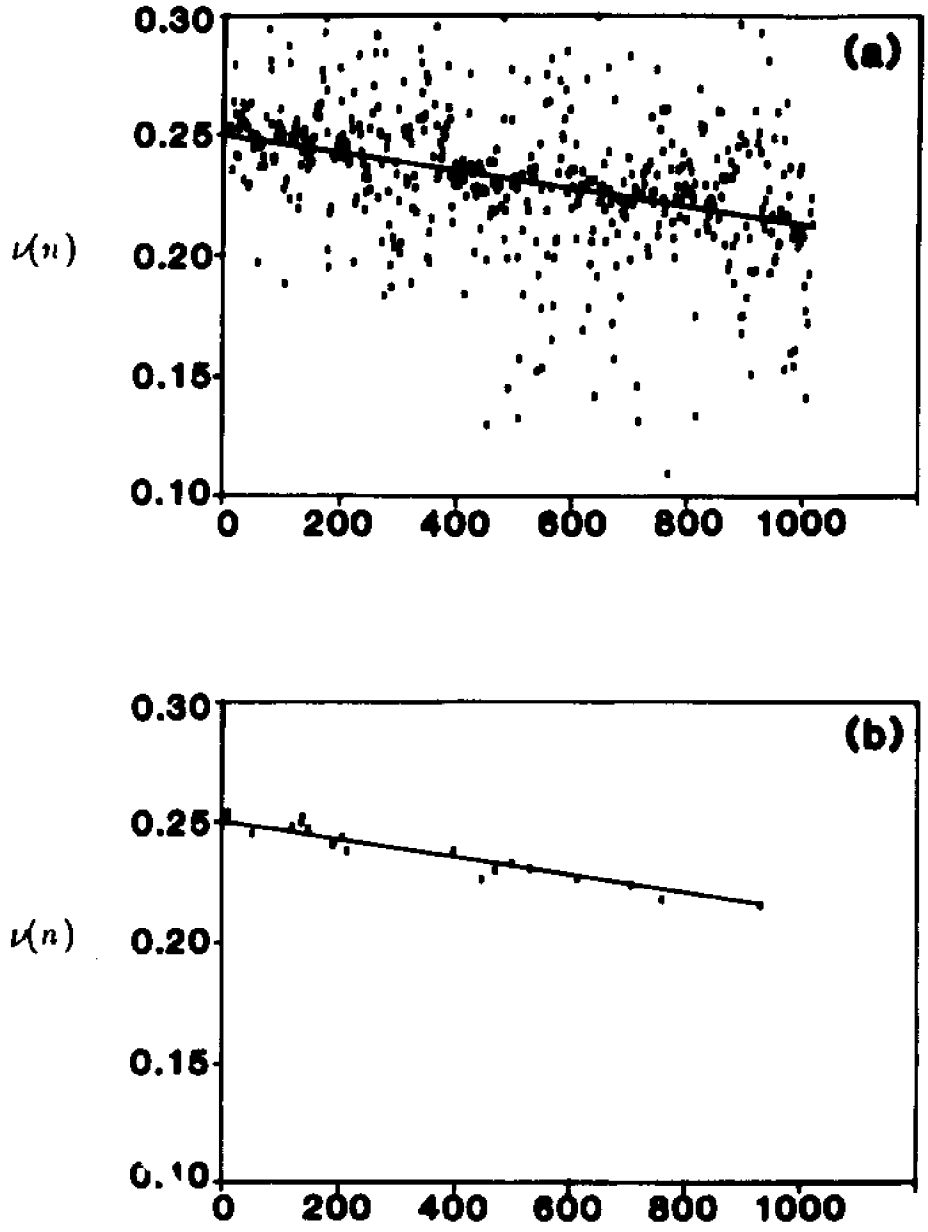

Figure 6. Results for simulated ultrasonic A-line in noise, S/N = 18 dB. (a) Standard, short-time Fourier transform centroid estimates using 32-point windows with 75% overlap. (b) WD based centroid estimates using 8-point windows with 75% overlap.

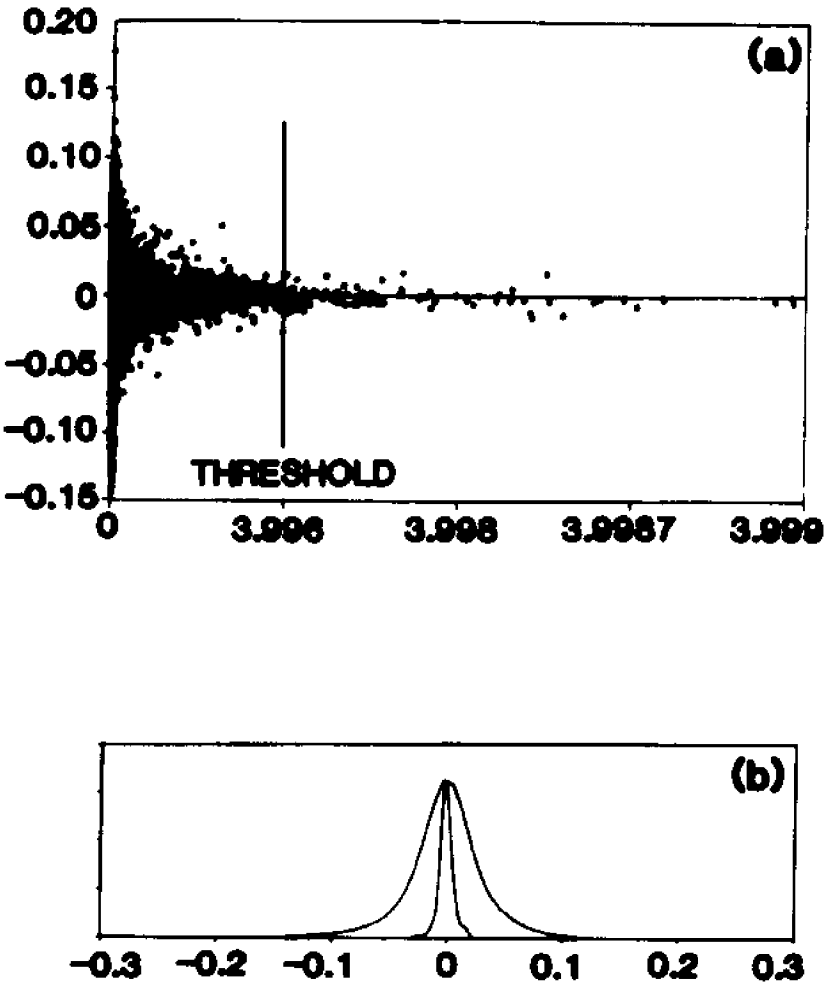

Figure 7. (a) Deviation of the centroid estimates from the built-in frequency trend (normalized to the sampling frequency) vs. magnitude of the corresponding dominant singular value, noise added to the signal, S/N = 18 dB. (b) Probability density of the linear regression residuals for short-time Fourier analysis method (wide spread) and for Wigner analysis method (narrow spread), noise added to the signal, S/N = 18 dB.

may be needed also. As can be observed in Fig. 7.a, the noise perturbs both the s.v.'s and the singular vectors. This affects the ability of the method to extract segments with stable frequency and the accuracy of the centroid estimate within each segment. Plots of the frequency estimation error probability density (see Fig. 7.b) indicate that the WD based method loses some of its advantage over the conventional technique. However, since the standard frequency estimation error is 7 times larger, the WD method requires still about 50 times less data for the same accuracy. In practice, the signal to noise ratio is usually higher than 18dB, and better improvement is expected.

5. Conclusions

Using the proposed method, accurate estimation of the local frequency trend with very little or no between line averaging is possible. Instead of brute force averaging, the regions of unstable frequency are identified and discarded by analyzing the singular values of the WD. For simulated ultrasonic A-lines, compared to the conventional short-time Fourier transform technique, the amount of data required for accurate frequency estimation is reduced by about two orders of magnitude. Although the WD based method is more complex, the actual number of computations per line is only somewhat larger since substantially shorter data windows are used. Therefore, this approach promises substantial savings in data acquisition and data processing time for the estimation of the attenuation by the frequency-shift method.

References

1. S. Leeman, L. Ferrari, J. P. Jones and M. Fink, "Perspectives on Attenuation Estimation from Pulse-Echo Signals," *IEEE Trans. Sonics Ultrasonics*, vol. SU-31, pp. 352-361, July 1984.

2. J. Ophir, T. H. Shawker, N. F. Maklad, J. G. Miller, S. W. Flax, P. A. Narayana and J. P. Jones, "Attenuation Estimation in Reflection: Progress and Prospects," *Ultrasonic Imag.*, 6, pp. 349-395, Oct. 1984.

3. M. Fink, F. Hottier and J. F. Cardoso, "Ultrasonic Signal Processing for In-Vivo Attenuation Measurement; Short-Time Fourier Analysis," *Ultrasonic Imag.*, 5, pp. 117-135, Feb. 1983.

4. R. Kuc, "Estimating Acoustic Attenuation from Reflected Ultrasound Signals: Comparison of Spectral-Shift and Spectral-Difference Approaches," *IEEE Trans. Acoustics, Speech Sig. Proc., vol. ASSP-32, pp. 1-6, Feb. 1984.*

5. J. Ophir, M. A. Ghouse and L. A. Ferrari, "Trade-offs in Attenuation Estimation Using the Zero-Crossing Technique," in press - *Ultrasonics in Medicine and Biology*, 1985.

6. T. A. C. M. Claasen and W. F. G. Mecklenbräuker, "The Wigner Distribution - A Tool for Time-Frequency Signal Analysis," *Philips J. Res.* 35, pp. 217-250, 276-300, 372-389, 1980.

7. W. Martin, "Time-Frequency Analysis of Random Signals," *Proc. ICASSP-82*, pp. 1325-1328, March 1982.

8. T. A. C. M. Claasen and W. F. G. Mecklenbräuker, "The Aliasing Problem in Discrete-Time Wigner Distributions," *IEEE Trans. Acoust. Speech, Signal Processing*, vol. ASSP-31, pp 1067-1072, Oct. 1983.

Chapter 8

Summary and discussion

Focus of this research has been on two generic time-frequency representations - the Wigner distribution and the ambiguity function. Two directions have been followed. These representations have been redefined to provide for scale-invariance. Properties of the scale-invariant representations have been analyzed in detail and shown to be well suited for the scale-invariant processing of signals and analysis of the scale-invariant systems.

The other research avenue focused on the data compression, enhancement and applications of the Wigner distribution in particular, although the discussion is valid more generally. It was shown that the Wigner distribution provides insight into the filtering action of the linear systems that is not available with conventional approaches. An outer product expansion was proposed and used for enhancement of the Wigner distribution. This provides for improved parameter estimation and detection of signals in the time-frequency plane. Moreover, it was shown that the expansion defines a non-linear, non-unitary signal transformation with the generalized "spectrum" of the signal determined by the set of expansion coefficients. The "spectrum" properties have been correlated with the physical characteristics of the signal. This, then, served as a basis for two different applications.

In one, the singular value spectrum was used to identify segments of an ultrasonic echo with unstable, noisy frequency, thereby enabling efficient estimation of the frequency shift along the region in the reflecting tissue. This is necessary for accurate measurement of the ultrasonic attenuation in tissue - a very extensively studied problem, but without much success. Spectrum

coefficients have been also successfully used in another area of signal processing - image analysis. They provided very good descriptors of shape that satisfy all standard requirements. Using the simple procedures successful classification of planar shapes was achieved.

A variety of applications for the scale-invariant Wigner distribution and ambiguity function remains to be explored. Some of the possibilities are: characterization of scale-invariant optical and electronic systems, scale-invariant parameter estimation, feature extraction and pattern recognition, Doppler processing, and non-linear spectrum spreading.

The transformation of the signal into its singular value spectrum seems to be a rather powerful tool for variety of signal processing applications. It takes advantage of the fact that representation of signals in time-frequency plane encodes more explicitly certain signal features, such as its time-bandwidth product, the complexity of frequency vs. time variation, and the complexity of signals in terms of the number of components and their spacing. Possibilities for further research seem very open here: in the classification of tissue states using ultrasonic echography, in the analysis of underwater acoustic transient signals, in speech analysis and recognition, in analysis of electroencephalographic and electromyographic signals, in 2-D shape description and classification for image analysis, target identification, biology, robotics, etc.